FINITE ELEMENT AND MECHANOBIOLOGICAL MODELLING OF VASCULAR DEVICES

A dissertation submitted for the degree of Ph.D.

Houman Zahedmanesh, B.Sc., M.Sc.

Dublin City University

Under the supervision of

Dr. Caitríona Lally

School of Mechanical and Manufacturing Engineering

March 2011

Declaration

I hereby certify that this material, which I now submit for assessment on the programme of study leading to the award of Ph.D. is entirely my own work, that I have exercised reasonable care to ensure that the work is original, and does not to the best of my knowledge breach any law of copyright and has not been taken from the work of others save and to the extent that such work has been cited and acknowledged within the text of my work.

Signed:_____ ID No.:_____ Date:_____

Publications Resulting from this Study

Peer Reviewed Journal Articles:

Zahedmanesh H., Lally C. (2011) A multiscale mechanobiological model using agent based models; Application to vascular tissue engineering, *Biomechanics and Modeling in Mechanobiology*, in press. doi: 10.1007/s10237-011-0316-0

Zahedmanesh H., Mackle J, Selborn A., Bodin A., Drotz C., Gatenholm P., Lally C. (2011) Bacterial cellulose as a potential vascular graft: Mechanical characterisation and constitutive model development, *Journal of Biomedical Material Research-Part B*, Vol.97, pp105-13.

Colombo A., Zahedmanesh H., Toner D., Cahill P., Lally C. (2010) A method to develop mock arteries suitable for cell seeding and in-vitro cell culture experiments, *Journal of the Mechanical Behavior of Biomedical Materials*, Vol.3, pp470-477.

Zahedmanesh H., Kelly D., Lally C. (2010) Simulation of a balloon expandable stent in a realistic coronary artery; Determination of the optimum modelling strategy, *Journal of Biomechanics*, Vol.43, pp2126–2132.

Zahedmanesh H., Lally C. (2009) Determination of the influence of stent strut thickness using the finite element method: implications for vascular injury and in-stent restenosis, *Medical and Biological Engineering and Computing*, Vol. 47, pp385-393.

Peer Reviewed Conference Proceedings:

Zahedmanesh H., Lally C., Simulation of remodelling in vascular scaffolds using agent based models and finite element analysis, *Proceedings of 17th Bioengineering in Ireland Conference, BINI, 2011, Galway, Ireland.*

Zahedmanesh H., Lally C., Simulation of remodelling in vascular scaffods using agent based models, *Proceedings of tissue engineering and regenerative medicine- EU meeting, 2010, Galway, Ireland.*

Zahedmanesh H., Lally C., A novel mechanobiological model of remodelling in vascular tissue engineered scaffolds, *Proceedings of 17th congress of the European Society of Biomechanics, 2010, Edinburgh, Scotland.*

Zahedmanesh H., Gatenholm P., Lally C., Bacterial cellulose, a potential vascular graft and tissue engineering scaffold, *Proceedings of ASME Summer Bioengineering Conference, 2009, Lake Tahoe, USA.*

Zahedmanesh H., Lally C., Bacterial cellulose as a potential vascular graft and tissue engineering scaffold; biomechanical considerations, *Proceedings of 15th Bioengineering in Ireland Conference, BINI, 2009, Limerick, Ireland.*

Internal Symposium Presentations:

Zahedmanesh H., Lally C., Bacterial cellulose as a tissue engineering scaffold and mechanobiology, *Faculty of Engineering and Computing Research Day, 2010, Dublin City University, Dublin, Ireland.* (The Award for the Best Presentation)

Zahedmanesh H., Lally C., Bacterial cellulose as a potential vascular graft and tissue engineering scaffold; biomechanical considerations, *Symposium for Mechanical Engineering Research & Practice, 2009, Dublin City University, Dublin, Ireland.* (The Award for Excellence in Presentation)

Invited Talks:

Zahedmanesh H., Lally C., Bacterial cellulose as a tissue engineering scaffold and mechanobiology, Biosynthetic Blood Vessels, Chalmers University of Technology, 2009, Gothenburg, Sweden.

Acknowledgments

Words cannot describe my sincere feelings towards those without whose support I was not in the position that I am today. I try to picture every single one of them and remind myself of the moments that we shared and their kind support.

When I review the years that I have spent in academia, undoubtedly my PhD supervisor Dr. Caitríona Lally has been the key figure. She is an ambitious, supportive, passionate and devoted supervisor who has an incredible ability to identify the potentials of her students and help them flourish those potentials. Every moment of the three years of working with her was a precious lesson for me to learn. I feel privileged to have been able to work with her because of her thorough knowledge and because of her endless passion for training competent biomedical engineers. She creates and promotes a creative research environment where research students can extend their imaginations, explore new methods and implement new ideas. Herewith, I would like to take the opportunity to express my most sincere gratitude towards her for this challenging, yet exciting and fruitful three years and wish to be able to continue my collaboration with her throughout the rest of my research career.

When it comes to gratitude, the first and the most beautiful names that come to my mind are Father and Mother. They are those who generously devoted their lives to my success and pictured their own happiness in my achievements. They are those who supported me in hardship and were enchanted by my every little success even more than myself. Only and only to remind myself of how much I owe them I would like to dedicate this thesis to my parents, Ali and Giti. I cannot thank my parents but not thank my younger brother Aryan who is now graduating as a young, intelligent and open minded electrical engineer. We shared lots of jokes and loud laughs on Skype and I enjoyed lots of philosophical discussions with him during these years which made living away from home much easier for me. I am so proud of him and I will be looking forwards to reading his PhD thesis someday soon.

I would also like to thank all of my friends and colleagues, Alberto, Vittoria, Artur, Evelyn and Joe with whom I shared very enjoyable and happy moments. I should also appreciate the very kind support that I received from the head of the school of mechanical and manufacturing engineering Prof. Saleem Hashmi, the assistance I received from the school technical staff, specifically Liam Domican, Keith Hickey, Chris Crouch and Jim Barry and also school secretary Suzanne Dockery.

In the end I would like to acknowledge the Irish Research Council for Science Engineering and Technology (IRCSET) for generously supporting this PhD through the Embark Initiative postgraduate scholarship.

Table of Contents

List of Figures

List of Tables

Nomenclature

$\lambda_j, j \in \{x, y, z\}$ or $j, \in \{r, \theta, z\}$	Principal Stretch;
I_j , $j \in \{x, y, z\}$ or $j, \in \{r, \theta, z\}$	Stretch Invariant;
$S_{ij}, i, j \in \{x, y, z\}$ or $i, j, \in \{r, \theta, z\}$	Components of the second Piola-Kirchhoff stress tensor;
$E_{ij}, i, j \in \{x, y, z\}$ or $i, j, \in \{r, \theta, z\}$	Components of the Green-Lagranian strain tensor;
$C_{ij}, i, j \in \{x, y, z\}$ or $i, j, \in \{r, \theta, z\}$	Components of the right Cauchy-Green deformation tensor;
W	Strain energy density function;
$\mu_p,\ \alpha_p, \alpha_p$	Ogden's hyperelastic material constants;
C	Compliance;
D_s, D_d	Graft diameter in systole and diastole respectively;
P_{sys}, P_{dias}	Systolic and diastolic pressures respectively;
$P_{amplitude}, P_{mean}$	Pulsatile flow amplitude and mean pressure respectively;
Freq.	Frequency of the pulsatile flow;
ε_{cyc}	Cyclic strain;
V_{fluid}	Pore fluid flow velocity;
DT	Cell doubling time;
σ	Stress;
p	Pore pressure;
K	Permeability;
φ	Porosity;
J	Deformation gradient;

Abstract

Finite Element and Mechanobiological Modelling of Vascular Devices

Houman Zahedmanesh

There are two main surgical treatments for vascular diseases, (i) percutaneous stent deployment and (ii) replacement of an atherosclerotic artery with a vascular graft or tissue engineered blood vessel. The aim of this thesis was to develop computational models that could assist in the design of vascular stents and tissue engineered vascular grafts and scaffolds. In this context, finite element (FE) models of stent expansion in idealised and patient specific models of atherosclerotic arteries were developed. Different modelling strategies were investigated and an optimal modelling approach was identified which minimised computational cost without compromising accuracy. Numerical models of thin and thick strut stents were developed using this modelling approach to replicate the ISAR-STEREO clinical trial and the models identified arterial stresses as a suitable measure of stent induced vascular injury.

In terms of evaluating vascular graft performance, mechanical characterisation experiments can be conducted in order to develop constitutive models that can be used in FE models of vascular grafts to predict their mechanical behaviour *in-situ*. In this context, bacterial cellulose (BC), a novel biomaterial, was mechanically characterised and a constitutive model was developed to describe its mechanical response. In addition, the interaction of smooth muscle cells with BC was studied using cell culture experiments. The constitutive model developed for BC was used as an input for a novel multi-scale mechanobiological modelling framework. The mechanobiological model was developed by coupling an FE model of a vascular scaffold and a lattice free agent based model of cell growth dynamics and remodelling in vascular scaffolds. By comparison with published *in-vivo* and *in-vitro* works, the model was found to successfully capture the key characteristics of vascular remodelling. It can therefore be used as a predictive tool for the growth and remodelling of vascular scaffolds and grafts.

Chapter 1

Introduction

1.1 Cardiovascular disease

Cardiovascular diseases (CVD) take the lives of millions of people in the world and impose considerable economic and social burden on societies. Being the largest cause of morbidity and mortality, CVD account for approximately 48% of deaths or 4.3 million deaths per annum in Europe and 40% of death (2 million) in the European Union alone based on 2008 statistics (EHN 2010). CVD affect the heart and blood vessels and can take many forms such as high blood pressure, coronary artery disease, aneurysm, heart disease and stroke. They are one of the leading causes of long term morbidity and loss to the labour market. CVD are strongly associated with socioeconomic conditions and differences in CVD rates constitute the biggest single cause of health inequalities within the European member states (Simoons 2003; Health-EU 2010). The financial burden for EU healthcare systems related to CVD has been estimated to be near €192 billion based on 2008 statistics, around 57% of which is due to healthcare costs, 21% due to productivity losses and 22% due to informal care of people with CVD (EHN 2010).

Coronary artery disease is a major type of CVD which is mainly due to development of atherosclerosis in coronary arteries and their consequent blockage which can ultimately lead to stroke or myocardial infarction. Coronary artery disease is the single most common cause of death in Europe and the European Union. Based on 2008 statistics, coronary artery disease accounts for 1.92 million deaths in Europe and over 741,000 deaths each year in the European Union per annum (AHA 2010b).

CVD and specifically atherosclerosis are linked to behaviours and lifestyles, therefore effective prevention strategies can be adopted to reduce the risk of atherosclerosis by better control over key factors such as smoking, nutrition and physical activity, alcohol consumption, and

psychosocial stress. However, once the disease develops the only effective treatment is surgical intervention. Currently two major surgical procedures are practiced to treat patients with atherosclerosis:

(i) Invasive surgical procedures such as open heart surgery where a vascular graft is used to bypass the diseased artery or fully replace it

(ii) Minimally invasive surgery including balloon angioplasty and stent deployment.

1.2 Objectives

Vascular grafts and stents are the main vascular implants used in the aforementioned surgical procedures. In bypass procedures usually an autograft such as the saphenous vein is used, however, in more than one third of the cases a suitable autograft is not available (Sarkar *et al.,* 2007b). This limitation has motivated development of artificial blood vessels including synthetic grafts and tissue engineered blood vessels. On the other hand different types of stents have been developed and there is an intense ongoing research to improve the performance of stents. The main issue with both of these devices is the problem of re-narrowing following their implantation partly due to over-proliferation of vascular smooth muscle cells (VSMCs) (Lemson *et al.,* 2000; Mitra *et al.,* 2006).

Several studies have elucidated the significant role of biomechanics in the performance of these devices and have highlighted the determining influence of biomechanics related factors on their short and long term implantation outcome. Computational methods offer several advantages in assessing the biomechanics of medical devices such as prediction of system behaviours, biomechanical design optimisation, and also efficiency and cost effectiveness in the design cycle. Given the advantages of computational methods, this study aims to develop computational models which can help to address the following key biomechanics related challenges in relation to vascular grafts and stents, (also see Figure 1-1):

(i) Optimise stent designs in order to minimise the re-narrowing of blood vessels following stent implantation due to in-stent restenosis.

(ii) Optimise the mechanical properties of vascular grafts and their design to minimise re-narrowing of grafts following implantation due to development of intimal hyperplasia.

(iii) Develop novel tissue engineering strategies informed by mechanics related cues in order to enhance the remodelling of vascular scaffolds and minimise intimal hyperplasia.

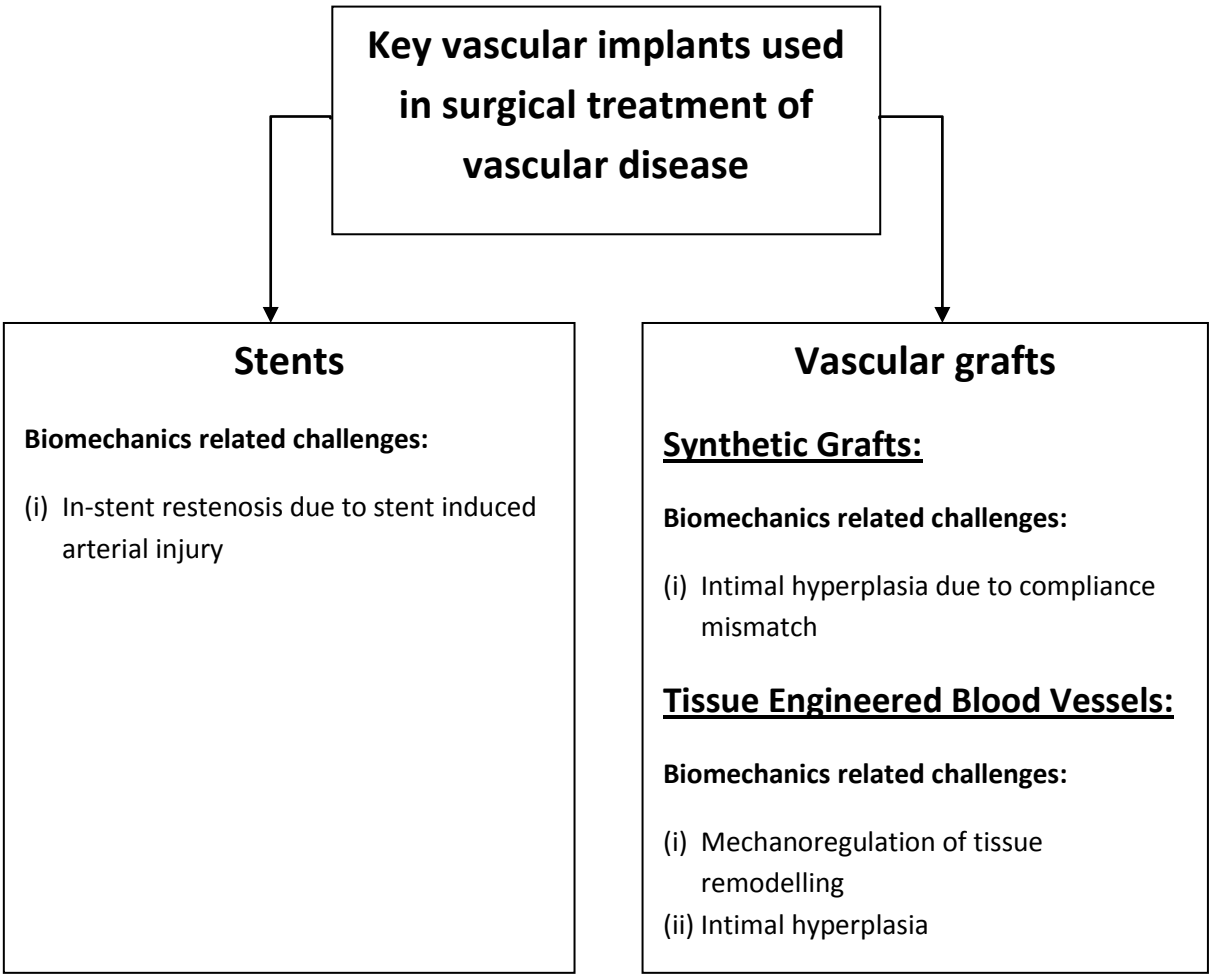

Figure 1-1: Overall objectives of this study

Chapter 2

Literature Review

2.1 Arteries, Structure and Diseases:

Arteries have the vital role of blood supply to organs in the body. In spite of their simple geometry and appearance as a tubular conduit for blood flow, arteries take advantage of a tremendously sophisticated and intriguing structure. This sophisticated structure of arteries helps regulate the blood flow and pressure in the farthest organs from the heart. Their passive viscoelastic response combined with their ability to actively contract depending on the physiological demands, complements the role of heart in the blood circulation system.

Arteries consist of three main layers, (i) the tunica intima, which is the innermost layer of an artery, (ii) the tunica media as the intermediate layer of arteries, and (iii) the tunica adventitia which is the outermost layer as can be seen in Figure 2-1. Arteries are generally categorised as *elastic* or *muscular* depending on the composition of the medial layer. In elastic arteries, the media contains comparably higher number of elastic laminae. In contrast, in muscular arteries the media is dominated by smooth muscle cells (SMCs) and the elastic content is lower. Large arteries are mainly classified as elastic arteries and the small diameter arteries and the arteries approaching the peripheral organs are classified as muscular (Rhodin *et al.,* 1980)

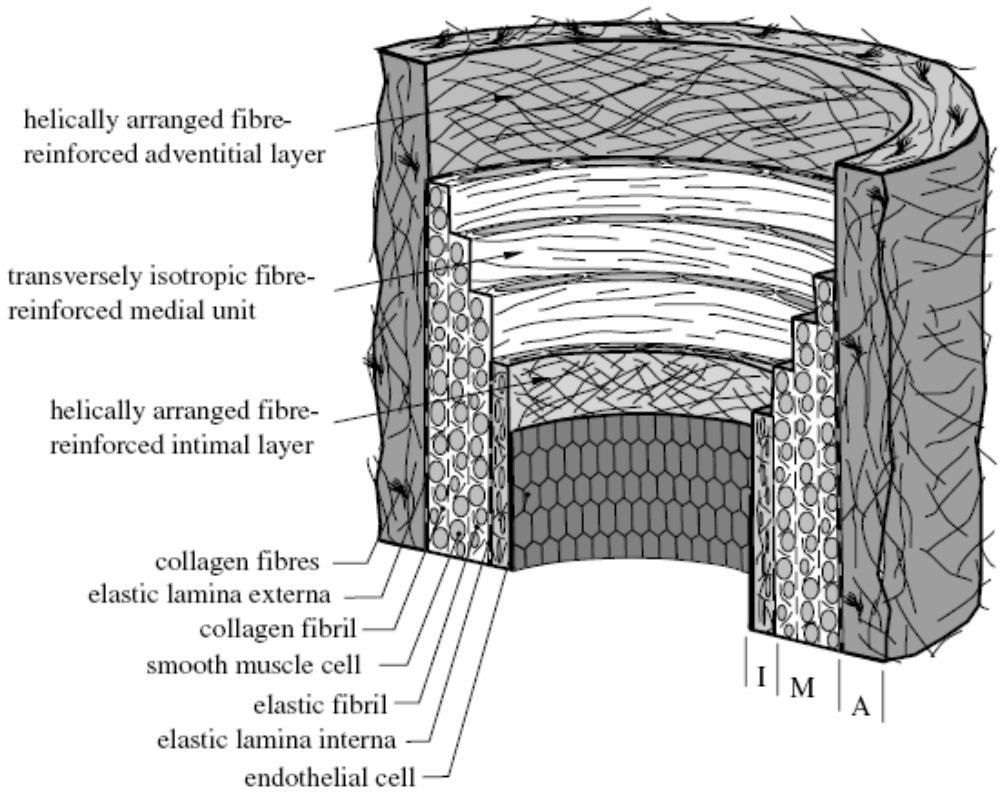

Figure 2-1 Diagram of a healthy elastic artery and its components, taken from Holzapfel *et al.,* 2000a.

The intima functions as an interface between the thrombogenic media and blood. This layer is composed of a single layer of endothelial cells lining a thin basal lamina (Rhodin *et al.* 1980). Along with ageing of arteries, a normal thickening of the intima occurs due to development of non-pathological intimal hyperplasia (Stary *et al.,* 1992; Subbotin 2007). This process is a non-atherosclerotic process and involves proliferation of intimal cells, mainly myofibroblasts, which leads to an increase of extracellular matrix containing mainly collagen fibres with dispersed smooth muscle cells through the layer (Canham *et al.,* 1989). The intima adapts itself overtime to baseline levels of stress. As a result, in aged human arteries the intimal layer has significant load bearing capacity (Holzapfel *et al.,* 2005a).

The media is mainly comprised of smooth muscle cells (SMCs), bundles of collagen fibrils, a network of elastin fibrils and proteoglycans, (Clark *et al.,* 1979; Pedrizzetti *et al.,* 2003). The collagen fibres are aligned in two transverse continuous helical orientations. The helix has a

small pitch, rendering the arteries strong enough in the circumferential direction to resist high blood pressures.

The adventitia mainly consists of fibroblasts and the ground-matrix where collagen fibres are organized in thick bundles. Collagen fibres mainly of type I (von der Mark 1981) are arranged within the ground matrix and form a fibrous tissue. Polarized light microscopy of the structure of adventitia has shown that collagen fibres form two helically arranged families of fibres with large dispersion from the mean orientation (Canham *et al.,* 1989).

Each of the arterial cell types play a vital role in the arteries and any disruption in their function will cause a pathological condition. Endothelial cells (ECs) which line the lumen of arteries create a barrier between the arterial wall and the blood vessel. ECs prevent thrombosis formation due to direct contact between blood and the arterial components. They also function as a layer which prevents proliferation of smooth muscle cells towards the lumen by synthesis of chemokines such as nitric oxide which has antiproliferative influence on the underlying SMCs (Lemson *et al.,* 2000). Also they prevent fusion of lipids in the blood flow into the medial layer which can create foam cells, an event that is postulated to occur in the early stages of atherosclerosis (Kleemann *et al.,* 2008). SMCs on the other hand synthesise extracellular matrix components such as elastin and collagen and are also in charge of vasoactive contraction of arteries. Fibroblasts, in the adventitia, produce extracellular matrix components, mainly collagen, which are organised in thick bundles strengthening the arterial wall.

Arteries are susceptible to many different diseases, most importantly atherosclerosis and aneurysms. Atherosclerosis is a disease where fatty material called plaque builds up in the lumen of arteries and makes them less flexible. Plaque build-up reduces the amount of blood and oxygen available for vital organs such as the heart and brain and consequently can lead to stroke and myocardial infarction, see Figure 2-2.

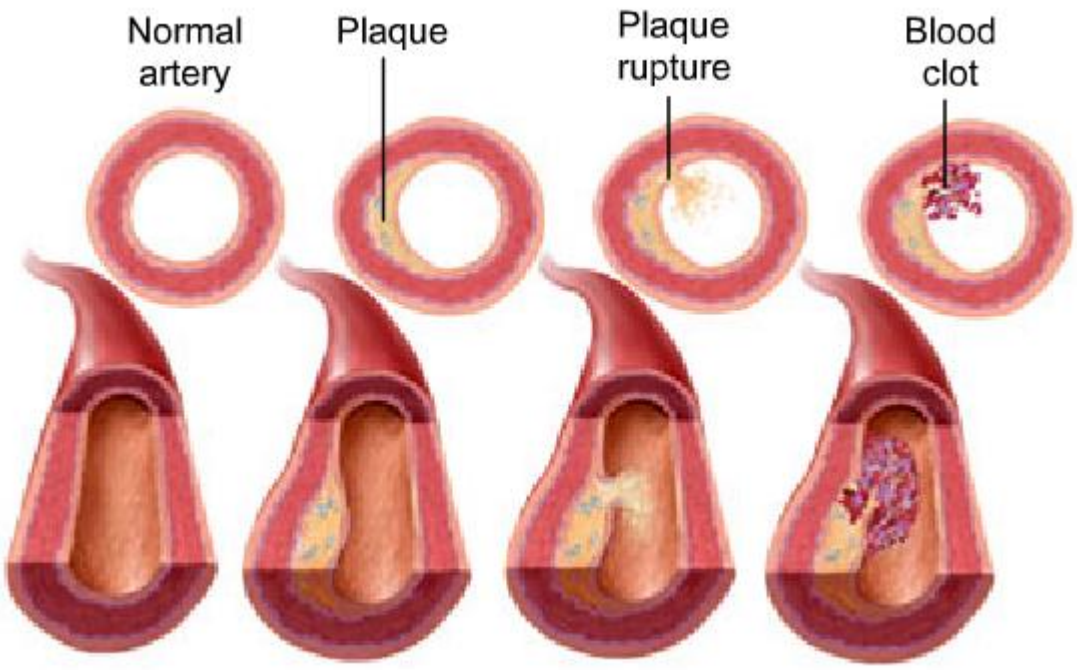

Figure 2-2: Progression of atherosclerosis, taken from AHA 2010a.

Atherosclerosis in arteries develops following a cascade of inflammatory events in response to accumulation of lipoproteins in the arterial wall (Steinberg 2005). It occurs in many different arteries such as the coronary arteries, aorta, carotid and even arteries approaching the extremities such as the iliac artery. It has been shown that atherosclerosis usually occurs in locations where blood flow perturbations take place such as near bifurcations. Damage to the endothelium can increase penetration of low density lipoproteins (LDL) into the intima and increase the risk of atherosclerosis (Steinberg 2005; Vukovic *et al.,* 2006). Formation of fatty streaks and accumulation of cellular and extracellular material between the intima and media are the first signs of an atherosclerotic plaque. Following penetration of lipoproteins into the arterial wall, immune cells (monocytes and T-cells) migrate from the circulatory system into the arterial wall and differentiate into machrophages. Machrophages then take up the accumulated lipoproteins and transform into foam cells. The macrophages and T-cells in the arterial wall then synthesise a wide variety of pro-inflammatory cytokines including the Interleukin family which are considered to be a key player in the chronic inflammation typical of atherosclerosis (Vukovic *et al.,* 2006; Kleeman *et al.,* 2008).

Accumulation of lipids and foam cells in the arterial wall consequently leads to atherosclerotic swelling of the arterial wall. The chronic inflammation increases the chemotactic migration and proliferation of SMCs from media to intima which, in turn also produce inflammatory mediators, monocyte chemoattractants and even take up LDL (Steinberg 2005). Smooth muscle cells are the predominant arterial cells in the larger atherosclerotic lesions and contribute to lesion formation and progression by synthesis of extracellular matrix products (Steinberg 2005).

Based on the American Heart Association, atherosclerotic plaques are classified into six types depending on the progression of the disease, see Figure 2-3. Atherosclerotic plaque *Type IV* and *type V* which are also referred to as *atheroma* and *fibroatheroma* respectively, may develop fissures, hematoma and thrombosis which makes them clinically relevant (Stary *et al.,* 1995). Mortality and morbidity due to atherosclerosis is mainly due to *type IV* and *type V* lesions in which disruptions of the lesion surface, hematoma or haemorrhage, and thrombotic deposits have developed. *Type IV* or *V* lesions with one or more of these additional features are classified as *type VI* and may also be referred to as *complicated lesions* (Stary *et al.,* 1995). Atherosclerosis has also been associated with development of aneurysms given that type IV, V and VI lesions appear to contribute to localised dilatations of the vascular wall and cause development of aneurysms (Stary *et al.,* 1995).

Atherosclerotic plaques are also categorised into stable and vulnerable plaques based on their risk of rupture. Stable plaques are characterised by a higher concentration of SMCs and collagen and lower amount of inflammatory cells. Although a stable plaque is usually thick and can cause a higher degree of stenosis but the thicker and stiffer fibrous caps in such plaques protects them from rupture and hence they constitute a less serious clinical problem. In stark contrast are the vulnerable plaques which are thinner and are richer in inflammatory and lipid-laden cells. These plaques have lower mechanical resistance and are prone to rupture specifically in the plaque shoulder region where the concentration of macrophages is higher. Plaques tend to rupture at sites of increased macrophage and reduced VSMC content. Rupture

of the plaque causes the contents of the lipid core to come into contact with blood clotting factors and creates blood clots and thrombosis which can occlude the blood vessel and cause stroke (Stoneman *et al.,* 2004).

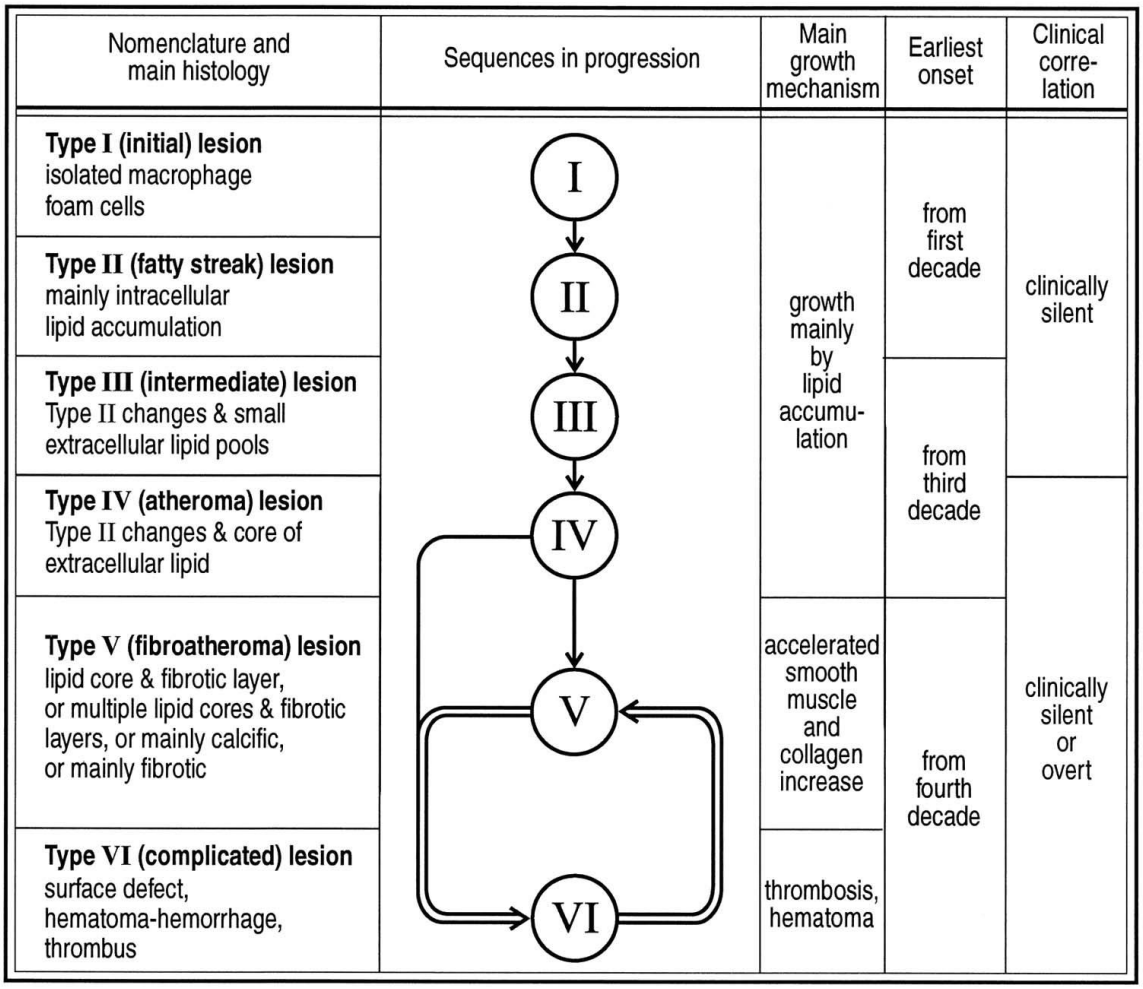

Figure 2-3: Types of atherosclerotic plaque and their characteristics, taken from Stary *et al.,* 1995.

Although healthy diet and life style can help prevent atherosclerosis, currently there are no pharmaceutical treatments for atherosclerotic plaques and in cases where the arteries are severely occluded due to atherosclerosis or where the plaque is prone to rupture the only possible treatment is surgical intervention. Several surgical techniques have been used to treat patients with severe arterial diseases such as atherosclerosis and aneurysms. These techniques can range from minimally invasive techniques including percutaneous transluminal balloon angioplasty and stent deployment to highly invasive methods such as open heart surgery for coronary bypass procedures or replacement of an aneurysmal abdominal aorta with a prosthetic graft.

Roughly one third of the patients with coronary artery disease undergo coronary angioplasty and stenting which constitutes nearly one million patients annually in the United States alone (Michaels *et al.,* 2002). The procedure takes 1 to 2 hours and is conducted using local anaesthesia on patients who are mildly sedated. Most patients stay overnight in the hospital for observation and are discharged the following morning. The patient can then resume normal activities in a week. Following the procedure the patients are treated with anti-platelet drugs such as *Clopidogrel* for a period of 30 days and *Aspirin* in the long term to prevent blood clotting on the stent.

However, there are cases where coronary angioplasty and stenting may not be performed (Michaels *et al.,* 2002). For instance when the coronary artery is too small, the plaque is highly vulnerable to rupture, the plaque is highly calcified and where there is a complete blockage that cannot be crossed with the balloon and stent. Under such conditions open heart bypass procedure is the only possible treatment.

In bypass procedures the surgeon needs a vascular graft to bypass the blocked portion of the coronary artery, see Figure 2-4. The most commonly used autografts are the saphenous vein from the leg, the internal mammary artery from the chest, and the radial artery from the arm. During the surgery a heart-lung machine maintains circulation while the surgeon operates on the heart. The patient is operated under general anaesthesia and stays 4 to 7 days under

observation in the hospital. It may take up to 3 months to fully recover from the surgery. However, in many cases a suitable autograft is not available due to previous use, inadequate calibre or varicosity and the surgeon needs to use a prosthetic graft. The coronary bypass surgery is a typical example of where prosthetic vascular grafts are needed for the treatment of vascular diseases. In addition there are many other cases where surgeons need prosthetic vascular grafts with high patency rates such as in patients who undergo dialysis and need vascular grafts to be implanted as arteriovenous fistulas and in patients with abdominal aortic aneurysms who need to replace the aneurysmal artery with a graft.

The prevalence of arterial diseases and the central role that stents and vascular grafts play in their successful treatment has motivated tremendous efforts towards improving their performance. In the following sections each of these devices are reviewed in more detail and their limitations and challenges are discussed.

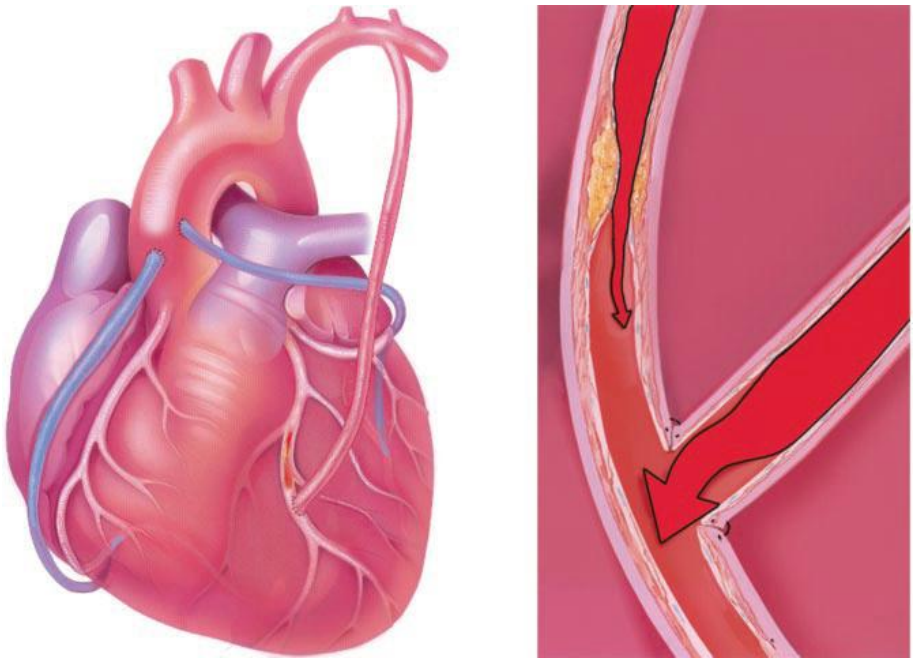

Figure 2-4: Schematic of a coronary bypass procedure; the bypass graft is connected to the aorta at the proximal end and to the atherosclerotic coronary artery downstream from the plaque, taken from Michaels *et al.,* 2002.

2.2 Vascular Devices

As discussed earlier, stents and vascular grafts are the two main devices used for the treatment of vascular disease. However there are several limitations and challenges with their use and outcome which has motivated tremendous endeavours to improve their design and performance. Many of these challenges have been associated with biomechanical factors. In this section, these two main vascular devices are explained and different aspects of their design are discussed specifically from a biomechanical and mechanobiological point of view which is the focus of this thesis.

It is worth mentioning that in this review vascular grafts are categorised into two groups, namely (i) synthetic vascular grafts and (ii) tissue engineered blood vessels, which are discussed separately. However, it should be acknowledged that with the recent developments in the field of biomaterials the difference between synthetic grafts as simple mechanical conduits, and tissue engineered blood vessels as live but artificial blood vessels is fading. This is due to the fact that the classical tissue engineering paradigm that involves *in-vitro* culture of patient cells into a scaffold and its implantation into body following *in-vitro* maturation, is being replaced in favour of a more practical approach towards developing off the shelf grafts which can be readily implanted into body to remodel and mature *in-vivo*.

2.2.1 Endovascular Coronary Stents

An estimated 652,000 percutaneous coronary interventions involving stent deployments were performed in the United States in 2006 to restore the blood supply to the hearts of patients suffering from cardiovascular diseases (AHA 2010a). Percutanesous coronary procedures have several significant advantages over open heart surgery, in particular the fact that they are minimally invasive procedures. Percutaneous coronary stenting was introduced as a solution to the elastic recoil of the atherosclerotic arteries following percutaneous angioplasty. In percutaneous angioplasty a balloon is used to permanently expand the stenosis and restore the blood flow, however, elastic recoil of the stenosed arteries usually minimises luminal gain.

The degree of this elastic recoil depends on the morphology of the atherosclerotic plaque. In cases where the plaque is eccentric the non-diseased segment of the artery may expand elastically under the pressure and the more rigid atherosclerotic plaque may remain undeformed. Therefore, luminal gain may be small following deflation of the angioplasty balloon. The majority of stents are delivered to the pathological region in a crimped configuration mounted on a folded balloon, at the tip of a percutaneously inserted catheter and expanded in the stenosed region by inflation of the folded balloon, see Figure 2-5. Following expansion they scaffold the deformed artery open and prevent its elastic recoil. In spite of the fact that stents have improved the luminal gain in comparison to angioplasty and proved to have a better long term outcome, new complications emerged after introducing stents into clinical use. Namely, intimal cells were found to proliferate due to the severity of the injury caused to the arterial wall by the stent often leading to excessive neointimal hyperplasia and re-stenosis of the artery (Grewe *et al.,* 2000; Mitra *et al.,* 2006).

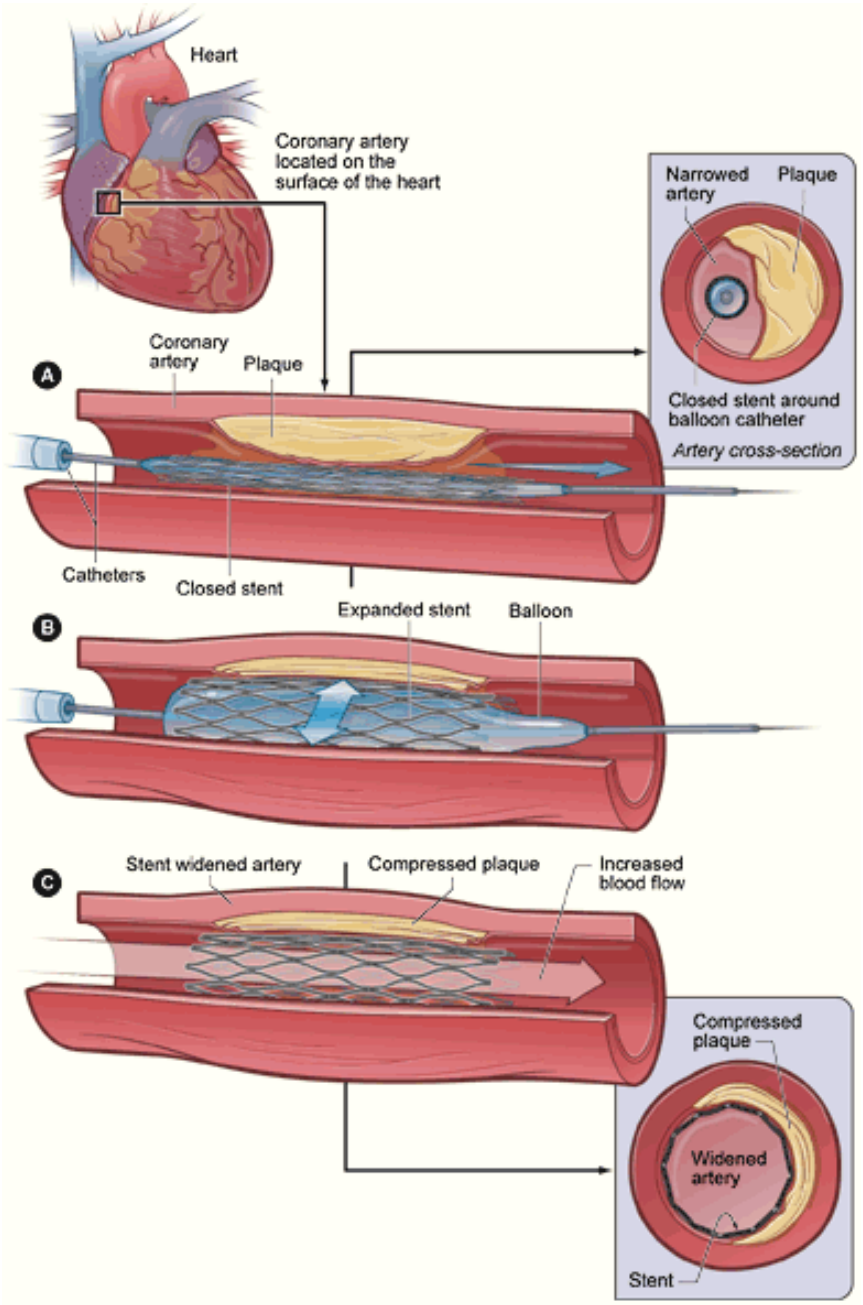

Figure 2-5: Schematic of a balloon expandable coronary stent deployment procedure, taken from NHLBI 2010.

In recent years drug eluting stents, coated with antiproliferative drugs, have reduced the restenosis rate compared to bare metal stents (Morice *et al.,* 2002; Sousa *et al.,* 2005; Hara *et al.,* 2006; Serruys *et al.,* 2006). Several mechanical factors linked to stent design and deployment have also been postulated to be involved in the development of this pathological condition however, which are not eliminated by such pharmaceutical interventions (Mc Clean *et al.,* 2002; Timmins *et al.,* 2007). In addition a higher rate of late thrombosis in drug-eluting stents due to their delayed healing (McFadden et al. 2004, Iakovou et al. 2005, Bavry et al.

2006, Daemen 2007) has raised uncertainty over their use urging researchers to focus further on improving the performance of bare metal stents by improving their mechanical design. The delivery of anti-proliferative drugs to surrounding tissue is also significantly influenced by the stent design (Hwang *et al.,* 2001). Endothelial denudation and vessel wall injury during stent deployment and alteration of the stress-strain field in the arterial wall following stent deployment are hypothesised to be some of the most important factors contributing to in-stent restenosis (Schwartz *et al.,* 1992; Kornowski *et al.,* 1998; Mitra *et al.,* 2006).

During the expansion of the stent, high stresses cause injury to the artery which leads into thrombosis formation in the arterial wall. The arterial injury initiates a cascade of inflammatory events which can lead to in-stent restenosis. After stent implantation adhesion of the thrombocytes at the injury sites are observed. These thrombocytes produce growth factors in the thrombosis sites and initiate chemotactic migration and proliferation of medial SMCs. The cytokines produced by the inflammatory cells not only serve as mitogens for SMCs but also upregulate synthesis of extracellular matrix by SMCs (Wieneke *et al.,* 1999; Welt *et al.,* 2002; Mitra *et al.,* 2006).

A close correlation has been observed between the degree of inflammation and the neo-intimal thickness which suggests that inflammation caused by the arterial injury plays a central role in the formation of in-stent restenosis (Wieneke *et al.,* 1999; Welt *et al.,* 2002; Mitra *et al.,* 2006). The laceration lesions are invaded by SMCs with mainly a synthetic phenotype. These cells produce extracellular matrix components such as collagen, elastin and proteoglycans and make up the intimal hyperplasia tissue. This inflammatory response usually takes up to 6 month after which further luminal loss is minimal (Wieneke *et al.,* 1999; Sousa *et al.,* 2005). Rupture of the internal elastic lamina is followed by a significant intimal hyperplasia and the severity of initimal hyperplasia is increased once the laceration extends to the media, external elastic lamina and adventitia respectively (Wieneke *et al.,* 1999). *Therefore the degree of vessel injury is a major determinant of the extent of restenosis and hence one key aspect of stent*

design is to minimise the stress level in the arterial wall following stent deployment while still obtaining luminal gain and blood flow restoration.

2.2.2 Synthetic Vascular Grafts

Currently, it is possible to replace large arteries with synthetic grafts made of materials such as polyester and expanded polytetrafluoroethylene (ePTFE) (Bäckdahl *et al.,* 2007), however their use is limited to large arteries given their thrombogenicity (Sarkar *et al.,* 2007a) and their high propensity to develop intimal hyperplasia (IH) (Pomposelli *et al.,* 1998, Tarry *et al.,* 1998, Helenius *et al.,* 2006). Development of suitable grafts to substitute for small size arteries (<6 mm in diameter), such as coronary arteries, still remains a daunting challenge due to the development of intimal hyperplasia and thrombus formation (Salacinski *et al.,* 2001). Due to these challenges only 50% of synthetic grafts survive even two years (Salacinski *et al.,* 2001).

The level of intimal hyperplasia has been found to depend on the graft material (Salacinski *et al.,* 2001). It has been found that the severity of intimal hyperplasia is highest in the anastomotic sites specifically in the distal anastomosis (Salacinski *et al.,* 2001). Very similar to the intimal hyperplasia occurring in the in-stent restenosis, it is known that intimal hyperplasia in the vascular grafts involves proliferation and migration of smooth muscle cells towards the lumen of the graft and excessive production of extracellular matrix. It is believed that SMCs, ECs, inflammatory cells (i.e. thrombocytes (platelets), monocytes, macrophages and cytokines (i.e. growth factors) are involved in development of IH in vascular grafts (Mitchell 2009).

Development of IH following synthetic vascular graft implantation procedures occurs through two major mechanisms, namely (i) immune system related, and (ii) compliance mismatch related (Lemson *et al.,* 2000; Salacinski *et al.,* 2001; Mitchell 2009). In the immune system related mechanism, the foreign body response activates macrophages and platelets which release growth factors such as TGF-β and PDGF which promote formation of a SMC dominated neo-intima layer on the luminal surface of the graft. The origin of these cells can be the vascular precursor cells in the blood stream which differentiate into SMCs and also SMCs from

the adjacent artery which proliferate and migrate towards the intima in the anastomotic site (Mitchell 2009).

Compliance is a mechanical property of a tube that expresses the change in diameter with respect to luminal pressure change. A direct relationship has been found between compliance of vascular grafts and their long term patency, see Figure 2-6. The compliance related mechanism which contributes to the development of IH is driven by wall stretch and fluid flow changes. It has been shown that increases in wall cyclic stretch inhibits rat vascular SMCs proliferation and enhances apoptosis (Morrow *et al.,* 2005) and in another study by Sotoudeh *et al.,* (2002) cyclic stretch was found to increase porcine VSMC apoptosis. The fact that over-proliferation of SMCs is the main mechanism involved in IH development (Subbotin 2007) suggests a strong link between the reduction in cyclic stretch due to low compliance of the grafts and the development of IH.

On the other hand, several studies have shown the influence of compliance mismatch on hemodynamic factors. Stewart *et al.,* (2004) numerically showed that low compliance of grafts disturbs the transport and distribution of growth factors and lowers the wall shear stress particularly in the vicinity of the distal suture in a model of an end-to-end anastomosis. In another study Stewart *et al.,* (1992) experimentally showed that under pulsatile flow, low graft compliance can trap particles less than 40 μm in size near the wall at the distal anastomosis suggesting that this may contribute to the development of intimal hyperplasia. Zones of low shear stress and flow separation in the anastomotic region cause platelet adhesion and activation which release growth factors (Lemson *et al.,* 2000).

Although the immune system related IH development may be treated by pharmaceutical interventions and surface modifications (Tseng *et al.,* 1998; Schepers *et al.,* 2006) the compliance mismatch related IH seems to be the achilles' heel of most available synthetic grafts and tissue engineered scaffolds. *Therefore, it is fundamental to build new vascular grafts which can exhibit a compliance response similar to arteries.*

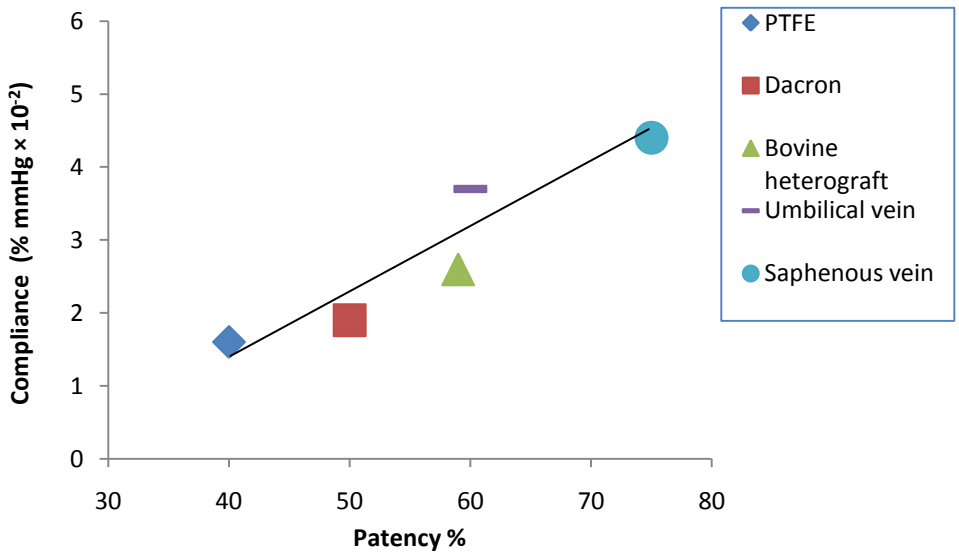

Figure 2-6: Influence of compliance on graft patency, adapted from Salacinski *et al.,* 2001.

2.2.3 Tissue Engineered Blood Vessels

The growing demand for development of substitutes for native blood vessels due to cardiovascular diseases and the limitations of the synthetic grafts have promoted tissue engineering approaches towards development of live blood vessels that can function close to that of the native vessels. A tissue engineered construct is composed of two main constituents, namely (i) scaffold and (ii) cells. Scaffolds confer mechanical integrity to the construct and provide a three dimensional structure onto which cells adhere and grow. Cells grow within the scaffold and are responsible for its biological functionality.

Since Weinberg and Bell (1986) reported *in-vitro* development of blood vessels using collagen as a scaffold and bovine aortic ECs, SMCs and adventitial fibroblasts, there have been significant improvements in the area of vascular tissue engineering. The general approach in tissue engineering is to seed cells on scaffolds and proceed by *in-vitro* culture of cells or *in-vivo* implantation. Scaffolds may be degradable where they are gradually resorbed and leave only the regenerated tissue, or alternatively they may be nondegradable and remain as a constituent of the generated tissue.

A successful tissue engineered blood vessel should be non-thrombogenic, non-immunogenic and should have similar mechanical compliance to native arteries (Nerem *et al.,* 2001;

Heyligers *et al.,* 2005). Several types of cells have been used for vascular tissue engineering including mature vascular cells such as SMCs and ECs, and also embryonic and adult stem cells (Isenberg *et al.,* 2006; Zhang *et al.,* 2007; Pankajakshan *et al.,* 2010). Also several different types of scaffolds have been used for engineering blood vessels including nature protein scaffolds, synthetic polymer scaffolds, decellularized vessels and hybrid scaffolds.

Natural proteins such as collagen, elastin and fibrin are extremely favourable given that they are highly biocompatible and create a perfect matrix for vascular cell attachment and growth. As a result collagen gels have been extensively used to engineer arterial constructs. However collagen gels suffer from lack of mechanical strength to withstand arterial blood pressure and consequently various techniques such as glycation, reinforcement with degradable and non-degradable meshes and sleeves, and electro-spinning have been used to strengthen collagen gel based scaffolds (Seliktar *et al.,* 2000; Berglund *et al.,* 2003; Isenberg *et al.,* 2003; Berglund *et al.,* 2004).

Elastin is another dominant extracellular matrix (ECM) protein which confers elasticity and recoiling to the blood vessels, however, its synthesis in most available scaffolds has proven very poor. This limitation has motivated the use of purified elastin as scaffolds, however, purified elastin scaffolds do not provide sufficient mechanical strength to be used as conduits in the arterial system (Hinds *et al.,* 2006). Therefore several methods such as using allogenic tissue support and incorporation of soluble elastin onto other types of scaffolds have been used (Pankajakshan *et al.,* 2010).

Another natural protein scaffold which has recently gained significant attention is fibrin. Cells have shown higher elastin and collagen synthesis in fibrin gels compared to collagen gel scaffolds (Long *et al.,* 2003; Pankajakshan *et al.,* 2010). Mature crosslinked fibin is relatively nonthrombogenic and nonreactive to platelets compared to other surfaces (Pankajakshan *et al.,* 2010). Albeit, similar to most other nature protein scaffolds one major limitation of fibrin is its low mechanical strength.

In addition several synthetic polymers have been used as scaffolds for arterial tissue engineering. Some of the important advantages of the synthetic polymers include their availability, low price and reproducibility. Polyglycolic acid (PGA) is widely used in vascular tissue engineering and was used by Niklason *et al.,* (1999) to produce an autologous graft which was later implanted into the arterial system. A poly(caprolactone)-poly(lactic acid), PCL-PLA, copolymer tube reinforced with woven PGA was successfully used to reconstruct the peripheral pulmonary artery in a 4-year-old girl (Shin'oka *et al.,* 2001) and later in twenty–three additional cases (Shin'oka *et al.,* 2005). Poly(L-lactic acid) PLLA (Mooney *et al.,* 1996), Poly (D,L-Lactic-co-Glycolic acid) PLGA (Mooney *et al.,* 1996), poly (4-hydroxybutyrate acid) (Opitz *et al.,* 2004), and co-polymer of PGA and polyhydroxyalkanoate (PHA) (Shum-Tim *et al.,* 1999) have been used as vascular scaffolds in the form of gels or electro-spun matrices. However one important limitation of their use is the cellular toxicity of their breakdown products which can cause adverse effects (Zhang *et al.,* 2007). In addition, in order to maintain their mechanical strength the rate of their resorption and the rate of tissue regeneration by cells should be equal which is a very challenging problem.

Decellularized vessels have also been extensively used as tissue engineering scaffolds and have shown good biocompatibility and have similar mechanical properties to that of native arteries. Decellularization is usually performed by detergents, enzyme inhibitors and buffers. Teebken *et al.,* (2000) successfully constructed vascular grafts by seeding human ECs and myofibroblasts on decellularized porcine aortas. However, the risk of trans-species infection transfer is a drawback and therefore the better solution would be decellularization of autologous vessels such as human autologous veins and culture of autologous cells under arterial conditions.

A novel biosynthetic biomaterial which has recently gained significant attention for vascular tissue engineering applications is Bacterial Cellulose (BC). BC is a polysaccharide produced by Acetobacter Xylinum Bacteria which exhibits high mechanical strength, high water content, high crystallinity and an ultra-fine highly pure nanofibril network similar to that of collagen

(Bäckdahl *et al.,* 2006). It is possible to fabricate BC tubes that can be used for the replacement of small to large size arteries with various dimensions (Bodin *et al.,* 2007). In addition, BC has been implanted into rats without eliciting any foreign body or inflammatory response (Helenius *et al.,* 2006) and it has been shown that the surface of BC induces the lowest thrombogenicity when compared to Dacron and ePTFE (Fink *et al.,* 2010). BC tubes have shown good mechanical strength exhibiting a burst pressure of up to 880 mmHg (Bodin *et al.,* 2007) Furthermore, BC tubes may have the potential to be used as tissue engineered blood vessel scaffolds given that SMCs grow and proliferate on them (Bäckdahl *et al.,* 2006; Bäckdahl *et al.,* 2008) and cultivation of ECs onto the lumen of BC tubes has led to development of a confluent layer of cells (Helenius *et al.,* 2006; Bodin *et al.,* 2007).

In spite of the favourable characteristics of BC for tissue engineering, in-depth investigation of the mechanical properties of BC is required to further support its clinical use as a vascular tissue engineering scaffold or graft. Specifically, the compliance response of BC tubes and their permeability should be investigated to ensure compliance matching with host arteries and suitable transport of nutrients and other vital chemicals within BC.

Two of the most important limitations which are common in the available scaffolds are their low burst pressure and compliance mismatch with host arteries. A method which has proven successful in improving these mechanical properties of the tissue engineered constructs is their *in-vitro* mechanical conditioning whereby the cell seeded scaffolds are cultured *in-vitro* and exposed to gradually increasing pulsatile flow and pressure. Several studies have shown improved extracellular matrix synthesis and mechanical properties in vascular tissue engineered constructs using this procedure (Jeong *et al.,* 2005; Stankus *et al.,* 2006; Hahn *et al.,* 2007). These observations highlight the key role of mechanics and mechanoregulation in vascular tissue engineering and necessitate in-depth mechanical characterisation of vascular scaffolds to ensure their potential for tissue engineering. In addition, the role of mechanical stimuli on remodelling and patterning of tissue engineered constructs has long been proven. For example, it is known that application of cyclic strain to VSMCs regulates their proliferation,

apoptosis, phenotype and orientation (Nikolovski *et al.,* 2003; Liu *et al.,* 2008; Colombo 2009). *Given that tissue level loads translate into mechanical stimuli for adherent cells through a scaffold, it is crucial to devise a suitable in-vitro mechanical stimulation regime and also to optimise the mechanical properties of vascular scaffolds in order to provide cells with optimal mechanical signals which enhance tissue regeneration and remodelling.*

2.3 Computational Modelling in Vascular Device Technology

As discussed in the previous section, mechanical factors significantly contribute to the performance of stents and vascular grafts. High stresses can cause injury to the arterial wall following stent deployment and the challenging issue of compliance and mechanoregulation in vascular grafts and tissue engineered blood vessels are important aspects of their design. Computational models have gained significant attention in the recent years to address the challenges involved in vascular device technology. Therefore this thesis is mainly focused on development of computational models which can address the aforementioned challenges with stents and vascular grafts. However, the most important building block required for the construction of such models is a thorough understanding of arterial biomechanics and development of precise constitutive models for arteries. Therefore this section starts with a review of arterial biomechanics and proceeds with a review of finite element (FE) modelling and mechanobiological modelling of vascular devices.

2.3.1 Arterial Biomechanics

A distinctive mechanical response of arterial tissues in a simple tensile test is their initial linear response with relatively large extension at low loads followed by stiffening at higher extensions, see Figure 2-7. This response is related to the distribution and configuration of collagen fibres which are initially wavy and in a crimped configuration. In the initial linear region of the force-extension curve of arterial tissue the load is mainly borne by elastin fibres. As the tissue is further stretched, collagen fibres straighten, reach their natural length and become more aligned with the direction of tension. Thereby, they resist further extension with their increased stiffness; a response which corresponds to the steeper region of the force-extension curve. This was well demonstrated by Roach and Burton (1959) by selectively digesting collagen and elastin from arterial samples and performing uniaxial extension tests on them. As can be seen in Figure 2-8, when trypsin was used to remove elastin, the remaining tissue demonstrated the mechanical response of collagen. Alternatively, when formic acid digestion was used, the remaining tissue demonstrated the mechanical response of elastin

fibres. In addition, the arterial wall matrix contains proteoglycans which are also mechanically relevant as it has been shown that their removal increases arterial wall stiffness (Pedrizzetti *et al.,*2003).

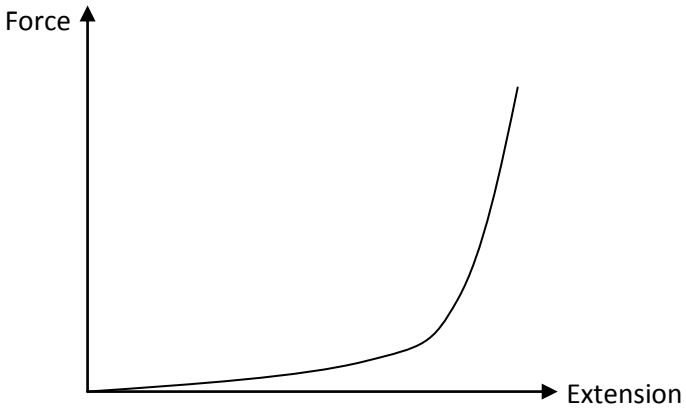

Figure 2-7: Characteristic J-shaped uniaxial tensile test curve of arterial tissues

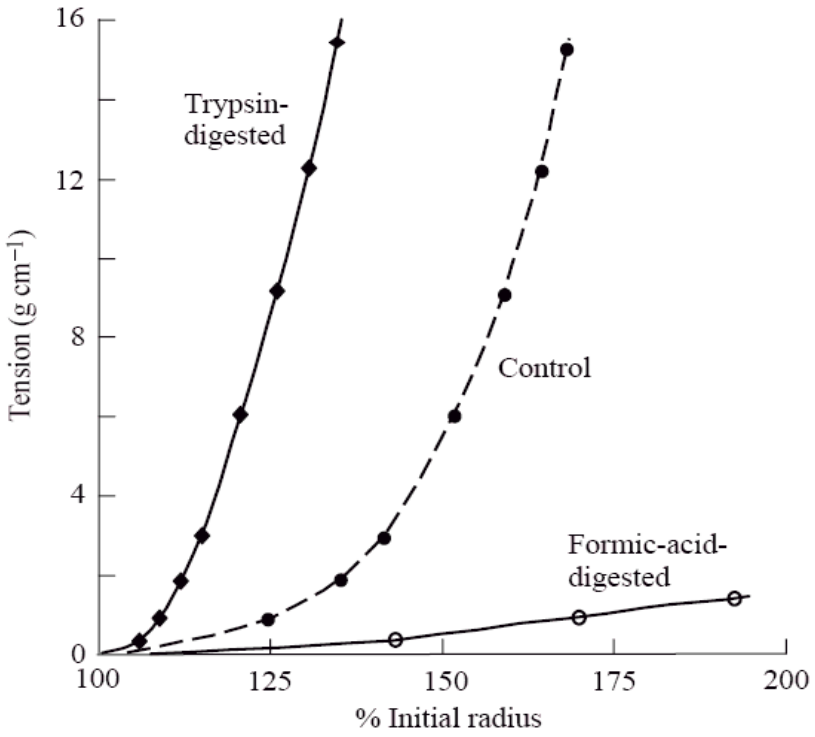

Figure 2-8: How elastin and collagen fibres affect arterial stress-strain response. Trypsin selectively digests elastin and formic acid selectively digests collagen, taken from Roach and Burton 1957.

The force-extension response of arterial tissue due to their sophisticated composite structure prevents any instability in the structure of arteries. The significance of this response is better explained by comparison with a rubber tube. The law of Laplace: T=PR, can be used to explain the inflation behaviour of thin cylinders, where T is the circumferential tension, P is the pressure and R is the internal radius, (Shadwick 1999). The nonlinear elastic behaviour of an artery and a rubber tube can be represented as a plot of T verses R. If Laplace relationships are plotted as straight lines for different pressures, the lines of each pressure intersect with the arterial response curve only at one point. In contrast in the case of the rubber tube there are two intersection points with the curve at pressure P_2, see Figure 2-9. This demonstrates the instability of the rubber tube at pressure P_2 which can cause irregular expansion of the tube at this pressure characterised by aneurysm like swellings at some locations. One can imagine the catastrophic consequences if such instability were to occur in an artery or a vascular graft; with possible aneurysm formation and consequent rupture.

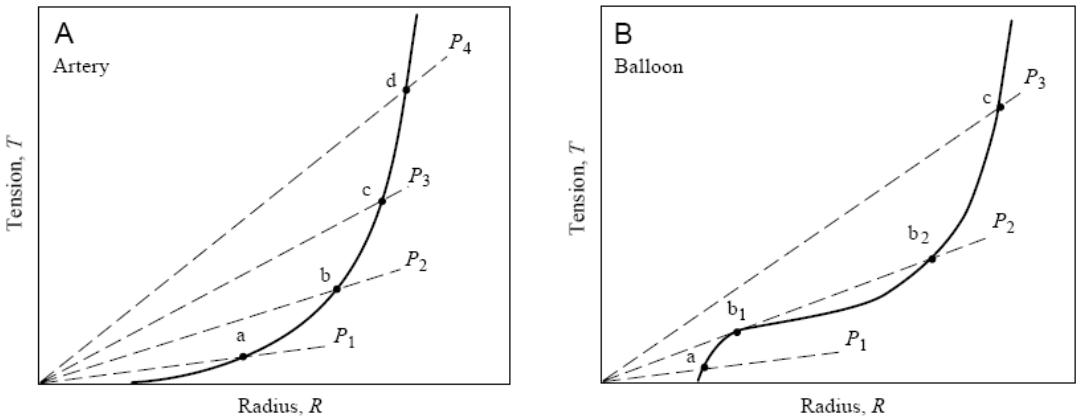

Figure 2-9: Comparison between radius-tension response of a rubber tube with arteries explaining how the structure of arteries prevents mechanical instability, taken from Shadwick 1999.

2.3.1.1 Constitutive Modelling of Arterial Tissues:

From a biomechanical point of view, mechanical characterisation of arteries requires development of their constitutive equations which can only be determined by experiments. The simplest experiments that can be performed on an artery is a uniaxial extension test whereby the stress-strain relationship of the artery under uniaxial loading is deduced. As discussed earlier, the stress-stiffening response of arteries deviates from Hooke's law given that Hooke's law only holds in the case of linearly elastic materials. In addition once arteries are subject to cyclicly varying strain, the stress-strain curves show a hysteresis loop with each cycle. This hysteresis loop diminishes with succeeding cycles and tends towards a steady state after a number of cycles, see Figure 2-10. In the context of mechanical characterisation and constitutive model development usually only the steady state stress-strain response is used and the first number of cycles which are applied to obtain steady state are called *preconditioning cycles* (Humphrey *et al.,* 2004).

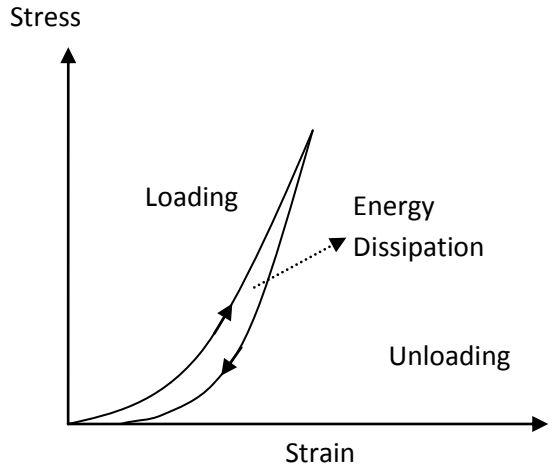

Figure 2-10: Noncoincident loading and unloading, evidence of viscous dissipation, adapted from Humphrey *et al.,* 2004.

One important property of arterial tissues is their high water content which renders the arterial tissue incompressible. Water itself is incompressible and the arterial wall is composed of approximately 70% water. Incompressibility is an important assumption which is used in the development of constitutive models for arteries or any other biomaterial with high water content such as hydrogels. It states that conservation of volume should hold, thereby the product of the principal stretches in a sample should be equal to one.

$$\lambda_1\lambda_2\lambda_3=1 \qquad \textbf{Equation 2-1}$$

Mooney (1940) for the first time developed a theory for the study of the mechanics of rubber-like materials. This work was followed by a number of studies such as the study by Treloar (1944) and Rivlin (1948a, 1948b) which shaped the seminal works on the theory of hyperelasticty for rubber-like materials.

Later, Tickner and sacks (1967) presented a theory for the study of arterial elasticity for the first time which was built on the approach developed earlier for rubber-like materials. The theory assumed a strain energy density function, *W*, for the material as a function of principal stretches ($\lambda_1, \lambda_2, \lambda_3$) or the stretch invariants (I_1, I_2, I_3). Usually rubberlike materials which can undergo large elastic deformations without permanent deformation are called hyperelastic materials. Strain energy density functions developed for hyperelastic materials are called hyperelastic constitutive equations. Although arteries are not perfectly hyperelastic materials given that they exhibit some hysteresis under cyclical loads, Fung reported in late 1960s that the behaviour of soft tissue tends not to depend strongly on the strain rate and hyperelastic models could model their behaviour reasonably well if the loading and unloading were treated separately as elastic. This concept was termed *pseudo-elasticity* and was first suggested by Fung given that the theory of viscoelasticity was much more difficult to implement than the theory of elasticity (Fung 1990).

For a hyperelastic material:

$$S_{ij} = \frac{\partial W}{\partial E_{ij}} = 2\frac{\partial W}{\partial C_{ij}} \qquad \textbf{Equation 2-2}$$

where:

S_{ij}= components of the second Piola-Kirchhoff stress tensor

E_{ij}= components of the Green-Lagranian strain tensor

C_{ij} =components of the right Cauchy-Green deformation tensor

Several forms of strain energy functions have been proposed to fit experimental stress-strain data obtained for different materials given that each function is suitable for certain material behaviours. To describe the stress-strain relationship of arteries Fung (1990) employed an exponential strain energy function of the form:

$$W = \frac{1}{2}c(e^{Q} - 1); \qquad \textbf{Equation 2-3}$$

$$Q = c_1E_{11}^2 + c_2E_{22}^2 + c_3E_{33}^2$$

$$+2c_4E_{11}E_{22} + 2c_5E_{22}E_{33} + 2c_6E_{33}E_{44}$$

$$+c_7(E_{12}+E_{21}) + c_8(E_{23}+E_{32}) + c_9(E_{13}+E_{31})$$

where c and $c_1 \_ c_9$ are material parameters obtained by fitting to the experimental stress-strain data and $E_{11} \_ E_{33}$ are the components of the Green-Lagrangian strain tensor. Fung (1990) showed that this strain energy density function could be used to obtain reasonable fits to data for various soft tissues including myocardium, arteries and skin.

In addition polynomial forms of the strain energy functions have been widely used to model soft tissues and biomaterials. An example of a widely used polynomial strain energy function for arterial tissue is the Mooney-Rivlin model, proposed by Mooney (1940) with its general form shown below:

$$W = \sum_{i,j}^{\infty} c_{ij}\,(I_1 - 3)^m\,(I_2 - 3)^n\,, a_{00} = 0 \qquad \textbf{Equation 2-4}$$

where c_{ij} are material constants, and $I_1\ and\ I_2$ are stretch invariants for the material as follows:

$$I_1 = \lambda_1^2 + \lambda_2^2 + \lambda_3^2$$

$$I_2 = \lambda_1^2\lambda_2^2 + \lambda_1^2\lambda_3^2 + \lambda_2^2\lambda_3^2 \qquad \textbf{Equations 2-5}$$

$$I_3 = \lambda_1^2\lambda_2^2\lambda_3^2$$

and $I_3 = 1$ for incompressible materials. In addition many polynomial strain energy density functions have been proposed and used to model hyperelastic materials which are formulated based on the principal stretches. The most widely used of such functions for arterial tissue, given its good capability to fit to different materials stress-strain data, is the model proposed by Ogden (1984) in the following form:

$$W = \sum_{p=1}^{N} \frac{2\mu_p}{\alpha_p}(\lambda_1^{\alpha_p} + \lambda_2^{\alpha_p} + \lambda_3^{\alpha_p} - 3) \qquad \textbf{Equation 2-6}$$

where μ_p and α_p are material constants. All the models discussed above are phenomenological models, meaning that they are just mathematical equations that can be derived by fitting to the experimental stress-strain data of the materials. Although the Ogden model is highly capable of fitting to stress-strain data obtained from soft tissue and rubber like materials, it is very important to determine the hyperelastic constants with high precision since the model response is highly sensitive to the constants and small changes in the number of significant digits may dramatically alter the model behaviour (Ogden *et al.,* 2004).

An alternative approach in soft tissue biomechanics is the mechanistic models which are informed by the structure of the material and study the tissue as a heterogeneous material. In this sense the parameters used in these models are not merely curve fitting constants and have physiological meaning. One prominent example of such a model is the model proposed by Holzapfel (2000b) which treats the arterial wall as a heterogonous material composed of a homogeneous ground matrix and two families of collagen fibres dispersed in the matrix at a specific angle and symmetric with respect to one another. Given that the model considers the presence of two families of collagen fibres, the model can capture the anisotropy of the arteries, see Figure 2-11.

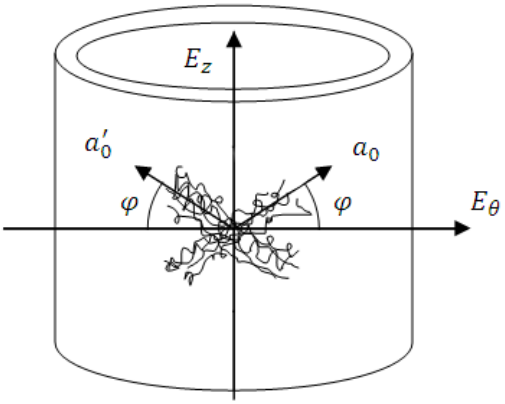

Figure 2-11: A schematic of the collagen fibre orientation in the constitutive model developed by Holzapfel *et al.,* (2000b) depicting the two families of collagen fibres and their helical orientation in the artery.

Holzapfel (2000b) accounted for the presence of the fibres in the ground matrix using a decoupled formulation for the isochoric (non-volume changing) strain energy function composed of two terms as follows:

$$W = W_{iso}(I_1) + W_{aniso}(I_4, I_6) \qquad \textbf{Equations 2-7}$$

$$I_4 = a_0 . C . a_0$$

$$I_6 = a_0' . C . a_0'$$

where a_0 and a_0' are the directions of collagen fibres present in the artery and *C* is the right Cauchy-Green strain tensor. Holzapfel then defined the strain energy function of the ground matrix using a simple neo-Hookean formulation and the strain energy stored in the collagen fibres using an exponential formulation as follows:

$$W_{iso}(I_1) = \frac{1}{2}\mu(I_1 - 3) \qquad \textbf{Equations 2-8}$$

$$W_{aniso}(I_4, I_6) = \frac{k_1}{2k_2} \sum_{i=4,6} \{\exp\left[k_2\,(I_i - 1)^2\right] - 1\}$$

where $\mu > 0, k_1 > 0\ and\ k_2 > 0$ are material constants.

In order to apply the aforementioned models or any similar ones for arterial tissue or similar biomaterials such as a vascular scaffold or graft (which ideally should have artery-like hyperelastic properties), the material constants have to be determined based on experimental tests. A strain energy density function should then be chosen which can best fit the stress-strain data of the material and satisfy the convexity condition of the strain energy function to assure stability of the model.

2.3.2 Finite element modelling of vascular devices

As discussed previously, reducing the risk of injury in the arterial wall is a key aspect of stent design. Computational models of stent deployment, such as FE models, are excellent tools for optimisation of stent designs and can be used along with experimental studies to improve the mechanical performance of stents by reducing the injury level in the arterial wall. In addition to being cost effective, computational models often offer the only solution to address some of the important challenges influencing stent design such as the estimation of stresses induced in the vessel wall and therefore the degree of vascular injury.

FE models of stent expansion enable quantification of the stress-strain field in the stents and also in the vessel wall following stent deployment and therefore provide insights into the various aspects of stent design that may reduce the risk of arterial injury.

One important advantage of computational models of stent deployment over *in-vivo* studies is that they enable the influence of the mechanical parameters of interest to be studied in isolation, while due to the several complex and intertwined biological, chemical and mechanical factors involved *in-vivo*, it is often difficult to associate the outcome of an *in-vivo* trial to one specific mechanical factor and further proceed to rectify that by optimising the stent design. A good example of this is the influence of stent strut thickness on in-stent restenosis. In recent years, several clinical trials have identified stent strut thickness as an independent predictor of restenosis (Kastrati *et al.,* 2001; Briguori *et al.,* 2002; Pache *et al.,* 2003). A clear conclusion from the many clinical studies on stent strut thickness is that stents with thinner struts have a lower restenosis rate, consequently, most of the current generation

of stents are produced with thinner struts using high strength materials such as cobalt–chromium alloys (Morton *et al.,* 2004). The ISAR-STEREO clinical trial focussed on the influence of stent strut thickness and compared the restenosis outcome for two stents with the same design but different strut thickness (Kastrati *et al.,* 2001). Although the study highlights the importance of stent strut thickness, it does not clearly elucidate the role and significance of the mechanisms by which stent strut thickness could lead to the higher restenosis rate.

From a mechanical perspective the effect of stent strut thickness can be twofold: (i) from a solid mechanical viewpoint where stresses induced in the artery are concerned, and (ii) from a hemodynamic viewpoint where blood flow perturbations due to strut thickness are concerned. *In-vitro* studies may not address each of these separate factors in isolation. Also several biological factors are involved *in-vivo*, such as the higher metal surface exposed to blood flow in thicker strut stents to which platelets can adhere and produce mitogenic growth factors, which make studying the role of a mechanism of interest extremely difficult. In contrast, computational models enable each different parameter involved in such a complex process to be studied in isolation. For instance, Duraiswamy *et al.,* (2007) studied the influence of stent strut thickness from a hemodynamics perspective and quantitatively showed that thicker stent struts lead to significantly larger recirculation zones and altered shear stress pattern in the vicinity of struts which can contribute to restenosis. In this context, FE simulations of stent deployment procedures can also be used to clarify the influence of stent strut thickness on the vessel wall stresses and provide enlightening guidelines for stent design.

Stent strut thickness is just one of the many factors involved in the stent design and the use of finite element method (FEM) is not limited to this factor. FEM can be utilised to study a wide range of design parameters in order to reduce arterial injury. Several studies have investigated the mechanical response of stents using the FEM and have suggested different strategies for their simulation (Lee *et al.,* 1992; Rogers *et al.,* 1999; Auricchio *et al.,* 2001; Prendergast *et al.,* 2003; Holzapfel *et al.,* 2005b; Lally *et al.,* 2005; Migliavacca *et al.,* 2005, 2007; Wang *et al.,* 2006; Gijsen *et al.,* 2008). Given the difficulties involved in construction of the model geometry

and the complex contact problem involved in the interaction of a balloon, stent and artery, many simplified methods have been used to model the complex mechanics of stent deployment. Balloons used for stent deployment are initially in a folded configuration. As the balloon unfolds it appears highly compliant however as its unfolded shape is reached the balloon becomes highly noncompliant. This complex procedure of balloon unfolding is difficult and very computationally expensive to model.

Four main strategies have been used in the literature for numerically modelling balloon expansion of stents which include; (i) direct application of a uniform pressure to the stent luminal surface (Dumoulin and Cochelin 2000; Migliavacca *et al.,* 2005; De Beule *et al.,* 2006; Early *et al.,* 2008), (ii) a rigid cylinder expanded by application of radial displacement (Hall and Kasper 2006; Takashima *et al.,* 2007; Wu *et al.,* 2007), (iii) stent deployment using a folded balloon model (De Beule *et al.,* 2008; Gervaso *et al.,* 2008) and (iiii) pressurisation of simple elastic cylinders with hyperelastic material properties neglecting the balloon folds (Ju *et al.,* 2008; Kiousis *et al.,* 2009).

Gervaso *et al.,* (2008) compared the first three strategies and concluded that a folded balloon model is necessary for accurate estimation of mechanical stresses. In spite of this, the computational costs and the effort involved in modelling folded balloons has urged many researchers to resort to alternative strategies which disregard the balloon model. In this context, Early *et al.,* (2008) proposed a method of stent expansion by direct application of a uniform pressure on the inner stent surface in conjunction with special function elements connected to the stent nodes which restrained stent expansion as the desired expansion diameter was achieved. However, no comparison with stent deployment using folded balloons was presented to fully support the use of this method and to elucidate its limitations. Although such a modelling strategy can significantly reduce the computation time and the effort involved in construction of a balloon model, the conditions under which it can yield accurate results is not well studied and the limitations of this method remain to be investigated.

On the other hand in the context of vascular grafts, FE modelling can help ensure compliance matching of vascular grafts with different host arteries. Given the availability of constitutive models for most host arteries in the literature, constitutive models for graft materials can be established by mechanical characterisation tests and implemented in FE models to optimise design variables such as material properties and geometrical parameters in order to ensure compliance matching of the grafts with different host arteries, reduce the risk of failure in the graft and also minimise stresses and therefore injury in the host arteries (Steinman 2003).

2.3.3 Mechanobiological modelling of vascular devices

The daunting complexities of biomechanical systems have motivated tremendous efforts towards developing novel computational models for predictive purposes and also to provide better understanding about these systems.

One important potential of computational models is that they enable the hypotheses about complex biological systems to be corroborated or refuted and hence constantly add to our knowledge about them (Nigg & Herzog 2001; Viceconti 2010). Computational models of the biomechanics of the skeletal system and cardiovascular system have significantly advanced in the recent years and have constantly added to our knowledge of the role of biomechanics ranging from progression of pathological conditions such as skeletal deformities (Subbaraj 1989), development of aneurysms (Watton *et al.,* 2009), fracture and wound healing (Geris *et al.,* 2010a; Geris *et al.,* 2010b), and stent implantations and its prognosis (Caiazzo *et al.,* 2009; Zahedmanesh *et al.,* 2009; Boyle *et al.,* 2010; Zahedmanesh *et al.,* 2010).

One important complexity which is specific to biomechanical systems is their regenerative ability to adapt their structure and properties in order to maintain homeostasis following any mechanical or biological perturbations. In many cases, however, this regenerative response of the biomechanical systems may derail into a maladaptive response. In-stent Restenosis following stent deployment (Hoffman *et al.,* 2000) and development of intimal hyperplasia (IH) following implantation of small calibre vascular grafts (Lemson *et al.,* 2000; Salacinski *et al.,* 2001; Zilla *et al.,* 2007) are examples of such maladaptive responses. In this context the global

response of the biological system which emerges at the tissue level as excessive luminal ingrowth stems from individual cell behaviour and interaction among cells. Cellular behaviours such as differentiation, proliferation, migration, protein and chemokine synthesis and cell death are influenced by the environmental factors such as extracellular matrix, chemicals, and forces and add up to emerge as complex responses at the tissue level. This intrinsic multi-scale behaviour of biological systems necessitates a multi scale modelling approach.

Two main approaches have been taken for modelling the response of multi cellular biological systems, (i) the continuum approach and (ii) the cell-based Approach (Byrne *et al.,* 2009). The continuum approach can be used to model the response of biological systems at all levels from cells to tissue. Although key cell responses such as cell density evolution can be modelled using partial differential equations (PDEs), one important limitation of this method is that PDEs may not capture the discrete nature of multi cellular biological systems consisting of individual cells and can become cumbersome when solving complex processes involving several variables (Hwang *et al.,* 2009). The other method used for modelling the response of multi cellular biological systems is the discrete approach. The global behaviour of a biological system results from discrete phenomena occurring at the cellular level, hence biological systems may be better modelled using discrete methods.

Two main discrete methods have been used for modelling the multi cellular biological systems, namely (i) Cellular Automata (CA) and (ii) Agent Based Models (ABM). Both methods can be defined as rule based models that take a bottom up approach. Each individual cell is modelled explicitly based on the rules of behaviour which are defined for it and the global system behaviour emerges through the local interactions among the cells based on the defined rules of behaviour at the cell level. Although the differences between (CA) and (ABM) are marginal, the main difference is that a lattice point needs to be defined for (CA) while (ABM) can be lattice free, meaning that cells can be at any location in the computational domain. This location is usually determined by solving either kinematic or dynamic equations of motion for each individual cell. Hence (ABM) can yield more realistic results given that no restriction is

imposed on the location of the cells in comparison to (CA) where the cells can only move through certain predefined lattice points. A hybrid modelling approach may be also adopted by combining both continuum and discrete methods (Gerlee *et al.,* 2008; Guo *et al.,* 2008).

With the emergence of tissue engineering as a promising technique in regenerative medicine, there is a genuine need for robust mechanobiological models for analysis of tissue engineered constructs. Tissue engineers need to consider a wide range of variables ranging from the type of scaffold material and its mechanical and morphological properties such as elasticity, porosity and permeability, to the best choice of cells and the optimum bioreactor parameters, such as the loading regime, to obtain a functional tissue engineered construct. In the context of vascular tissue engineering, and specifically in the case of low calibre vessels, complexities arise mainly due to development of IH where vascular smooth muscle cells (VSMCs) over-proliferate into the lumen of the construct and ultimately occlude the blood flow.

Optimally a vascular scaffold should allow the vascular cells to populate the scaffold and remodel it into a tissue similar to the artery by producing extra-cellular matrix components; however, it should prevent over-proliferation of cells towards the lumen. IH in vascular grafts and tissue engineered blood vessels (TEBVs) occurs due to an imbalance between inhibitory and proliferative mechanisms which control the growth of VSMCs. Scaffold properties such as porosity and permeability are vital to ensure nutrient transport and waste removal in a TEBV. On the other hand, the elasticity of the construct, usually measured as compliance in the context of vascular grafts/scaffolds, plays a pivotal role in vascular scaffold remodelling as cyclic strain has a significant anti-proliferative and pro-apoptotic influence on VSMCs (Colombo 2009). In addition, fluid flow in a scaffold is influenced by cyclic strain (Buijs *et al.,* 2009) and is therefore also dependant on the elasticity of the scaffold when it is subject to pulsatile pressure in the arterial system. The importance of the role of compliance is further supported by the outcome of vascular graft implantations which suggest a direct relation between the compliance of vascular grafts and their long term patency (Salacinski *et al.,* 2001).

Another key factor in regulating the proliferative response of VSMCs, is a functional endothelium. In the absence of a functional endothelium, inflammatory cells such as macrophages and platelets are recruited to the lumen of the scaffold/graft and secrete mitogenic and chemotactic factors such as Platelet Derived Growth Factor (PDGF) which have a proliferative influence on VSMCs (Lemson *et al.,* 2000). However, to date most available vascular grafts/scaffolds have shown a very poor endothelialisation rate in the human body (Zilla *et al.,* 2007). Given the central role of VSMCs in success or failure of TEBVs, it is necessary to better understand the mechanobiological mechanisms which regulate VSMC growth dynamics in vascular tissue engineered constructs and mechanobiological models can be utilized for this purpose.

Several mechanobiogical models have been developed using the continuum approach (Coletti *et al.,* 2006; Andreykiv *et al.,* 2008; Issaksson *et al.,* 2008) and also the cellular automata approach (Byrne *et al.,* 2007; Stops *et al.,* 2010) combined with robust numerical methods such as the FEM. However, in spite of the significant role of mechanoregulation in vascular tissue engineering (Seliktar *et al.,* 2003; Jeong *et al.,* 2005; Hahn *et al.,* 2007; Xu *et al.,* 2008) and the central role of VSMCs in this context, mechanobiological models of VSMC tissue engineered constructs are scarce and the available mechanobiological models are mainly focused on skeletal tissue engineering and fracture healing.

On the other hand, even though lattice free agent based models have been extensively used in modelling multicellular biological systems (Walker *et al.,* 2004; Baily *et al.,* 2007; Thorne *et al.,* 2007; Merks *et al.,* 2008; Li *et al.,* 2008; Pappalardo *et al.,* 2009), these models are merely biological and mechanoregulation is rarely included to these studies. The few mechanobiological models which have used lattice free agent based models have resorted to calculation of the mechanical stimuli (i.e. stress/strain) using simple analytical equations rather than using more robust numerical methods such as FEM (Peirce *et al.,* 2004; Ausk *et al.,* 2006; Geris *et al.,* 2010c). This is mainly due to the fact that lattice free agent based models are

computationally expensive and coupling them with numerical methods such as FEM is challenging.

Given that cyclic strain due to pulsatile blood pressure is the prevalent mechanical load that VSMCs are exposed to in an artery, several studies have been dedicated to the study of the influence of cyclic strain on VSMCs (Chapman *et al.,* 2000; Durante *et al.,* 2000; Morrow *et al.,* 2005; Wang *et al.,* 2006; Colombo *et al.,* 2009). It has been shown that physiological cyclic strain (less than 15% amplitude) has an anti-proliferative influence on VSMCs and also increases the apoptosis rate of VSMCs (Chapman *et al.,* 2000; Morrow *et al.,* 2005; Colombo *et al.,* 2009; Kona *et al.,* 2009).

In a recent *in-vitro* study by Colombo (2009) which was dedicated to the study of the role of cyclic strain on VSMCs, bovine aortic SMCs were cultured under cyclic strain with varying mean and amplitude. The study concluded that physiological cyclic strain has an anti-proliferative influence on VSMCs and that the relationship between cyclic strain and proliferation and apoptosis rate depends on the amplitude of the cyclic strain rather than on the mean value of the cyclic strain. The consistency of these findings on human VSMCS was also verified by conducting the same experiments on human Iliac SMCs (Colombo 2009). Conversely, pathological values of cyclic strain (>15%) have been found to play a conflicting role and increase proliferation in VSMCs (Numaguchi *et al.,* 1999; Kozai *et al.,* 2005; Halka *et al.,* 2008; Kona *et al.,* 2009).

In addition, physiological cyclic strain has been shown to upregulate synthesis of ECM products such as collagen and Elastin (Kona *et al.,* 2009). On the other hand pore fluid velocity within a tissue engineered construct can significantly improve nutrient delivery and waste removal which in turn increases the proliferation rate and reduces cell death. Cartmell *et al.,* (2003) studied the effect of medium perfusion rate on cell growth and ECM synthesis within human trabecular bone scaffolds seeded with osteoblast-like cells and showed a significant increase in DNA content in perfused samples compared to statically grown samples. In another study by Volkmer *et al.,* (2008) cell death occured in the central region of a statically cultured bone

matrix scaffolds following 5 days culture, whilst in contrast, perfusion bioreactors successfully prevented cell death in the scaffold. Culture of VSMCs on vascular scaffolds have also resulted in a higher number of VSMCs and improved mechanical properties when cultured in perfusion bioreactors compared to the static culture (Jeong *et al.,* 2005; Stankus *et al.,* 2006; Hahn *et al.,* 2007). Therefore from a mechanobiological modelling stand point, cyclic strain and pore fluid flow are two key mechanical regulators of VSMC growth in a vascular tissue engineered construct which have to be given specific consideration.

2.4 Summary

Several biomechanical factors are involved in the design and application of vascular devices. In this context, stents and vascular grafts need to be given specific attention as they are the two key devices widely used in the treatment of cardiovascular disease. In order to improve the performance and outcome of stents and vascular grafts, however, the following crucial biomechanical challenges remain to be more fully understood and quantifiable:

- Arterial Injury due to high stresses conferred to the arterial wall following stent deployment which is considered to be the main cause of in-stent restenosis.
- Mechanical compliance mismatch of vascular grafts with that of host arteries which leads to development of intimal hyperplasia and consequent loss of patency specifically in low calibre arteries (<6mm diameter).
- The growth and remodelling of vascular tissue engineered blood vessels which is highly dependent on mechanical factors such as mechanical properties of the scaffold and external mechanical stimulation.

Computational modelling is a robust and efficient platform to develop new strategies and designs in order to overcome the aforementioned challenges. Computational modelling of stent deployment is the only possible method to precisely quantify the stresses induced in the arterial wall and therefore the risk of arterial injury due to stent deployment. As a result, FE models of stent deployment are widely used for design optimisation and as a preclinical testing platform to improve the performance of stents by reducing the risk of injury to the arterial wall. However, FE simulations of stent deployment are computationally expensive and it is therefore necessary to investigate the different modelling strategies to determine an optimal strategy which offers the lowest computational cost combined with high accuracy. In Chapter 3, different modelling strategies are investigated and Chapter 4 proceeds to showcase the application of the optimal modelling strategy determined in Chapter 3 to investigate the influence of stent strut thickness on the arterial wall stress levels.

On the other hand, in the case of vascular grafts, FE models can be used to ensure compliance matching of vascular grafts with different host arteries. Given the availability of constitutive models for most host arteries in the literature, constitutive models for graft materials can be established by mechanical characterisation tests and implemented in patient specific FE models to optimise design variables such as material properties and geometrical parameters in order to build vascular grafts custom-tailored to match any specific artery and patient. Such a procedure will minimise intimal hyperplasia and will prevent graft rupture and arterial injury due to high anastomotic stresses. Chapter 5 is therefore used to showcase how mechanical characterisation experiments can be conducted in order to develop constitutive models that can be used in FE modelling of vascular grafts to predict their mechanical behaviour *in-situ*. In this context, bacterial cellulose as a novel biomaterial was deemed to be a suitable candidate and therefore the method was specifically applied to bacterial cellulose tubes.

Also computational models can be used in vascular tissue engineering to decipher the important role that mechanical factors i.e. scaffold mechanical properties and external mechanical stimulation play in regulating the growth dynamics of VSMCs and remodelling of the scaffolds. Such a model can be used as a tool to optimise the mechanical properties of vascular scaffolds and pinpoint an optimal *in-vitro* mechanical stimulation regime that would enhance remodelling and prevent intimal hyperplasia. However to-date, no such computational study dedicated to development of a mechanobiological model for vascular tissue engineering applications exists. In Chapter 6, therefore, a novel mechanobiological modelling framework is presented that addresses this challenge.

Chapter 3

Simulation of a balloon expandable stent in a realistic coronary artery; Determination of the optimum modelling strategy

Computational models of stent deployment in arteries have been widely used to shed light on various aspects of stent design and optimisation. In this context, modelling of balloon expandable stents has proved challenging due to the complex mechanics of balloon-stent interaction and the difficulties involved in creating folded balloon geometries. In this study, a method to create a folded balloon model is presented and utilised to numerically model the accurate deployment of a stent in a realistic geometry of an atherosclerotic human coronary artery. Stent deployment is, however, commonly modelled by applying an increasing pressure to the stent, thereby neglecting the balloon. This method is compared to the realistic balloon expansion simulation to fully elucidate the limitations of this procedure. An alternative balloon simulation procedure is also presented to overcome many of the limitations of the applied pressure approach by using elements which restrain the stent as the desired diameter is achieved.

3.1 Materials and methods

A FE model of a patient specific atherosclerotic coronary artery and the ACS Multi-Link RX DUET stent was constructed and the stent was expanded within the artery using three different strategies as defined by the following case studies:

i) A uniformly increasing pressure, to a maximum value of 16 atm, was directly applied to the inner stent surface.

ii) A uniformly increasing pressure was directly applied to the inner stent surface to achieve an inner stent diameter equal to the fully expanded balloon (3.5mm) in conjunction with connector elements which restrained the stent expansion beyond this diameter. One end of these connector elements was connected to the

nodes on the stent outer surface and the other end was connected to the ground (i.e. the initial coordinates of the same node prior to deformation).

iii) Expansion of the stent using a realistic three-fold balloon inflated to a diameter of 3.5 mm using a maximum pressure of 16 atm.

To generate the simulations pertaining to each case study, the FE models require a number of inputs: namely the geometry of the stent, the atherosclerotic coronary artery, and the three-fold balloon; the material properties of the stent, artery and balloon; and the appropriate application of loading and boundary conditions, as described below.

3.1.1 Model Geometry

A patient derived model of an aged atherosclerotic human coronary artery was constructed based on digitised 3D angiography images provided by the 3D imaging laboratory, Division of Cardiology, School of Medicine, University of Colorado, USA. The images were obtained using a method developed and described by Messenger et al. (2001) to obtain an accurate 3D geometry of the lumen of an atherosclerotic artery. The vessel wall dimensions were generated based on assigning a healthy arterial wall thickness of 0.5 mm at the proximal end of the vessel, upstream from the stenosed region, by offsetting the lumen contour by 0.5 mm. This outer diameter was then extrapolated across the stenosed region of the vessel to define both healthy vessel wall and atherosclerotic plaque regions. The model was subsequently meshed using ANSYS (Canonsburg, PA, USA) assigning 6 elements through the thickness of the healthy artery wall and three elements through the plaque thickness. The vessel was divided into three layers; intima, media, and adventitia. The thickness of each arterial layer was discretised by two elements and the thickness of each layer was assigned using ratios of adventitia, media and intima to the wall thickness of 0.38, 0.33, and 0.29 respectively consistent with the data reported by Holzapfel *et al.,* (2005a). Eight node linear brick, reduced integration elements with hourglass control (ABAQUS element type C3D8R) were used to mesh the atherosclerotic coronary artery. The total number of elements used to mesh the

atherosclerotic coronary artery was 29,400 which was chosen based on mesh sensitivity studies (see Appendix A-A.1). All elements were checked to ensure that no distorted elements were generated. In addition, element distortion control was used to prevent inaccuracies arising from excessive distortion of elements in the contact regions.

A full three-dimensional FE model of the stent was generated and meshed in ANSYS based on the ACS MultiLink RX Duet manufactured by Guidant/Advanced Cardiovascular Systems. The stent has an interconnected-ring design, struts with rectangular cross-sectional areas and width and thickness of 100 µm and 140 µm, respectively. The length of the stent was 15 mm consisting of seven rings in the longitudinal direction with six crowns in each ring. The stent inner radius in the crimped configuration was 0.72 mm, with a corresponding outer radius of 0.86 mm. The stent dimensions were extrapolated from the handbooks of coronary stents (Serruys *et al.,* 1998; Serruys *et al.,* 2000).

To generate the stent model, a procedure previously reported by Lally *et al.,* (2005) was adopted. The stent geometry was initially modelled in an opened-out, planar configuration utilising a Cartesian coordinate system. The volume of the stent was discretised by eight node linear brick, reduced integration elements with hourglass control (ABAQUS element type C3D8R). The model of the stent was meshed with two elements through the thickness and a total number of 30,768 elements which was opted based on mesh sensitivity studies. Finally, the nodal coordinates of the meshed model were transferred from the Cartesian coordinate system into a cylindrical coordinate system where the planar configuration was wrapped to generate the cylindrical structure of the stent.

In order to create the geometry of a three-fold crimped balloon, the geometry of a fully expanded balloon was generated in ProEngineer (Needham, MA, USA) with a diameter of 3.5 mm and was exported into ABAQUS (SIMULIA, Providence, RI, USA). The imported geometry was meshed using 4-node doubly curved shell elements with reduced integration and hourglass control, (ABAQUS element type S4R). The balloon was then deflated in an explicit simulation by application of a negative pressure of 0.01 MPa on its inner surface using general

contact and with the proximal and distal ends fully constrained. Symmetry boundary conditions were applied on the balloon nodes at every 120 degrees in the circumference using the CONSTRAINTS command in ABAQUS so as to deflate the balloon into a tri-wing configuration. Later the wings were folded circumferentially onto one another in a subsequent step by application of pressure to one side of each wing while the base of each wing was fully constrained in order to generate the three-fold crimped balloon configuration, see Figure 3-1.

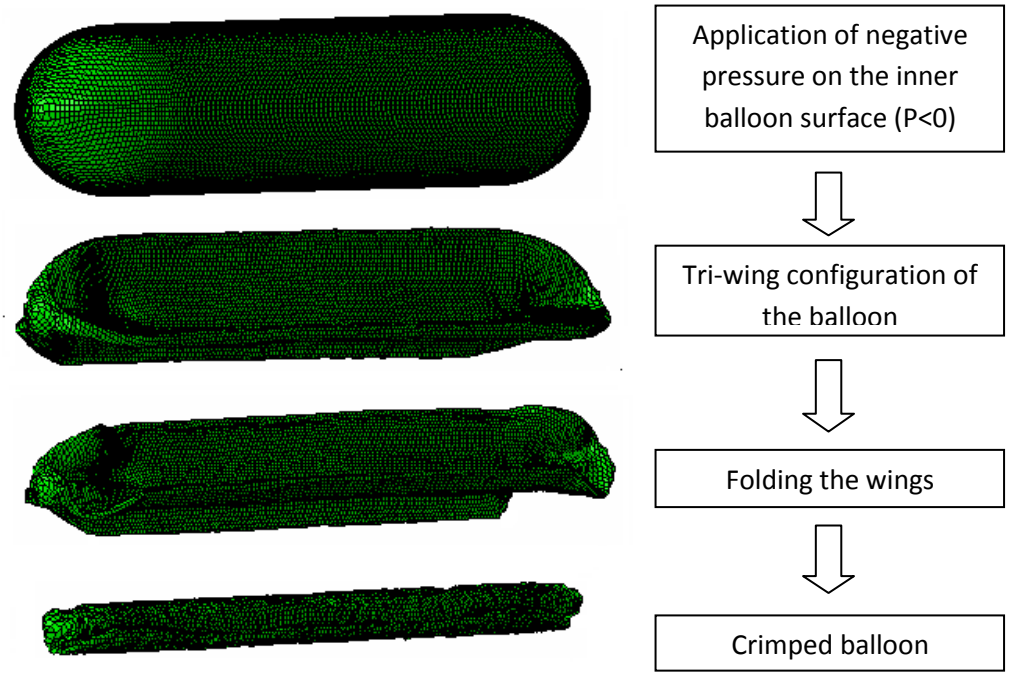

Figure 3-1: The process of creating the three-fold balloon geometry.

3.1.2 Material Properties

Layer specific human coronary arterial wall properties were assigned to the artery, consisting of the intima, media and adventitia based on the data from Holzapfel *et al.,* (2005a). Human cellular atherosclerotic intimal plaque properties were assigned to the localised plaque based on the available published data from Loree *et al.,* (1994). The material of the intima, media and adventitia and plaque were defined using Ogden hyperelastic constitutive equations (Ogden 1972):

$$W = \sum_{i=1}^{N} \frac{2\mu_i}{{\alpha_i}^2}\left(\bar{\lambda}_1^{\,\alpha_i} + \bar{\lambda}_2^{\,\alpha_i} + \bar{\lambda}_3^{\,\alpha_i} - 3\right) + \sum_{i=1}^{N} \frac{1}{D_i}(J-1)^{2i} \qquad \textbf{Equation 3-1}$$

Where $\bar{\lambda}_i$ denotes the deviatoric principal stretches, J is the elastic volume strain and μ_i, α_i and D_i are the hyperelastic constants, and *N* represents the order of the equation.

The constitutive equations were determined by fitting to the circumferential stress-strain data of human coronary artery as published in Holzapfel *et al.,* (2005a) and the tensile stress-strain data of cellular atherosclerotic plaque published in (Loree *et al.,* 1994).

A non-linear regression routine, available in ABAQUS, was used to obtain the constitutive models that best fit the experimental data. The stability of the material constitutive models was checked using the routine available in ABAQUS. The hyperelastic coefficients used for artery/plaque models are summarized in Table 1. The arterial components and atherosclerotic plaque were assumed to be nearly incompressible. This assumption was imposed by specifying a Poisson's ratio of 0.49, infinitesimal values for D_1, and zero for D_2 and D_3 in the hyperelastic constitutive equations describing the materials, see Table 3-1.

Table 3-1: Coefficients of the Ogden hyperelastic constitutive models (Zahedmanesh and Lally 2009)

Ogden hyperelastic model constants	Intima	Media	Adventitia	Plaque
μ_1 (Pa)	-7'037'592.77	-1'231'144.96	-1'276'307.99	93'726.43
μ_2 (Pa)	4'228'836.05	875'118.59	846'408.08	-
μ_3 (Pa)	2'853'769.62	453'616.46	438'514.84	-
α_1	24.48	16.59	24.63	8.17
α_2	25.00	16.65	25.00	-
α_3	23.54	16.50	23.74	-
D_1	8.95×10^{-7}	5.31×10^{-6}	4.67×10^{-6}	4.30×10^{-7}

The stress-strain response of the stent was applied based on data from a study by Murphy *et al.,* (2003) on the mechanical behaviour of the 316L stainless steel stent struts. The linear elastic response of the material was described as an isotropic material with a Young's Modulus of 196 GPa and Poisson's Ratio of 0.3. A piecewise linear function was used to represent the non-linear plasticity through a von Mises plasticity model with isotropic hardening.

The balloon was modelled as an isotropic, linear-elastic material, with a Young's modulus of 900 MPa and Poisson's Ratio of 0.3 based on the data published by Gervaso *et al.,* (2008).

3.1.3 Boundary Conditions

The two ends of the coronary artery were tethered using connector elements which were assigned elasticity characteristics. One end of these elements was connected to the end nodes of the artery and the other end was connected to the ground. The elasticity of these elements was chosen to be 1000 N/m which assured that the ends of the artery were constrained.

The load used for the expansion of the stents in case study (i) and (iii) was 16 atm which was applied on the inner surface of the stent and the inner balloon surface, respectively. This value is the maximum clinically permissible pressure for the expansion of most stents (Serruys *et al.,*

1998, 2000). However in case study (ii) a maximum load of 30 atm was applied to the stent inner surface to fully expand the stent to a diameter equivalent to the diameter achieved using the balloon model. Restraining connector elements were applied to every node of the stent however to ensure that the diameter of stent did not exceed the desired diameter due to the application of this clinically meaningless pressure of 30 atm.

All of the restraining connector elements were attached to ground and assigned a length of 1.113 mm to ensure that the stent expanded from its crimped state to a final expansion diameter of 3.5 mm. Given that the stent is symmetric in the circumferential direction the two ends of the restraining connector elements could have been connected between circumferentially symmetric nodes of the stent. However in many cases stents are not symmetric in the circumferential direction and therefore one end of the connector elements must be connected to the ground while the other end is connected to the stent nodes. In this study although the stent is circumferentially symmetric, in order to maintain the generality of the approach, one node of each of the connector elements was always connected to the ground.

In order to model the adhesion of the balloon to the catheter in case study (iii), the two end nodes of the balloon were connected using a connector element which was assigned a maximum length equal to the balloon length in the folded configuration and allowed for possible balloon bending. In addition the end nodes of the balloon were constrained in the tangential direction.

The general contact available in ABAQUS explicit was used to model the contact between the stent, balloon, and artery using frictionless contact with the default properties in all models. In addition, in all of the case studies three circumferentially symmetric nodes in the middle of the stents were constrained in the axial direction.

ABAQUS explicit was used in this study given its robust general contact algorithm and its ability to handle highly deformable materials well. However, when performing a quasi-static analysis using the explicit approach it is vital to ensure that the inertial forces are negligible throughout

the simulation and do not cause unrealistic dynamic effects. Therefore, in this study the ratio of kinetic energy to the total strain energy was consistently maintained lower than 5%. This criterion was proposed by Kim *et al.,* (2002) and ensures that the dynamic effects are negligible. In order to respect this criterion the simulation times were set to three seconds in all case studies.

3.2 Results

The method proposed in this study to create the three-fold balloon geometry combined with a patient derived model of the coronary artery in case study (iii) enabled a realistic simulation of the stent deployment, see Figure 3-2.

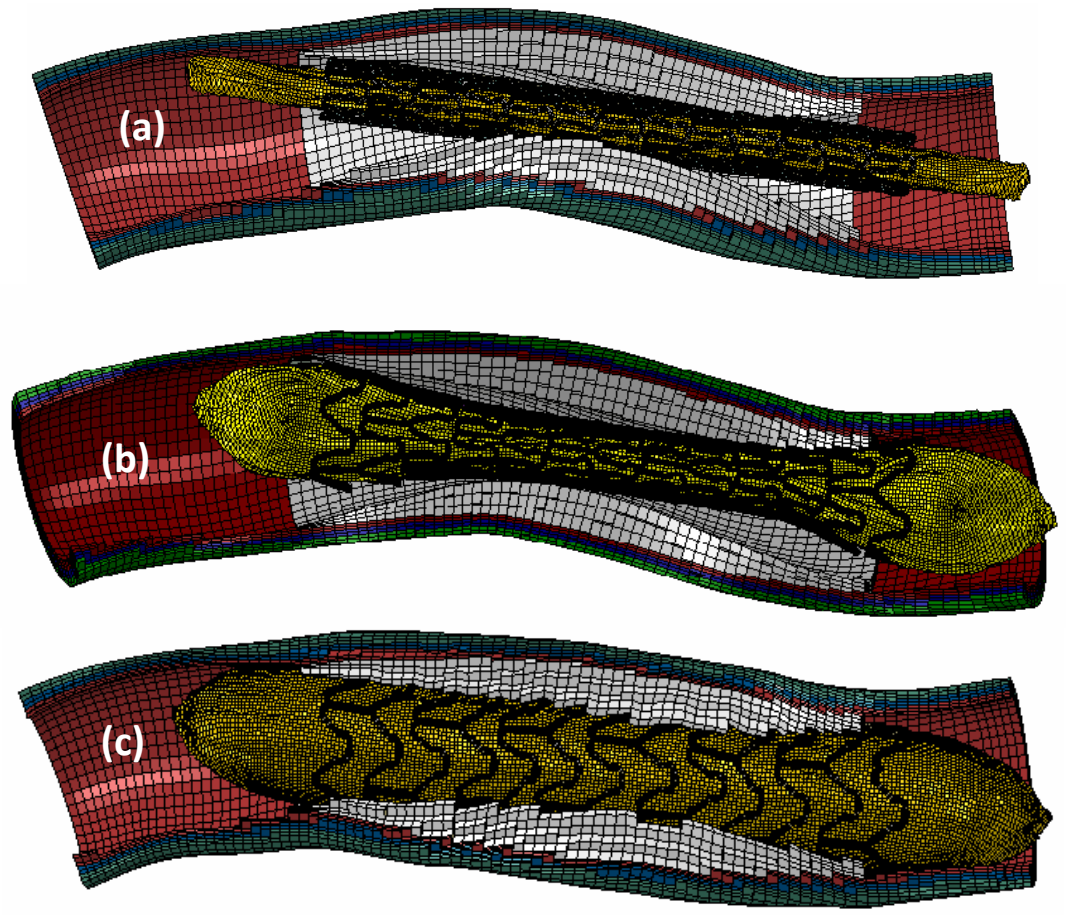

Figure 3-2: Assembly of layer specific stenosed coronary artery, stent and balloon in the (a) crimped configuration prior to expansion, (b) dog-boned configuration upon pressurisation (c) following full expansion. The adventitia, media, intima, and the atherosclerotic plaque are represented by green, blue, red and grey respectively.

Stent deformation response in this case study showed significant differences when compared with the results obtained from case studies (i) and (ii). The deformation of the stent was investigated by studying the pressure-expansion response, flaring of the stent widely known as *dog-boning* and *foreshortening* which represents the shortening of the stent length.

According to Kiousis *et al.,* (2009) the *dog-boning* of the stent may be defined using the following ratio:

$$Dogboning\ (DB) = \frac{D_{distal} - D_{central}}{D_{distal}} \qquad \textbf{Equation 3-2}$$

and the *foreshortening* of the stent may be defined as:

$$Foreshortening\ (FS) = \frac{L_{deformed} - L_{undeformed}}{L_{deformed}} \qquad \textbf{Equation 3-3}$$

Where D_{distal} and $D_{central}$ represent the diameter at distal and central locations of the stent and $L_{deformed}$ and $L_{undeformed}$ represent the deformed and undeformed length of the stent respectively.

In all case studies, *dog-boning* occurred upon pressurization, however in case study (iii) where the stent was expanded using a balloon model, the *dog-boning* was more pronounced and initiated at a lower pressure. The maximum *dog-boning* percentage in case study (iii) reached 49% at a pressure of 4 atm. In contrast, in case study (i) and (ii) this value reached a maximum of 19% at a pressure of 14.4 atm. The final *dog-boning* after stent recoil however was identical in case studies (ii) and (iii) with a value of 6%. This value was found to be 19% for case study (i), see Figure 3-3.

The overall pressure-diameter response in the mid-stent region in all case studies was determined as a function of pressure, see Figure 3-4.

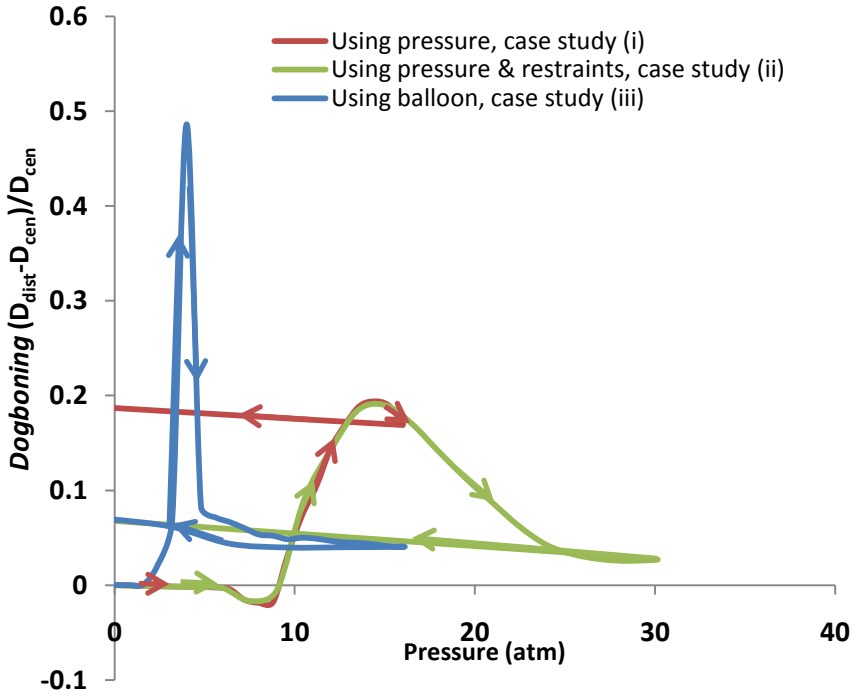

Figure 3-3: Dog-boning of the stent as a function of the applied pressure throughout the deployment process.

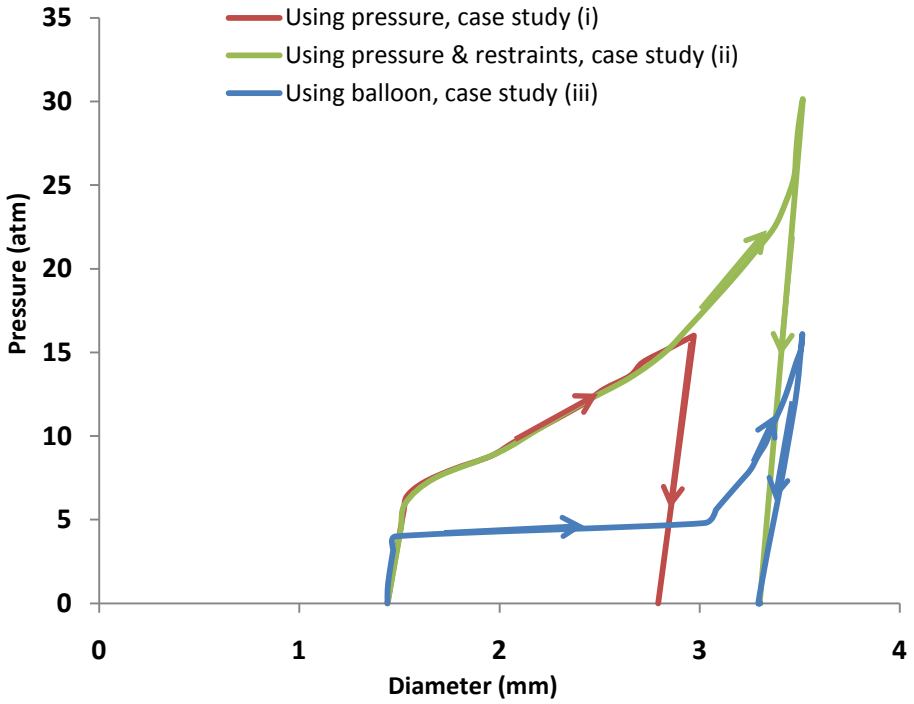

Figure 3-4: Pressure–diameter relationship of the stent throughout the deployment process.

Comparison of the curves illustrates a significantly different pressure-expansion response in case study (iii) in which the stent-balloon assembly showed a highly compliant response as the pressure reached 4 atm and the diameter increased rapidly from 1.5 mm to 3 mm, see Figure 3-4. This highly compliant response cannot be generated using direct application of a uniformly increasing pressure. A similar response consistent with the results of case study (iii) has previously been reported in experimental studies of stent deployment (Migliavacca *et al.,* 2008; Kiousis *et al.,* 2009).

The most significant difference in the stent deformation pattern, however, was found in the foreshortening curves, see Figure 3-5.

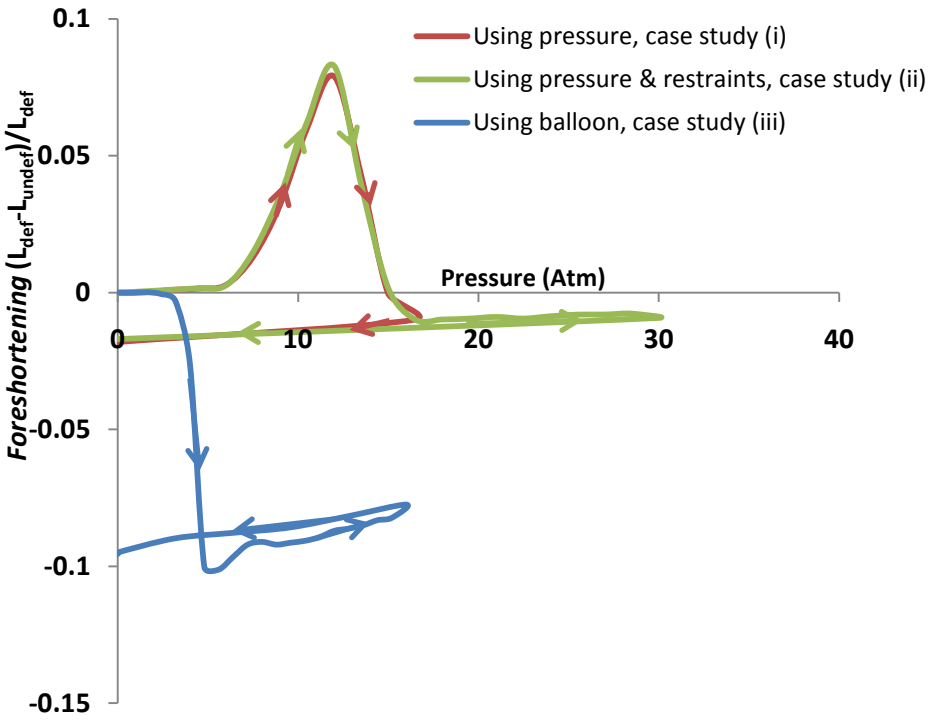

Figure 3-5: Foreshortening of the stent as a function of applied pressure throughout the deployment process.

Case study (iii) shows a foreshortening response with negative values at all pressures reaching a maximum foreshortening of -10% at a pressure of 5.6 atm. In contrast the foreshortening response in the other case studies takes positive values over a wide range of pressures with a maximum value of +8% in case study (ii). Clearly, direct application of uniform pressure on the stent inner surface in case studies (i) and (ii) leads to elongation of the stent in the 0 to 15 atm pressure range. On the contrary, expansion of the stent using the balloon model predicts shortening of the stent in the longitudinal direction which is consistent with the findings of experimental studies on very similar stents (Kiousis *et al.,* 2009).

Exploring the stresses in the vessel wall showed that the highest stresses occurred in the plaque and intima. In case studies (ii) and (iii) the von Mises stresses induced in the arterial tissue were of very similar magnitudes with maximum values of approximately 950 kPa and 170 kPa in the plaque and intima, respectively, and the predicted stress fields were comparable, see Figure 3-6. Comparison of the maximum stresses in case studies (i) and (iii), however, revealed the maximum von Mises stresses in the plaque and intima to be almost 65% lower in case study (i), see Figure 3-6. Moreover, the percentage of the tissue volume stressed over a certain threshold, to the total volume of the tissue, was calculated based on the stress value at the element integration points and quantifying the volume of plaque and intima tissue stressed at high levels within the vessel also proved very similar in case studies (ii) and (iii), see Figure 3-7.

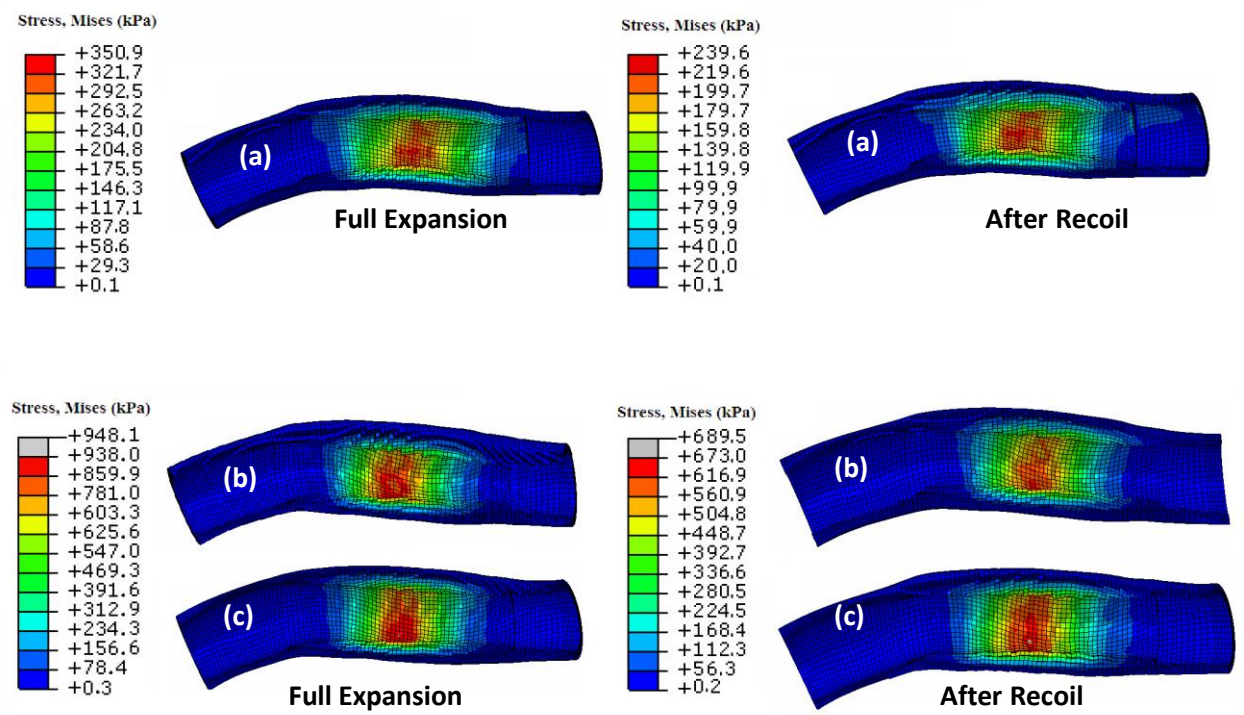

Figure 3-6: Von Mises Stresses in the stenosed vessel (a) applying uniform pressure to the stent, case study (i), (b) applying uniform pressure to the stent using restraining elements, case study (ii) and (c) using the balloon model, case study (iii).

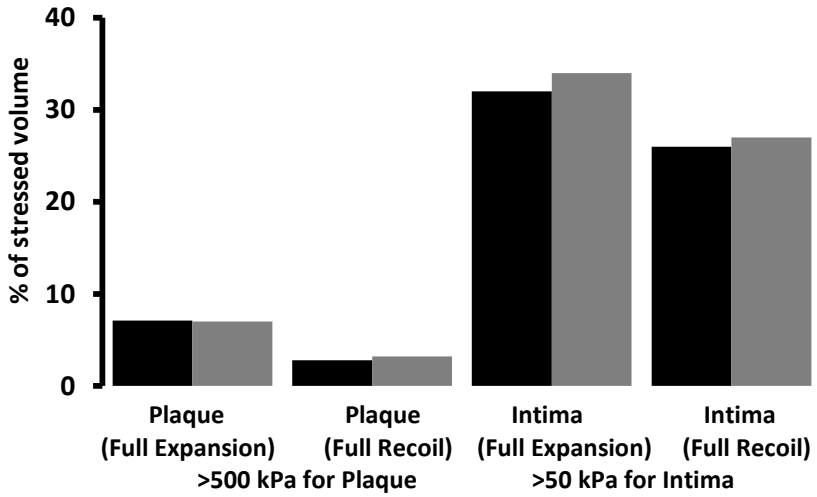

Figure 3-7: Percentage volume of plaque tissue stressed above 500kPa and of intimal tissue stressed above 50kPa using uniform pressure with restraining elements (Black) and a folded balloon (Grey).

In addition, investigating the stresses in the stent, a maximum von Mises stress of 761 MPa was found in the stent expanded using the balloon which is 4% and 10% higher than that predicted in case study (ii) and (i) respectively. The highest stresses in the stent occurred at the

base of the crowns where the crown joins the longitudinal struts and also in the crown tips in all cases.

3.3 Discussion

Simulation of stent expansion by direct application of pressure to the stent inner surface has been widely used in the literature as a means of reducing the computational costs of modelling the deployment of balloon expandable stents (Lally *et al.,* 2005; Early *et al.,* 2008; Gijsen *et al.,* 2008). Discarding the balloon model from the simulation reduces the contact problem from stent-artery and stent-balloon contact pairs to only a stent-artery contact problem and simulation time, memory requirements, and further simulation complications are significantly reduced as a result. A few studies have compared the different modelling strategies to propose the optimal modelling technique. Gervaso *et al.,* (2008) compared simulation of stent deployment in an idealised vessel by direct application of pressure to the inner stent surface and also by using a folded balloon model and concluded that modelling the balloon is essential to accurately estimate the level of injury to the arterial wall. In another study by De Beule *et al.,* (2008), the same two scenarios were compared in a free expansion simulation (without inclusion of any vessel) and the pressurisation technique was found to be an over simplification which could not yield accurate results. Consistently, in this study comparison of case study (i) and case study (iii) illustrates that application of the clinically relevant pressures to the stent inner surface neither results in accurate estimation of the stress-strain field in the arterial wall nor is it able to predict the transient response, final deformed configuration and stresses of the stent.

The results of case study (ii), however, elucidate that this scenario may have the potential to reasonably predict the stress-strain field in the vessel wall. Although this result is shown for a particular case of the Multilink stent and a specific vessel geometry, the stresses in the vessel wall during deployment of any particular stent are mainly dictated by the expansion diameter of the stent and therefore provided that the desired expansion diameter is achieved, utilising the method presented in case study (ii) may suffice to model stent deployment.

This study illustrates that estimation of the transient response of the stent such as pressure-diameter, *dog-boning* and *foreshortening* is clearly not possible by direct application of pressure to the stent inner surface and requires utilisation of a balloon model. Nevertheless in certain cases where the objective is the estimation of the final vessel wall stress/strain field following full stent expansion and recoil, use of the method outlined in case study (ii) may be adopted as an optimal method in terms of reduced computational costs. In this study a 6% error in the estimation of the stent length on full expansion and recoil in case study (ii) did not cause any significant alteration in the vessel wall stress magnitudes or spatial distribution. However, caution should be exercised when using this method as excessive elongation of the stent during direct application of pressure could alter the spatial distribution of the stresses in the vessel wall.

Although this study presents a simulation of a balloon expandable stent in a patient derived vessel geometry using a realistic three-fold balloon and a three layered vessel, some limitations still exist in this study. The most important limitations of this study are associated with the vessel wall material properties. Damage to the vessel wall and residual stresses in the artery were not included in the material properties of the vessel wall. However, given that this is a comparative study which investigates the different modelling strategies, inclusion of damage and residual stresses in the vessel wall material model was deemed beyond the scope of this work. In addition, human coronary arteries generally exhibit an anisotropic response in the axial and circumferential directions due to collagen fibre orientation. The response of the vessel wall during stent expansion, however, is mainly dictated by its circumferential mechanical properties and therefore in this study the material properties of human coronary arterial layers in the circumferential direction were assigned to the models using an isotropic material model.

Although no experimental studies were carried out in this work to verify the numerical results obtained, the experimental work carried out by Kiousis *et al.,* (2009) on very similar stent designs shows pressure-diameter, *dog-boning* and *foreshortening* responses consistent with

the results of case study (iii) and provide clear evidence to support the accuracy of this approach, see Figure 3-8.

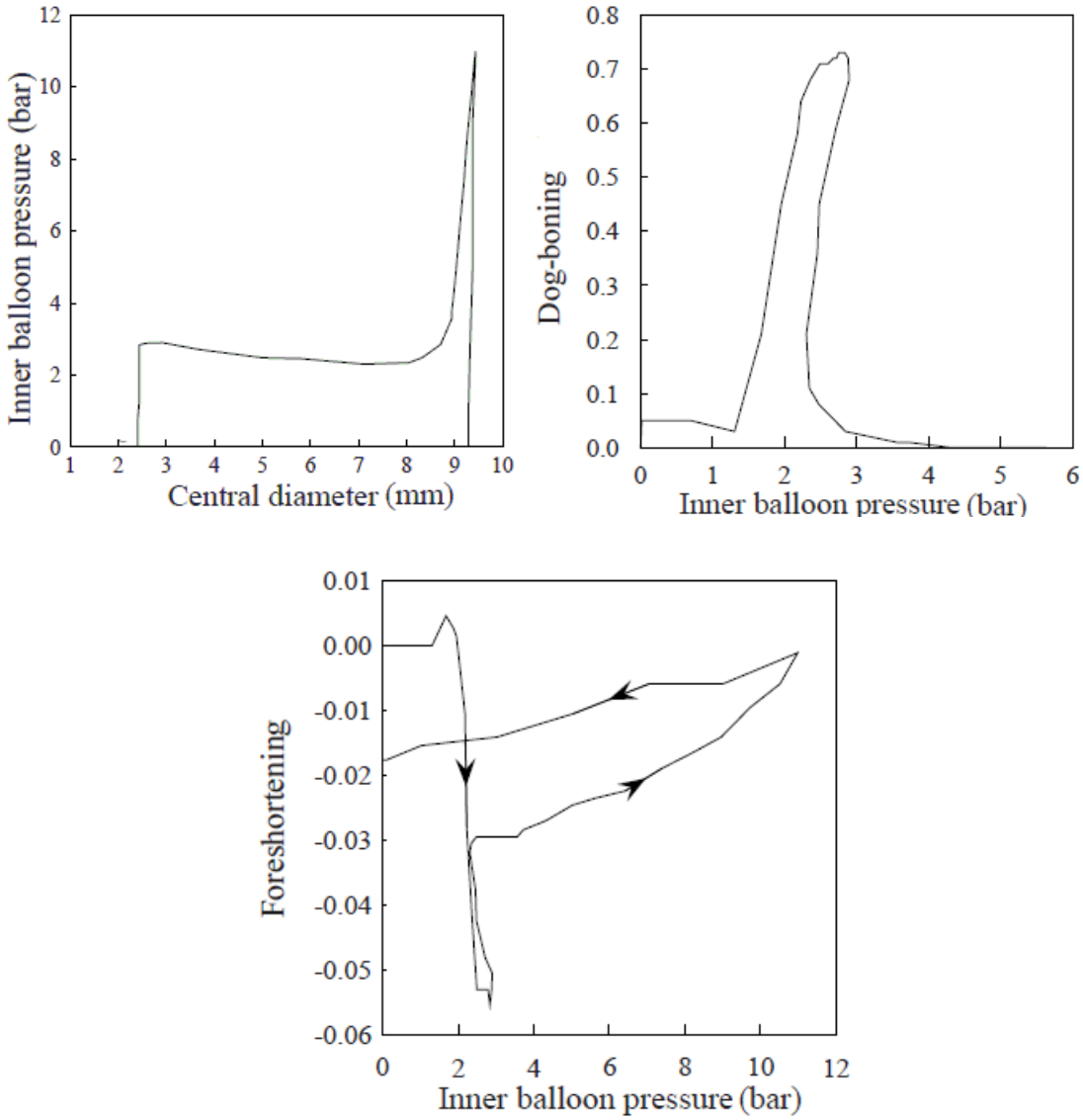

Figure 3-8 : Experimental results from Kiousis et al. 2009 on the pressure-diameter, dogboning and foreshortening responses of a balloon expandable Express Vascular LD ™ balloon-stent system under free expansion with a design very similar to the stent modelled in this study.

Chapter 4

Determination of the influence of stent strut thickness using the finite element method: implications for vascular injury and in-stent restenosis

Many clinical studies, including the ISAR-STEREO trial, have identified stent strut thickness as an independent predictor of in-stent restenosis where thinner struts result in lower restenosis than thicker struts. The aim of this study was to more conclusively identify the mechanical stimulus for in-stent restenosis using results from such clinical trials as the ISAR-STEREO trial. The mechanical environment in arteries stented with thin and thicker strut stents was investigated using numerical modelling techniques. FE models of the stents used in the ISAR-STEREO clinical trial were developed and the stents were deployed in idealised stenosed vessel geometries in order to compare the mechanical environment of the vessel for each stent. The stresses induced within the stented vessels by these stents were compared to determine the level of vascular injury caused to the artery by the stents with different strut thickness.

4.1 Materials and methods

In the study presented here, FE models of two stents with identical design but different thickness were developed and the stents were deployed in an idealised stenosed vessel in order to compare the mechanical environment of the vessel for each stent. The stents were expanded and deployed within the arteries to scaffold open the stenosed arteries, in line with that which was carried out in the ISAR-STEREO trial. Two case studies were investigated to determine the influence of stent strut thickness on the vessel wall;

(i) Both stents were expanded to the same initial maximum stent diameter

(ii) Both stents were expanded to achieve the same final maximum stent diameter taking stent recoil into consideration.

Case study 1 represents the clinical situation since stents are routinely expanded under fluoroscopy to achieve a ratio of 1.1:1 between the stent diameter and the proximal and distal diameter of the host vessel (de Quadros *et al.,* 2006).

FE analyses were carried out to compare the stresses induced within the stented vessels by these stents, and hence to evaluate the potential of arterial injury caused by stents with different strut thickness. To generate these numerical simulations, the FEM requires a number of inputs; the geometry of the stents and the stenosed coronary arteries, the material properties of the stents and the artery, and the appropriate application of loading and boundary conditions, as described below.

4.1.1 Model Geometry

The FE models of the stents were generated and meshed in ANSYS (Canonsburg, PA, USA) and were generated based on the stents used in the ISAR-STEREO Trial, namely the ACS RX MultiLink and the ACS MultiLink RX Duet (Kastrati *et al.,* 2001). Both stents are manufactured by the same company, namely Guidant/Advanced Cardiovascular Systems. Both stents have a similar interconnected-ring design, struts with rectangular cross-sectional areas and a width of 100 µm but different strut thickness. The strut thickness of the ACS RX MultiLink ($Mlink_{thin}$) is 50 µm and the strut thickness of the ACS MultiLink RX Duet ($Mlink_{thick}$) is 140 µm. Full three-dimensional models of the stents were developed to determine the expansion characteristics of the stents after stent deployment. The main dimensions of the stents were extrapolated from a handbook of coronary stents (Serruys *et al.,* 2000). Both stents are available in a range of lengths, whilst the length of the stents investigated in this study was 7.2 mm. For this length, the MultiLink stents consist of six rings in the longitudinal direction with six crowns in each ring.

For both stent models, all of the parameters, such as the length and width were kept constant and the only variation between the two designs was the thickness of the struts. Both stents were simulated with an inner radius of 0.72mm, with a corresponding outer radius of 0.77mm for the $Mlink_{thin}$ and 0.86mm for the $Mlink_{thick}$.

The stents are not symmetrical in the longitudinal direction, however, symmetry is observed in the circumferential direction. Due to the circumferential symmetry, only one third was modelled in the circumferential direction with the full length in the longitudinal direction. The stent geometry was initially modelled in three-dimensional Cartesian coordinate system, representing the stent in an opened-out, planar configuration. The volumes of $Mlink_{thin}$ and $Mlink_{thick}$ were discretised by means of eight-noded isoparametric, three-dimensional brick elements. The models of $Mlink_{thin}$ and $Mlink_{thick}$ were meshed with two and three elements through the thickness respectively, see Figure 4-1. All elements were checked to ensure that no distorted elements were generated. The stent mesh comprised a total number of 7794 elements for $Mlink_{thick}$ and 4592 elements for $Mlink_{thin}$. The nodal coordinates of the meshed model were transferred from a Cartesian coordinate system into a cylindrical coordinate system, using a procedure previously reported (Lally *et al.,* 2005) whereby the planar configuration was wrapped to represent the cylindrical structure of the stents.

The FE software used to solve the models was ABAQUS (SIMULIA, Providence, RI, USA). ABAQUS explicit was utilized for its robust general contact algorithm and stability which enables modelling of very soft hyperelastic materials. The General contact algorithm in ABAQUS explicit with no friction between the contacting bodies was considered for the analysis which enforces contact constraints using a penalty contact method. The default parameters were used to define the contact between the artery and the stent.

Each simulation model composed two bodies, the stent and the stenotic coronary artery. The thickness of atherosclerotic human coronary arteries range from 0.56 mm to 1.25 mm, depending upon the location of the arteries on the surface of the heart (van Andel *et al.*, 2003). For this reason, a thickness of 0.8 mm was chosen to represent the stenosed coronary artery with the atherosclerotic localised plaque. The stenotic coronary artery was modelled as a straight 0.5 mm thick vessel with a localised plaque 0.3 mm thick and an internal radius of 1.3 mm, see Figure 4-1. Eight node linear brick, reduced integration elements with hourglass control (ABAQUS element type C3D8R) were used to mesh the atherosclerotic coronary artery.

Six elements were assigned through the thickness of the arterial wall. The vessel was divided into three layers; initima, media and adventitia. The thickness of each arterial layer was discretized by two elements and each layer was of equal thickness. This closely complied with the ratio of the thickness of adventitia, media, and intima which have been reported as 0.40±0.03, 0.36±0.03, and 0.27±0.02, respectively in (Holzapfel *et al.,* 2005a). Six elements were assigned through the plaque thickness in the central region. The atherosclerotic artery was meshed by a total of 121,440 elements and 135,969 nodes, see Figure 4-1.

Figure 4-1: FE models of the atherosclerotic coronary arteries with crimped (A) Multilink thin and (B) Multilink thick stents.

4.1.2 Material Properties

Layer specific human coronary arterial wall properties were assigned to the artery, consisting of the intima, media and adventitia based on the data from Holzapfel *et al.,* (2005a). Human cellular atherosclerotic intimal plaque properties were assigned to the localised plaque based on the available published data from Loree *et al.,* (1994). The material of the intima, media and adventitia and plaque were defined using third order Ogden hyperelastic constitutive equations as described in Chapter 3 and published in (Zahedmanesh and Lally 2009).

The properties of 316L stainless steel were assigned to the stents' material. The stress-strain relationship of 316L stainless steel for $Mlink_{thin}$ (strut thickness of 50 µm) and $Mlink_{thick}$ (strut thickness of 140 µm) in the FE models in this study were described by the mechanical behaviour of the struts tested by Murphy *et al.,* (2003), see Figure 4-2.

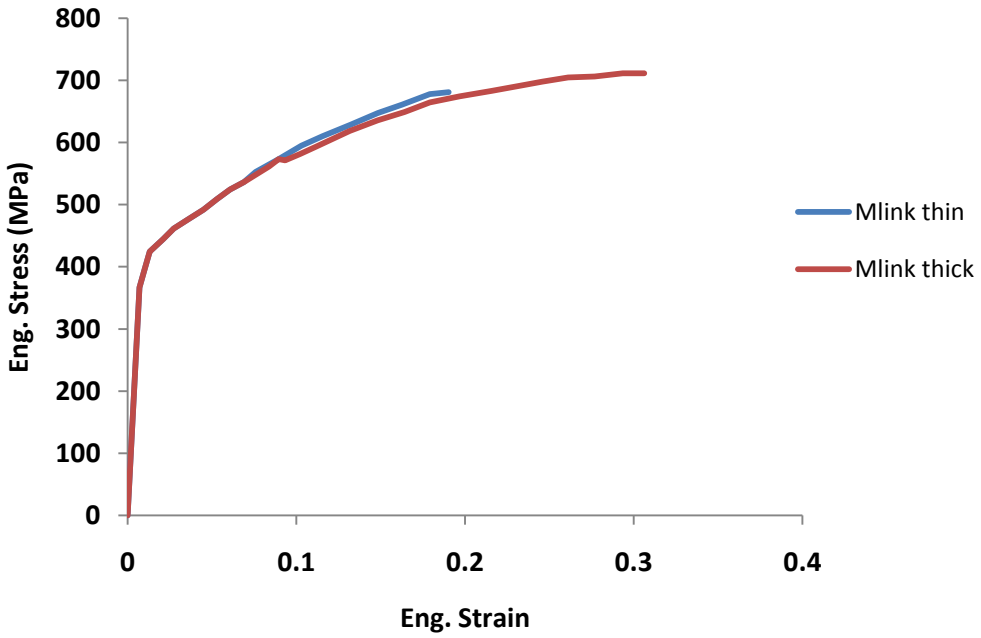

Figure 4-2 : Stress-strain response of the thick and thin stent struts, adapted from Murphy *et al.* 2003.

The material was described as an isotropic material with the linear elastic region of the curve defined through the bulk material values for 316L stainless steel; Young's Modulus of 196GPa, Poisson's Ratio of 0.3. A piecewise linear function was used to represent the non-linear plasticity through a von Mises plasticity model with isotropic hardening.

4.1.3 Boundary Conditions

The stent deployment involved expansion of the stent by the application of an internal pressure on the inner stent surface (loading), and removal of the internal pressure (unloading). A uniform, radial pressure was applied as a surface load to the internal surface of the stent increasing temporally in magnitude as a smooth step. Connector elements were utilized in ABAQUS to stop the stent from further expansion as the desired expansion diameter was achieved based on the optimal method described in Chapter 3. These elements were connected to the centre of the stent (ground) on one end and to the stent nodes on the other end. These connector elements simulate expansion of a stent with a non-compliant angioplasty balloon as they prevent the stent from expanding beyond the balloon diameter.

Two cases were studied to compare the effect of stent strut thickness. In the first case study, both $Mlink_{thin}$ and $Mlink_{thick}$, were expanded to the initial maximum external diameter of 3.22 mm, and were allowed to recoil. In the second case study, the stents were expanded to different diameters in such a way as to achieve the same final maximum external diameter following radial recoil (3.08 mm). These values were chosen in order to expand the central stenosis in the vessel to the diameter of the proximal and distal non-atherosclerotic vessel lumen. As the diameter of the stent was found to be non-uniform in different parts of the stent following expansion, the maximum external diameter achieved by the stent was opted as a criterion for the case studies.

For both case studies the same FE models were simulated, the only difference being the amount of pressure applied. For case study 1, 0.9 MPa (9 atm) was applied to $Mlink_{thin}$ and 1.5 MPa (15 atm) was applied to $Mlink_{thick}$, to achieve the same initial maximum external stent diameter of 3.22 mm. For case study 2, the pressure required to expand $Mlink_{thin}$ and $Mlink_{thick}$

were 1 MPa (10 atm) and 1.5 MPa (15 atm), respectively, to achieve the same final maximum external stent diameter (3.08mm).

Cyclic symmetry boundary conditions were imposed on the nodes of the stent and artery in the circumferential plane of symmetry. The ends of the stent were free from any constraints. Displacement boundary condition was applied to both ends of the vessel to account for *in situ* prestretch of the vessel. Axial *in situ* prestretch was chosen to be 1.05 which is typical of coronary arteries. This is the upper band of the axial *in situ* stretch of 1.044±0.006 in coronary arteries reported by Holzapfel *et al.,* (2005a).

In addition, element distortion control was used to prevent incorrect results in the contact region where excessive distortion of elements could occur.

When performing a quasi-static analysis with the explicit approach it is necessary to ensure that the inertial forces are negligible and do not cause unrealistic dynamic effects. It has been shown that by maintaining the ratio of kinetic energy to the total strain energy less than 5% dynamic effects are negligible (Kim *et al.,* 2002). This criterion was adopted for the quasi-static analyses presented here.

4.2 Results

Radial displacements were measured at key locations on each stent through the loading and unloading process of the stents' expansion. The radial recoil throughout both structures of $Mlink_{thin}$ and $Mlink_{thick}$ was found to be highly non-uniform. The lowest values of recoil were observed at the proximal and distal ends of the stent structures because of lower plaque thickness at the two ends and the radial recoil was higher for the $Mlink_{thin}$ when compared with $Mlink_{thick}$, see Table 4-1.

Radial recoil was in the order of 3-9%, which is higher than that reported by the manufacturers for the laser cut stainless steel multilink stents (1.7-4.8%) (Serruys *et al.,* 1998; Surreys *et al.,* 2000). This is due to the fact that recoil is generally reported for free expansion of stents whilst the presence of the stenotic artery around the stent increased the radial recoil of the stents.

Investigating the stresses induced in the arteries by the two stents with different strut thickness it was found that the $Mlink_{thick}$ induced 15% higher stress values in intima than the $Mlink_{thin}$ on loading to achieve the same initial maximum stent diameter, see Figure 4-3. However, it was on unloading that the greatest difference in the mechanical environment of the vessels was observed. After removal of the expansion pressure the maximum external diameter of $Mlink_{thin}$ and $Mlink_{thick}$ was found to be 3.02 mm and 3.08, respectively. As a result of the higher recoil in the $Mlink_{thin}$ 64% lower stresses were present in the intima with 17% lower stresses induced in the plaque of the vessel scaffolded by this stent, see Figures 4-3 & 4-4. The percentage stress volume defined as the percentage of the tissue volume stressed over a certain threshold to the total volume of the tissue was also calculated. Quantifying the volume of plaque and intima tissue stressed at high levels within the vessel it was found that the $Mlink_{thick}$ had higher volumes of tissue stressed at high levels particularly in the intima following recoil, see Figure 4-5.

Table 4-1: Radial recoil in the stents

Stent	Pressure (atm)	Stent expanded diameter (mm)	Stent diameter following recoil (mm)	Distal End	Centre	Proximal End
$Mlink_{thick}$	15	3.22	3.08	4.54%	5%	4.88%
$Mlink_{thin}$	10	3.40	3.08	6.95%	9.63%	6.52%
$Mlink_{thin}$	9	3.22	3.02	6.56%	6.93%	5.8%

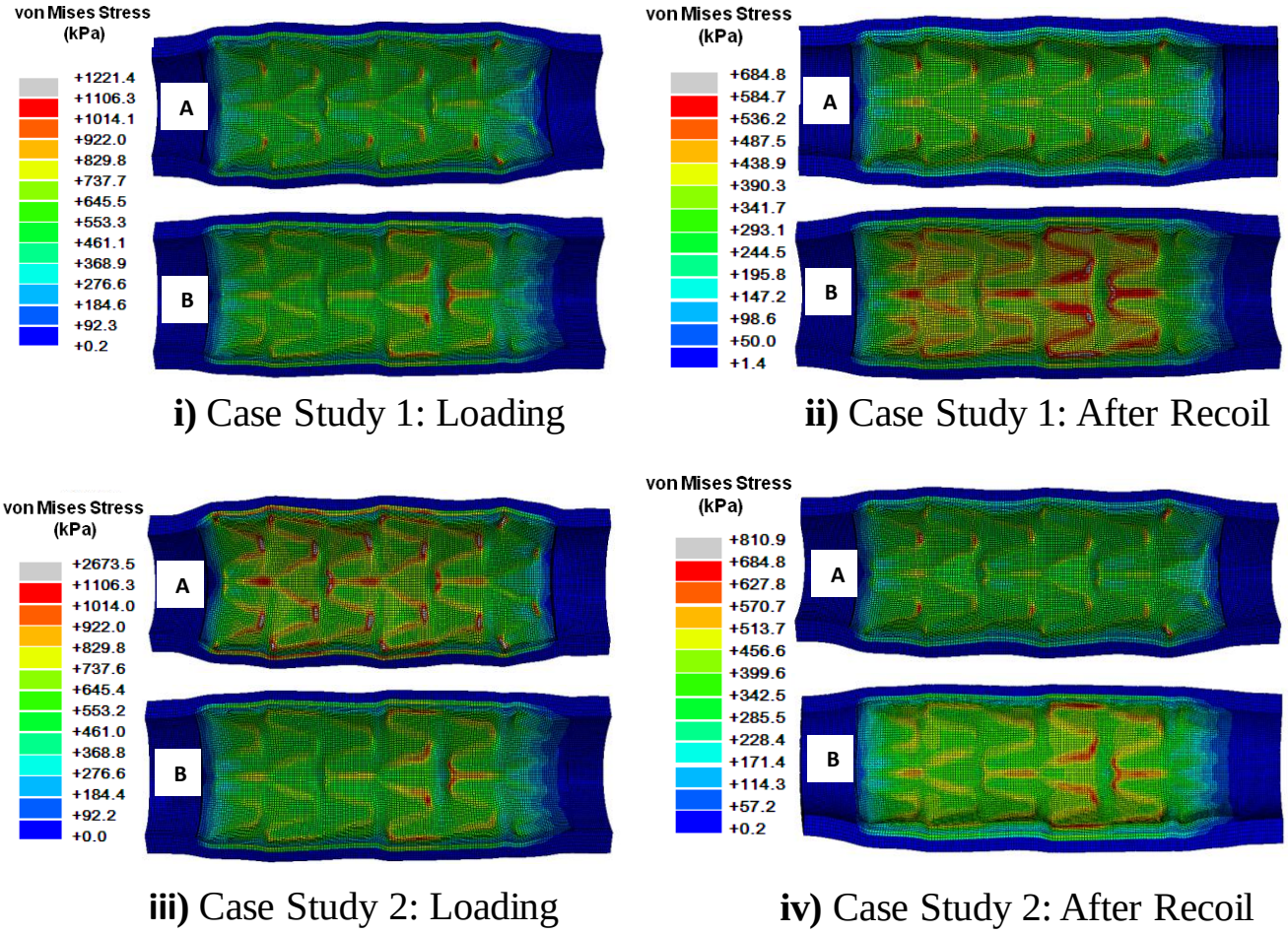

i) Case Study 1: Loading

ii) Case Study 1: After Recoil

iii) Case Study 2: Loading

iv) Case Study 2: After Recoil

Figure 4-3: von Mises stresses in the stenosed vessels stented with (A) Multilink thin and (B) Multilink thick stents.

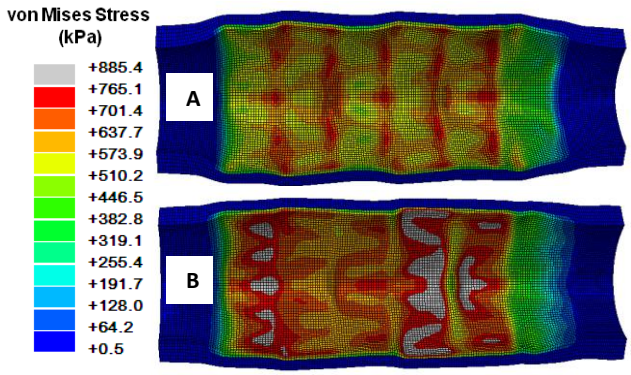

i) Case Study 1: Loading

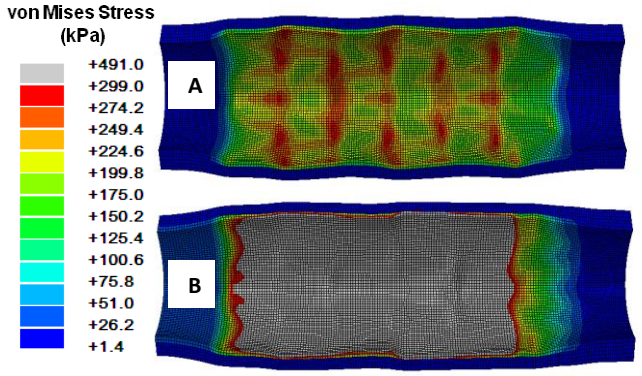

ii) Case Study 1: After Recoil

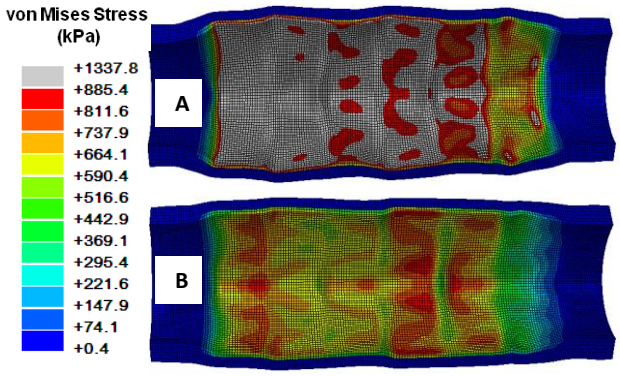

iii) Case Study 2: Loading

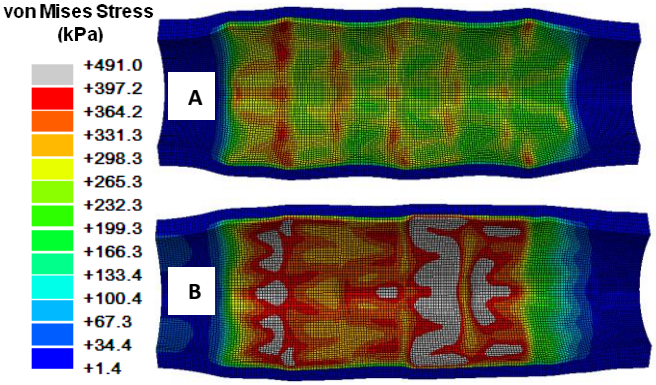

iv) Case Study 2: After Recoil

Figure 4-4: von Mises stresses in the intima of the stenosed vessels stented with (A) Multilink thin and (B) Multilink thick.

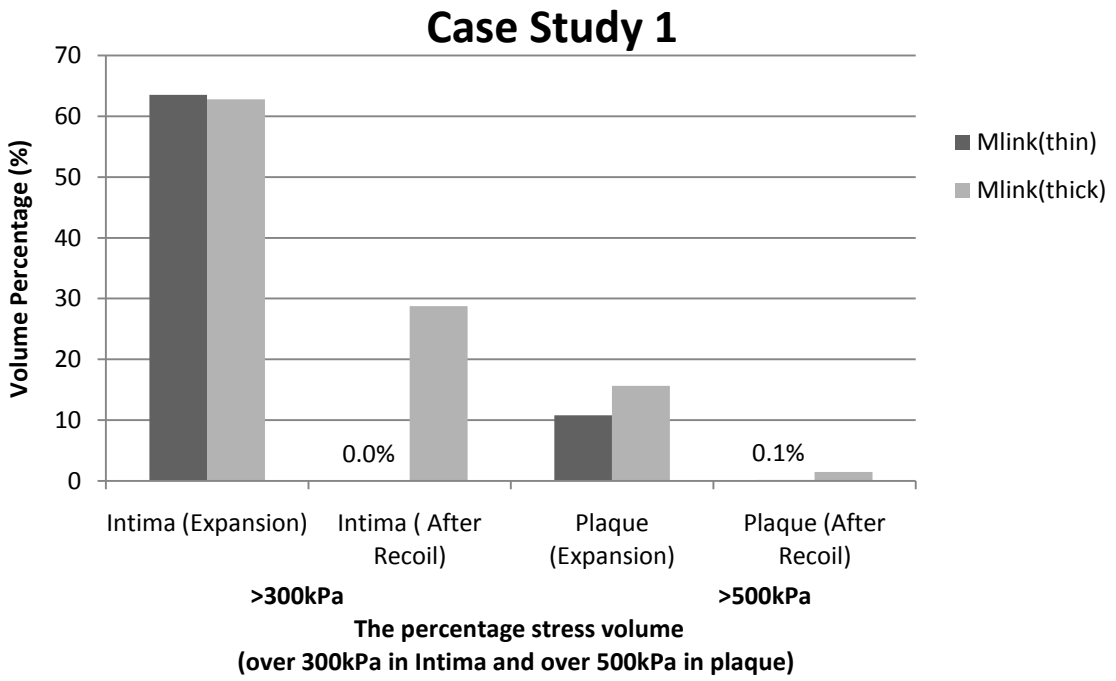

Figure 4-5: The percentage stress volumes of case study one calculated for intimal tissue stressed over 300kPa and plaque tissue stressed over 500kPa

Stresses in the vessel were also investigated for case study 2, where the stents were expanded to achieve the same final maximum stent diameter. Due to the higher radial recoil observed for the $Mlink_{thin}$ it was necessary to expand it to 3.4 mm and the $Mlink_{thick}$ to 3.22 mm initial maximum external diameter to achieve a final maximum external diameter of 3.08 mm in both stented vessels. Investigating the stresses in the vessels, it was found that due to the higher expansion diameter of the $Mlink_{thin}$ on loading it induced considerably higher stress magnitudes and volumes in the plaque tissue localised where the stent crowns contacted the plaque and intima, see Figures 4-3 & 4-4. Removal of the lumen pressure on the stents lowered the stresses in the vessels, however, 23% higher stresses were induced in intima by $Mlink_{thick}$ following recoil, see Figures 4-6.

The results of these models also show that in all cases the plaque and intima of the atherosclerotic vessels undergo significantly higher stresses when compared to the media and adventitia of the vessels, see Figures 4-3, 4-4, 4-5, 4-6.

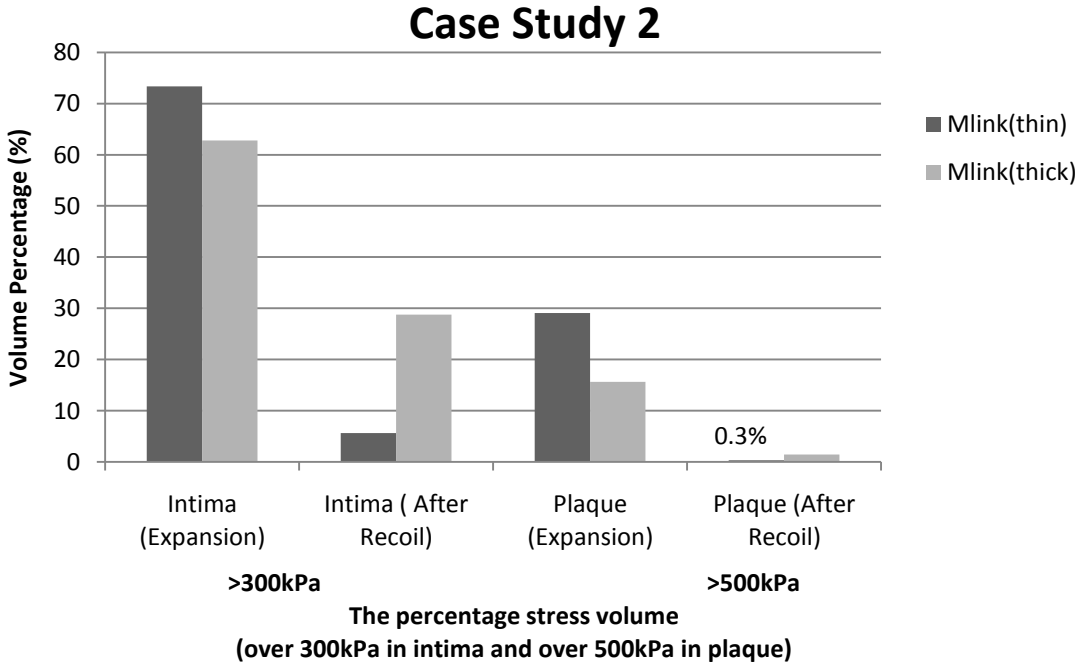

Figure 4-6: The percentage stress volumes of case study two calculated for intimal tissue stressed over 300kPa and plaque tissue stressed over 500kPa

4.3 Discussion

The results of this study show the influence of stent strut thickness on the stresses within a vessel. If, as in the ISAR-STEREO clinical trial, two stents with the same design are expanded to the same initial maximum stent diameter the recoil of the thinner strut stent will cause lower stresses to be induced in the vessel, both acutely during the procedure, and chronically. The stresses induced in the vessel on unloading, particularly in the intima, may act as a chronic stimulus for cell proliferation where the artery attempts to lower these stresses by vessel thickening. The lower lumen gain, but lower acute and chronic stresses, in the thinner strut stented vessel may ultimately result in less injury and aggressive healing response.

This hypothesis and the results from this numerical modelling study are supported further by the ISAR-STEREO clinical trial results whereby the diameter stenosis immediately after the procedures showed the thin-strut group had less optimal lumen gain but this was found to have significantly reversed at 6-month follow-up (see Figure 1 in (Kastrati *et al.,* 2001)).

The results from case study 2 show that, although a thinner strut stent may be favourable when compared to a thicker strut stent, it only applies in cases where both stents are expanded to the same initial maximum stent diameter. Expansion of the thinner strut stent to a higher diameter to achieve the same final maximum stent diameter as the thicker strut stent results in considerably higher acute stresses at loading, however, at unloading the thicker strut stent induces 23% higher intimal stresses. Clearly therefore many stent designs, even thick strut stents, could potentially offer a solution to restenosis if the optimum expansion diameter was considered such that stresses in the vessel were maintained low.

Manufacturers quote the recoil of stents but only for free expansion and these compare very well to those predicted using numerical models of free expansion. However, experience from our lab using commercially available stents has shown that recoil is significantly higher in stented vessels when compared to that quoted by manufacturers for free expansion (Toner *et al.,* 2007). This is also clearly demonstrated in the models presented here and it demonstrates the need for accurate numerical models of medical devices.

Clearly therefore, a major concern in the response of a vessel to a stent is the stent recoil which influences the stresses induced in the vessel, however, overall stent compliance may also be a factor influencing restenosis. A more flexible, compliant stent may recoil more than a thicker strut, more rigid stent and may also therefore allow greater conformability and scaffolding in a tortuous vessel. In addition, arterial vessels contain living cells, such as smooth muscle cells (SMCs), which are conditioned to thrive in a cyclic strain environment. Stenting lowers vessel compliance and consequently reduces the cyclic strain on these cells (Vernhet *et al.,* 2001). Altering the cyclic strain on SMCs may cause cells to proliferate as has been indentified in studies on the influence of cyclic loading versus static cells in culture (Morrow 2005). Specifically, in the study by Colombo (2009) it has been found that reduction of cyclic strain due to stenting in mock coronary arteries increases the proliferation of VSMCs which can implicate in-stent restenosis. A thinner strut stent may stiffen a vessel to a lesser extent when

compared to a thicker strut stent resulting in the cells experiencing closer to the normal cyclic strain stimulus.

The main observations from this study, however, are that a thinner strut stent induces considerably lower chronic vessel stresses when expanded to the same initial diameter as a thicker strut stent and marginally lower when expanded to the same final diameter as a thicker strut stent. Given the lower clinical restenosis rates observed for such thinner strut stents it may be postulated that there is a critical chronic stress or injury level above which intimal hyperplasia occurs which ultimately results in restenosis. It is this critical stress level that needs further investigation in clinical trials. Guidelines on this critical stress level in arteries would enable preclinical testing tools to provide better design solutions to the problem of in-stent restenosis.

Some limitations of this study include the use of only circumferential tensile test properties and therefore defining the arterial layers as isotropic materials, however, this assumption is plausible as the dominant mechanical properties of the arterial wall during stent deployment are the circumferential properties. Residual stresses and blood pressure were not included in the vessels, however, given the comparative nature of this study the results are not compromised. In addition, the tissues were assumed to be purely elastic and damage accumulation within the atherosclerotic vessel was not accounted for as it was deemed beyond the scope of this study.

Another factor which has been hypothesised to contribute to the onset of in-stent restenosis is alterations in the fluid flow within a vessel, and particularly abnormal wall shear stresses. Factors such as the separation and recirculation of the blood downstream from the stent struts have been shown to be influenced by strut spacing (Duraiswamy *et al.,* 2007). Although blood flow within the stented vessels has not been investigated as part of this study, it is possible that alterations in fluid flow would also vary with strut thickness and therefore influence the potential for restenotic growth within a stented vessel.

In the ISAR-STEREO trial, stent strut thickness was not strictly the only difference between the two stent designs implanted. The design of the two models is very similar except for a slightly decreased number of inter-ring articulations in the thick-strut stent (ACS Multi-Link RX DUET) when compared to the thin strut stent (ACS RX Multi-Link). The clinical study itself, however, did not consider these differences significant and therefore simply considered the study an investigation of strut thickness. In this study we have adopted a similar approach by solely investigating the influence of the strut thickness variation and using the ACS Multi-Link RX DUET stent design only.

Clearly however, the results from the numerical models in this study demonstrate that an optimum stent design should recoil sufficiently to prevent overstressing the vessel wall whilst maintaining patency of the vessel. This study also provides evidence that preclinical testing using numerical modelling can provide insights into the optimum loading for a particular stent design to reduce the stimulus for in-stent restenosis.

Chapter 5

Bacterial cellulose as a potential vascular graft: Mechanical characterisation and constitutive model development

Bacteria Cellulose (BC) is a novel emerging biomaterial which has shown good potential for arterial grafting and vascular tissue engineering. Given that compliance mismatch is one of the main factors contributing to the development of intimal hyperplasia in vascular replacement conduits, an in depth investigation of mechanical properties of BC is required to further support its use in cardiovascular grafting applications. The aim of this study was to mechanically characterise bacterial cellulose (BC) and also study its potential to accommodate vascular cells. To achieve these aims inflation tests and uniaxial tensile tests were carried out on BC samples. In addition, dynamic compliance tests were conducted on BC tubes and the results were compared to that of arteries, saphenous vein, ePTFE and Dacron grafts. In addition, bovine smooth muscle cells and endothelial cells were cultured on BC samples and histology and fluorescent imaging analysis were carried out to study cell adherence and biocompatibility. Finally, a method to predict the mechanical behaviour of BC grafts in situ was established, whereby a constitutive model for BC was determined and used to model the BC tubes under inflation using FE analysis.

5.1 Materials and methods

5.1.1 Bacterial Cellulose tubes

Bacterial cellulose tubes were manufactured by *Biosynthetic Blood Vessels (BBV)*, *Gothenburg, Sweden* and provided for mechanical characterisation experiments. The tubes were produced by BBV through fermentation of *Acetobacter xylinum* subsp.*sucrofermentas* BPR2001, trade number 1700178™, submerged in glass tubes of 70 ml by using a silicone support (Ø4 mm, AvantaPure) as an oxygen permeable material. An oxygen ratio of 100% was blown into the oxygen permeable material at a rate of 100 ml/min. A complex media was used as described previously (Bodin 2007). Four cellulose colonies were grown for two days in a rough flask yielding a cell concentration of 3.7×10^6 cfu/ml and later the bacteria were liberated from the resulting cellulose by vigorous shaking. 2.5 ml of the bacterial suspension was added to each fermentation vessel. The fermentation was completed after 7 days and the BC tubes were purified by heating them in 0.1 M NaOH at 60°C for 4 hours and thereafter repeatedly in Millipore™ water. The BC tubes were steam sterilized (20 minutes, 120°C) and stored in a refrigerator for subsequent mechanical characterisation.

5.1.2 Inflation tests

Inflation tests were performed on six bacterial cellulose tubes with 4 mm luminal diameter to study the behaviour of the bacterial cellulose tubes under the physiological pressure range. 5 cm long bacterial cellulose tubes were cut and fixed onto the fittings of a custom built test rig, see Figure 5-1. The tubes were inflated using a hydrostatic pressure of a water column ramping from 0 to 160 mmHg. Expansion of each tube was determined by measuring the outer diameter of the tube using a precise video extensometer (MESSPHYSIK Material Testing, Austria) and relating it to the measured initial diameter corresponding to zero pressure. The tubes were tested applying no axial prestretch and preconditioning of the tubes was carried out before recording expansion by applying ten cycles of pressurization ranging from 0 mmHg to 160 mmHg to minimise hysteresis and achieve repeatability.

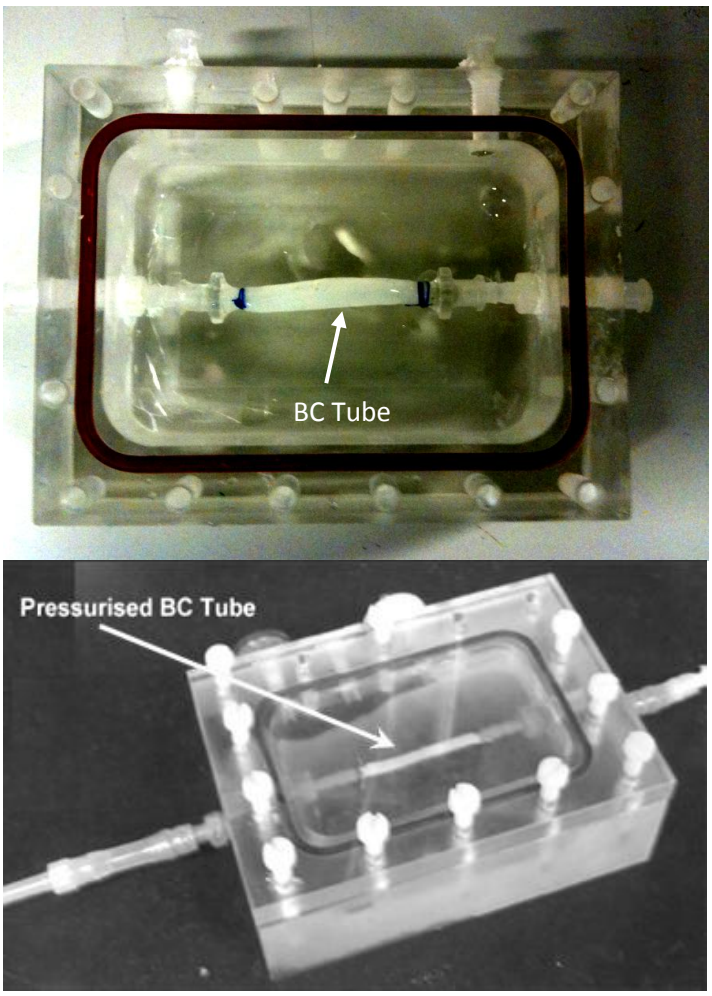

Figure 5-1: Custom built inflation and compliance test rig

5.1.3 Tensile tests

Uniaxial tensile tests were carried out on samples obtained from the bacterial cellulose tubes immediately following the inflation tests to establish the stress-strain response of bacterial cellulose and later establish the constitutive material model. The tubes were cut open along the axial direction and flat sheets of bacterial cellulose were obtained. Axial and circumferential strips were cut out of the tubes. As the structure of BC shows no preferred direction in fibre dispersion an isotropic behaviour was expected in the axial-circumferential plane. This was confirmed by testing axial samples and comparing with the circumferential test results. The tubes did not spring open upon axial cutting indicating that no significant residual stress was present in the tubes. The strips were tested using a Zwick displacement controlled tensile testing machine utilising a 20 N load cell and the video extensometer was used to verify

that no slippage occurred in the grips and to record the strain in the tests. The thickness of each sample was measured using microscopy images of the cross section of the samples which showed an average thickness of 0.635±0.2 mm and an average luminal diameter of 4.18±0.12 mm for the BC tubes.

Given the tubes were preconditioned during the inflation tests, the uniaxial tensile tests were performed immediately following the inflation tests without further preconditioning being performed. A preload of 0.001 N was specified for the tensile test machine as the criterion to initiate recording strain in all tensile tests. The samples were stretched to full failure with a strain rate of 0.25 mm/s, however the dependence of the stress-strain response on strain rate was studied beforehand and proved insignificant. As the samples had the same width within and outside the grips they occasionally broke at the grips due to stress concentrations at the grip edges. Where this occurred the ultimate tensile strength data was disregarded. This limitation was due to the small diameter of the BC tubes rendering preparation of dog bone shaped samples difficult. The stress was determined by dividing the instantaneous load by the original cross sectional area and the stretch value was derived by dividing the instantaneous gauge length by the original gauge length.

5.1.4 Constitutive modelling

The concept of pseudo-elasticity was utilized and the loading response was modelled using a hyperelastic formulation. The following Ogden strain energy function, of order three, for an isotropic incompressible material was implemented (Ogden 1972):

$$\bar{W} = \sum_{i=1}^{3} \frac{2\mu_i}{{\alpha_i}^2}\left(\bar{\lambda}_1^{\alpha_i} + \bar{\lambda}_2^{\alpha_i} + \bar{\lambda}_3^{\alpha_i} - 3\right) \qquad \textbf{Equation 5-1}$$

where $\bar{W}$ denote the isochoric strain energy per unit of reference volume of the incompressible hyperelastic material, $\bar{\lambda}_i$ denotes the deviatoric principal stretches and μ_i and α_i denote the hyperelastic constants which are established based on the uniaxial tensile test data. The nonlinear regression routine available in Abaqus (Simulia, Providence, RI, USA) was

used to determine the model that best fit the tensile test data. Although it is possible to fit to each individual sample, the average characteristic tensile properties of BC is of interest in this study and therefore the average characteristic tensile behaviour was chosen to obtain the hyperelastic constants. No restriction was imposed on the material constants and Drucker stability criteria (Hibbett and Karlsson 1998) available in Abaqus, was utilised to ensure the stability of the model. This confirmed that the second derivative of the strain energy function with respect to strain remained positive definite and that the material model was convex.

5.1.5 Numerical simulations

A FE simulation of the inflation test was carried out based on the constitutive material model established and the results were compared to the results obtained from the experiments. As uniaxial tensile tests are theoretically insufficient to fully characterise the three dimensional response of an isotropic incompressible material, the numerical simulation of the inflation test was used to assess the accuracy of the material model. A 5 cm long cylindrical tube geometry was generated. The thickness and diameter of the tube were defined as 0.635 mm and 4.18 mm respectively, on the basis of the average of those measured from the six bacterial cellulose tubes tested. A uniform luminal pressure ranging from 0 mmHg to 160 mmHg was applied. The tube was fully constrained at the two ends thereby representing the tethering applied experimentally and the expansion of the tube was determined as the outer diameter divided by the initial outer diameter corresponding to zero luminal pressure. The tube was meshed by linear hexahedral elements with reduced integration and hybrid formulation and composed of a total of 47,670 elements with three elements through the thickness, chosen on the basis of a mesh sensitivity study, (see Appendix A-A.2).

5.1.6 Compliance measurement

Diametrical compliance, defined as the inverse of Peterson's elastic modulus and expressed in percent per millimetre of mercury $\times 10^{-2}$, was determined as follows:

$$C = \frac{D_S - D_d}{D_d (P_S - P_d)} 10^4 \qquad \textbf{Equation 5-2}$$

where D_s and D_d are the tube diameter in systole and diastole and P_s and P_d are systolic and diastolic pressures respectively (Tai *et al.,* 2000).

Compliance tests were carried out on five BC tubes. The tubes were tethered longitudinally on the same rig used for the inflation tests applying no longitudinal prestretch. The rig was then connected to a pulsatile flow pump (Harvard Apparatus, USA) and the external diameter of the tubes was measured using the video-extensometer. A pediatric pressure catheter (Abbot, IL, USA) connected to a pressure sensor (DTXPlus, BD, NJ, USA) and an amplifier and monitoring device (TA-100, CWE, PA, USA) were utilised for real time measurement of the intraluminal pressure. The mean luminal pressure was increased from 30 to 120 mmHg in increments of 10 mmHg and the compliance values were determined at each mean luminal pressure by application of a pulse pressure of 60 mmHg amplitude consistent with the experiments carried out by Sarkar *et al.,* (2006).

5.1.7 Cell culture experiments

Bovine aortic SMCs (Coriell AG08504, NJ, USA) were seeded on the luminal and abluminal surfaces of the BC tubes using a rotational seeding technique. The tubes were mounted on the fittings of a custom built bioreactor similar to the rig shown in Figure 5-1 and autoclaved. Later a suspension of SMCs (0.4 million cells/ml) in RPMI 1640 (Sigma R8758) supplemented with 10% fetal bovine serum (Sigma F9665) and 1% Penicillin-Streptomycin (Sigma P4333) was placed into the lumen of the BC tubes and also into the bioreactor space surrounding the BC tube to seed the abluminal surface. The bioreactor was mounted on a rotator and placed in an incubator for 24 hours rotating at a speed of 2 rpm to allow homogeneous and confluent cell

adherence to the BC surfaces. No adhesion molecule was used for SMC culture. Following rotational SMC seeding for 24 hours the bioreactor was connected to a CELLMAX™ flow loop and cultured with a media flow of 10.7 ml/min and a pulsatile pressure of 14-21 mmHg for 28 days in a humidified atmosphere of 95% air, 5% CO_2 and a temperature of 37 °C. The culture medium was changed every 2 days. In addition, in a separate experiment, bovine ECs (Coriell AG08594, NJ, USA) were seeded (125,000 cell/cm^2) on the luminal surface of flat BC samples pretreated for 1 hour with 20 µg/ml fibronectin (Sigma F1141) and were cultured statically for a period of 5 days using the same medium and culture conditions as used for SMCs.

In order to analyse the cell scaffold interaction the samples were vigorously rinsed with phosphate buffered saline to ensure that non-adhering cells were washed off. Samples were then fixed in a 10% buffered formalin solution overnight. The nuclei of the cells on the BC samples were stained using DAPI and the actin filaments were stained using Phalloidin (Sigma-Aldrich, St. Louis, MO). In addition separate samples obtained from the BC tubes with SMCs were embedded in paraffin and sectioned using standard protocols and were stained using hematoxylin (Sigma-Aldrich, St. Louis, MO) and counter stained with Eosin-Y (Sigma-Aldrich, St. Louis, MO). The stained samples were observed using a fluorescent microscope (Olympus BX51) and images were taken using an integrated camera (Olympus DP30BW).

5.2 Results

5.2.1 Uniaxial tensile tests

The stress-strain behaviour of all samples tested was found to be highly nonlinear. The cross section of bacterial cellulose tubes are composed of two distinct inner and outer layers with a denser inner layer and a more porous outer layer (Bäckdahl *et al.,* 2006). The characteristic tensile test curves are comprised of four distinct regions; an initial nonlinear region which extends to the initiation of failure in the inner layer, a second region which is associated with the propagation of failure in the inner layer until rupture of this layer, a third region where only the outer layer remains intact and bears the load until a final region where complete failure occurs, see Figure 5-2. The ultimate tensile strength was determined based on the initial failure of the samples and was found to be 311±29 kPa for all samples that failed within the gauge length of 10 mm.

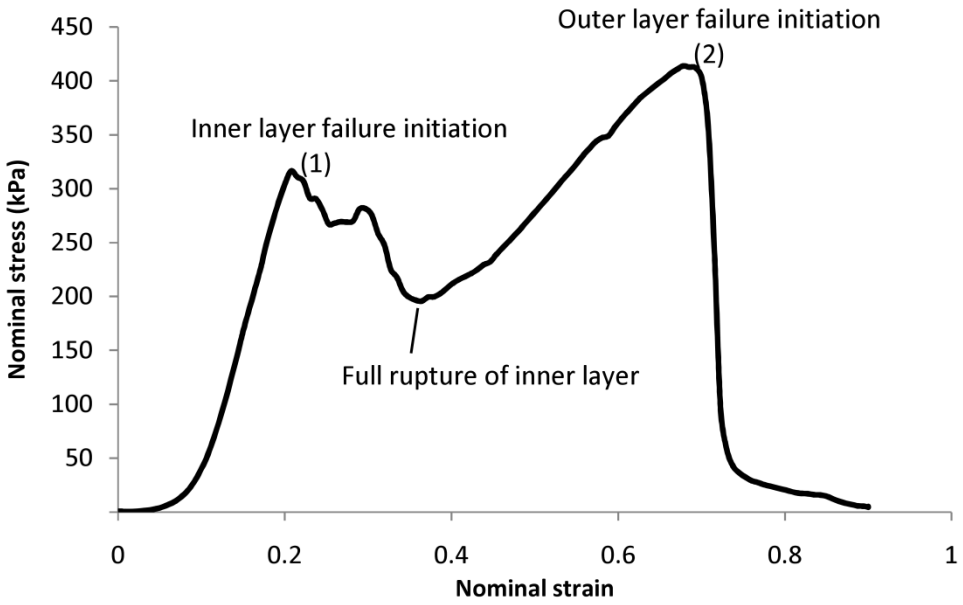

Figure 5-2: Characteristic tensile test curve of bacterial cellulose tubes.

The stress-strain response of the bacterial cellulose shows variation amongst the samples, see Figure 5-3, however a dominant average characteristic behaviour can be seen in samples 3 to 7 with samples 1 and 10 exhibiting the highest and lowest stiffness behaviour, respectively. Axial and circumferential strips did not exhibit different tensile responses which could be due to the absence of a preferred fibre orientation of cellulose fibres. The stress-strain response of bacterial cellulose in uniaxial tensile tests reveals a nonlinear stress stiffening behaviour comprising a toe and a heel region very similar to that of arteries, see Figure 5-3.

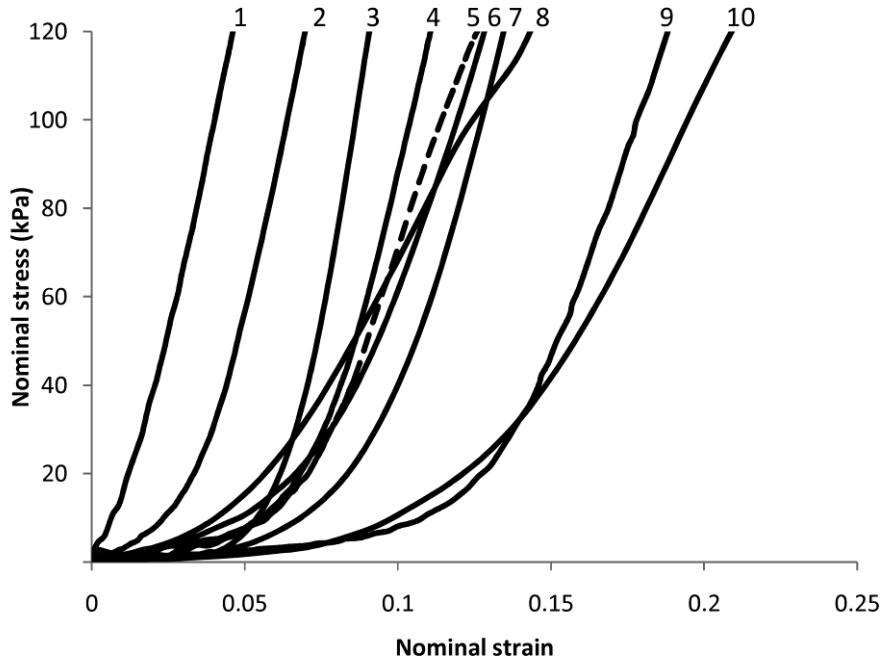

Figure 5-3: Tensile stress-strain response of the preconditioned bacterial cellulose specimens, sample 5 (dashed line) is chosen as the average characteristic curve.

This nonlinear stress stiffening response could be attributed to the gradual recruitment of cellulose fibres upon loading which is analogous to the function of collagen fibres in arteries (Holzapfel 2000b; Holzapfel *et al.,* 2005a). This stress stiffening response is necessary in materials chosen for grafts and tissue engineered scaffolds if the compliance of arteries is to be matched. In contrast, many synthetic graft materials have linear stress-strain behaviour. The stiffness of PTFE, one of the most widely used synthetic graft materials, is significantly higher than that of BC, see Figure 5-4.

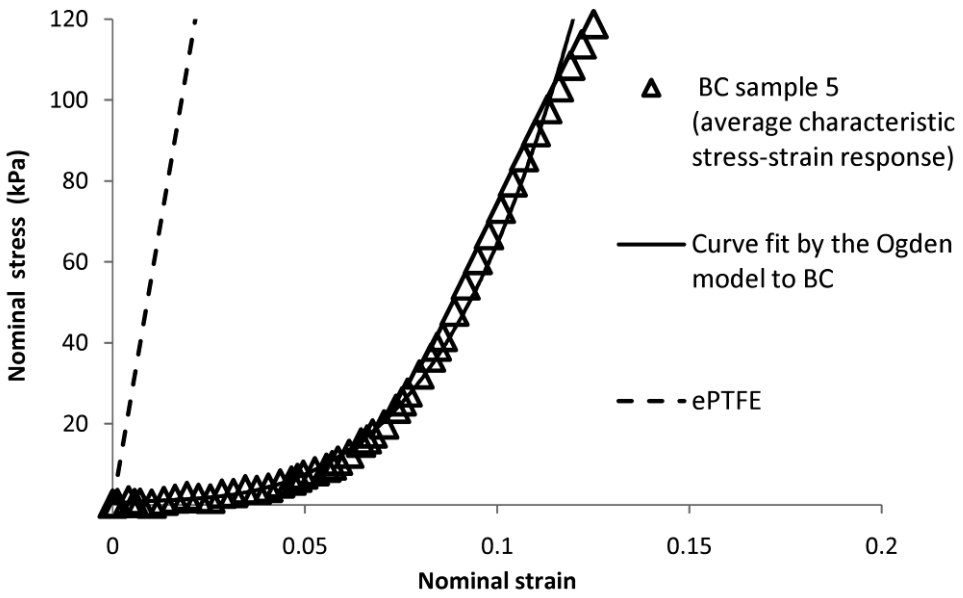

Figure 5-4: Curve fits to the tensile test data by the constitutive model proposed (ePTFE data adapted from Catanese *et al.,* 1999)

5.2.2 Inflation tests and related numerical simulations

Figure 5-5 shows the pressure-expansion curves of inflation tests obtained for six bacterial cellulose tubes. The tests show a nonlinear pressure-expansion response consistent with the uniaxial stress-strain response of the material. The stress-strain curve of sample 5, which exhibits the average characteristic stiffness, was chosen to determine the hyperelastic constants of the constitutive model for BC and the constants that yielded the best fit to the experimental data by least-squares error were determined, see Table 5-1. The fit of the constitutive model to the stress-strain tensile test results is given in Figure 5-4. The average pressure-expansion curve obtained from the inflation tests, along with the pressure-expansion curve calculated from the numerical simulation of the inflation test using the hyperelastic constitutive model, is also shown in Figure 5-5. Clearly the constitutive model proposed captures the nonlinear response of the bacterial cellulose tubes and compares very well with the average experimental inflation test results.

Table 5-1: Hyperelastic constants used for modelling characteristic tensile response of BC tubes (Zahedmanesh *et al.,* 2011a).

Hyperelastic constants	Value
μ_1 (Pa)	-40,841,700.4
μ_2 (Pa)	25,961,863.1
μ_3 (Pa)	14,911,467.2
α_1	6.860,889,05
α_2	8.517,152,27
α_3	3.735,167,42

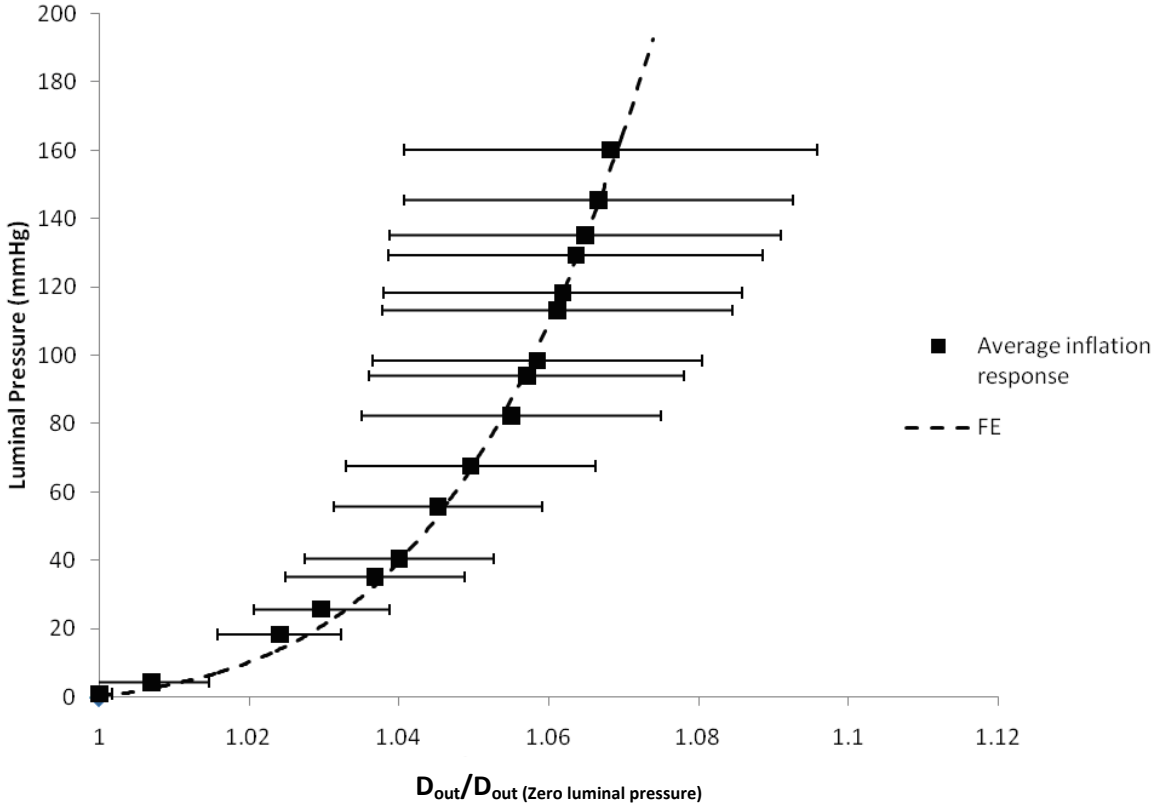

Figure 5-5: Inflation test results and comparison with numerical results. Error bars represent the standard deviation amongst 6 BC tubes.

5.2.3 Compliance tests

Compliance test results of the five bacterial cellulose tubes are demonstrated in Figure 5-6. BC tubes exhibit varying compliance over the mean luminal pressure range of 30 to 120 mmHg and the compliance value lowers with luminal pressure increases. A significant variation in the compliance values of the tubes was observed which is consistent with the variations observed in tensile and inflation test results. The mean measured compliance of the tubes was found to be 4.27±1.51 % per mmHg$\times 10^{-2}$ obtained over a mean luminal pressure range of 30 mmHg to 120 mmHg.

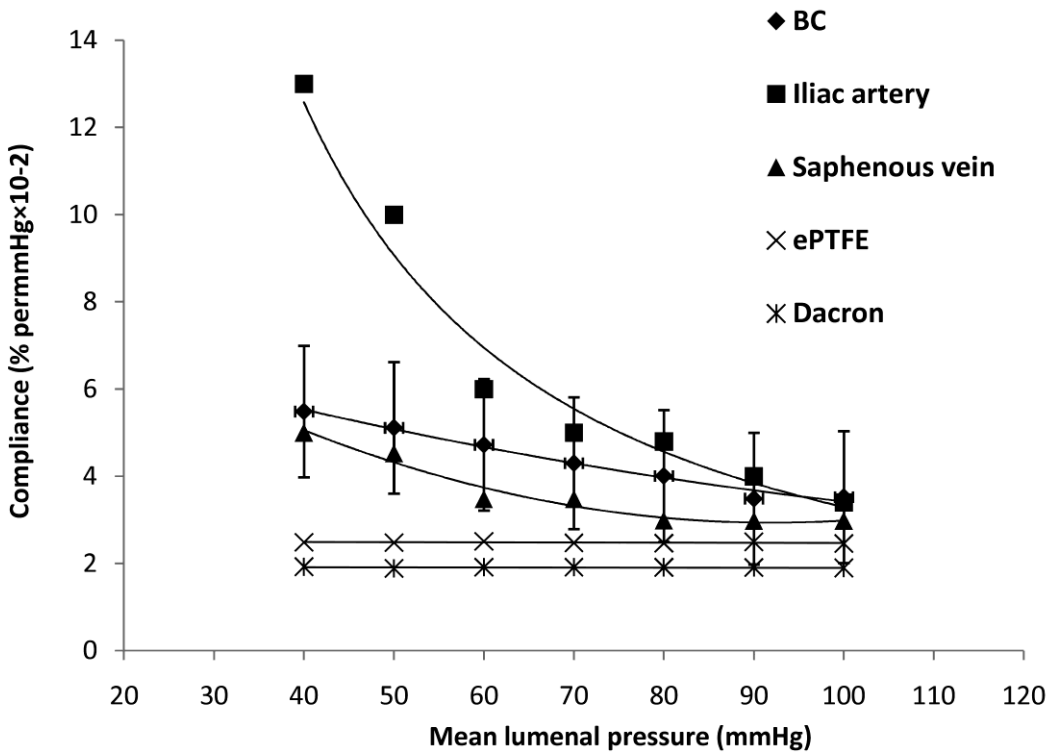

Figure 5-6: Average compliance of the bacterial cellulose tubes in comparison to human iliac artery and widely used grafts. Error bars represent the standard deviation for the five BC tubes. (Saphenous vein, Artery, Dacron and ePTFE data adapted from Sarkar *et al.,* (2006))

5.2.4 Cell culture experiments

Following 28 days of culture, SMCs infiltrated more than 100 µm into the abluminal side of the BC tubes where BC has a more porous structure, see Figure 5-7. In addition the cell culture experiments showed a confluent layer of SMCs adhere on the luminal side of the BC tubes, see Figure 5-8. However, there was no significant SMC infiltration from the luminal side into the BC due to the lower porosity and highly packed fibrous structure on the luminal side of the BC tubes. Also, culture of ECs on the luminal side of the BC tubes resulted in good adhesion to the luminal surface treated with fibronectin following 5 days of culture, see Figure 5-9.

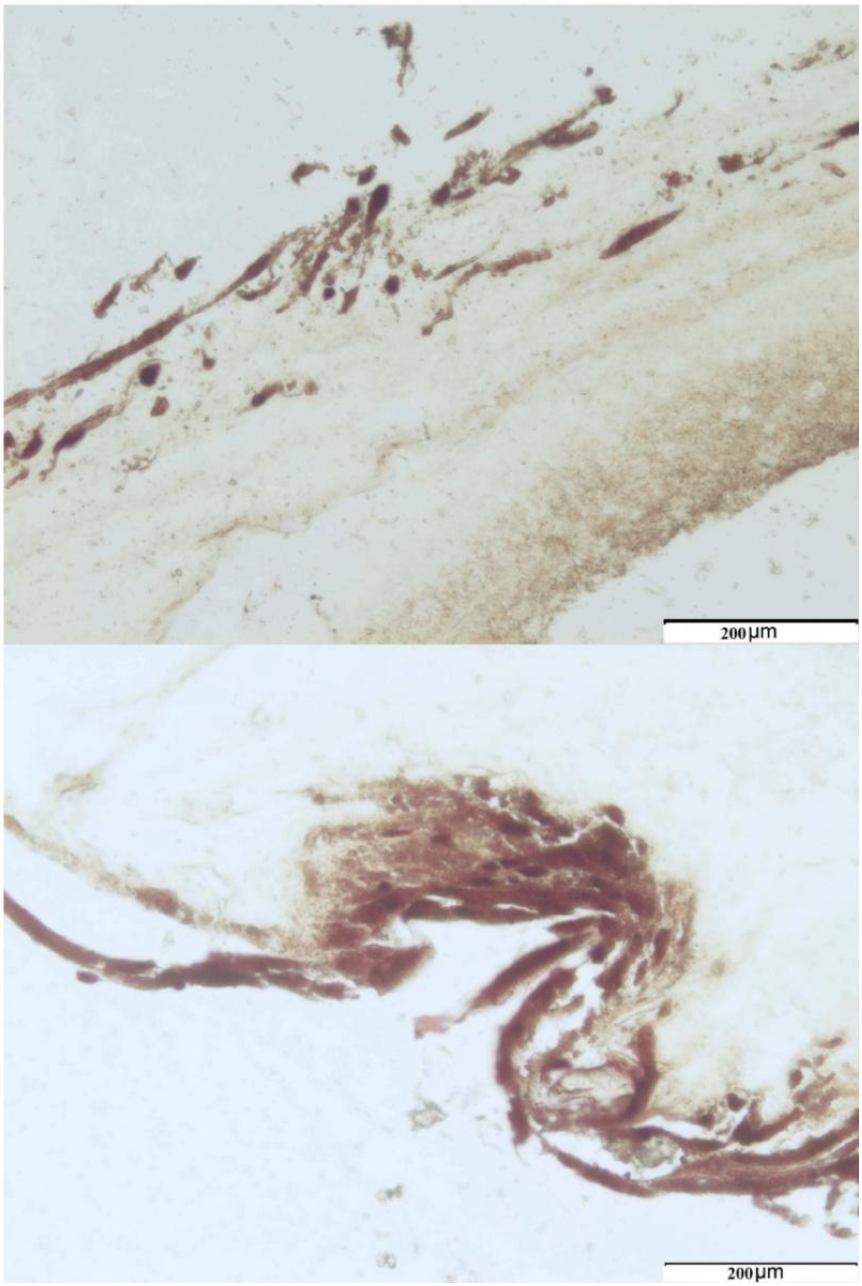

Figure 5-7: Histological images of cross sections of bacterial cellulose tubes (abluminal side) with SMCs cultured for 28 days stained with H&E. The images show more than 100 µm of SMC infiltration into the abluminal side of the BC tubes (Scale bars represents 200 µm).

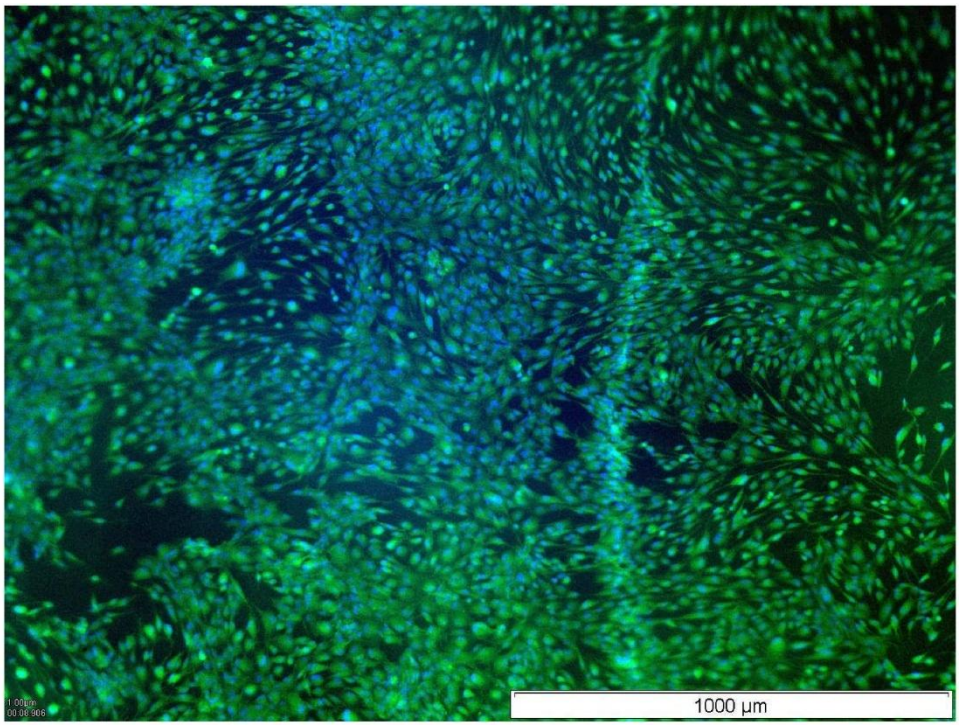

Figure 5-8: DAPI and Phalloidin stained fluorescent image of the luminal surface of a BC tube seeded with SMCs following 28 days of culture.

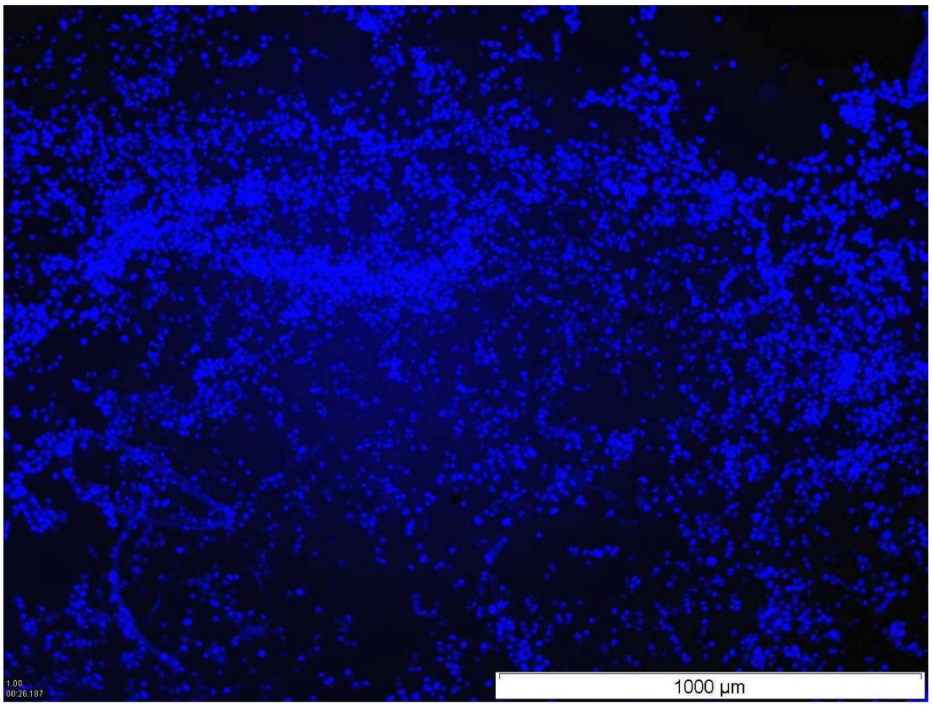

Figure 5-9: DAPI stained fluorescent image of ECs adhering to the luminal surface of a BC sample following 4 days of culture.

5.3 Discussion

To-date the saphenous vein has been the 'gold' standard autograft for bypass procedures due to poor patency of available synthetic grafts, particularly as small calibre vessel substitutes (Catanese *et al.,* 1999). The lack of availability of the saphenous vein in one third of cases due to varicosity, previous use or incompatible calibre (Sarkar *et al.,* 2007b) has encouraged development of vascular grafts and tissue engineered blood vessels. However most grafts suffer from poor patency rates due primarily to thrombogenicity and intimal hyperplasia (IH) (Tai *et al.,* 2000).

Thrombosis formation in vascular grafts depends primarily on the surface properties of the grafts and is due to activation of a cascade of events at the blood-graft interface which ultimately lead to formation of thrombin, a vital component in blood that facilitates cleavage of fibrinogen to fibrin. Fibrin eventually polymerizes to a network that is a main constituent of thrombosis. In a recent study by Fink *et al.,* (2010) the material induced blood coagulation of ePTFE and Dacron, the two most widely used vascular grafts in clinical application, was compared with that of BC and it was concluded that BC induced the least and slowest activation of the coagulation cascade.

Interestingly, the compliance response of bacterial cellulose tubes reveals a behaviour very similar to that of saphenous vein, see Figure 5-6. The compliance of bacterial cellulose tubes lowered from a value of 5.96 % per mmHg$\times10^{-2}$ at a mean luminal pressure of 30 mmHg to 3.15 % per mmHg$\times10^{-2}$ at 120 mmHg which is in fact higher than that of saphenous vein, ePTFE and Dacron. This varying compliance response, characteristic of arteries and saphenous vein, is not exhibited by grafts such as ePTFE and Dacron and may be the key characteristic contributing to graft thrombosis during hypotensive states (Salacinski *et al.,* 2001).

The interaction of bacterial cellulose with vascular cells, such as that demonstrated here for SMCs, may even suggest adaptive remodelling of bacterial cellulose grafts *in-vivo* and hence better compliance matching with host arteries in the long term. This is supported by the work

of Greisler *et al.,* (2004) where cellular ingrowth was found to increase the compliance of woven polyglactin 910 grafts implanted into rabbits. In addition, in the work by Roy *et al.,* (2005) decellularisation of porcine carotid arteries was found to significantly reduce arterial compliance. Production of elastin fibres by vascular cells such as SMCs (Seliktar *et al.,* 2003; Patel *et al.,* 2006) in the remodelling process of BC grafts could further improve their compliance response in the long term following implantation. The similarity of the cellulose fibre structure in BC with the collagen network in arteries suggests that elastinogenesis in the remodelling process in BC grafts could create a similar structure to arteries. Elastin fibres would then bear the load at lower pressures allowing for high extension while the cellulose fibres would be progressively recruited with the increase of luminal pressure, functioning like collagen fibres in arteries and therefore enhancing the compliance response. This speculation however, needs to be investigated by *in-vitro* and *in-vivo* implantation experiments. Studies have shown that production of extracellular matrix components in tissue engineered scaffolds serve to improve the ultimate tensile strength and suture holding properties of the tissue engineered blood vessels (Xu *et al.,* 2008) and consequently given its biocompatibility, BC may serve as an excellent candidate for tissue engineering if not as a graft. The biodegradability of BC in a physiological environment, however, remains to be investigated by *in-vivo* experiments in order to better understand the long term evolution of its mechanical properties following implantation.

The pressure-inflation response of the FE model based on the established constitutive model is shown in Figure 5-4. By comparing the numerical simulation results and the experimental results of inflation it can be seen that the numerical model does capture the characteristic response of the BC tubes during inflation. Although the constitutive model is based on the average characteristic tensile behaviour of BC, the numerical model of the inflation captures the characteristic response of BC tubes on inflation and the presented approach can be applied to the stress-strain curves obtained from each tube to predict the response of the related tube upon inflation. Considering the ready availability of accurate constitutive models for most host

arteries in the literature numerical models of BC-artery anastomosis can be now used to design BC grafts with optimum geometrical and tensile properties to achieve the highest compliance matching with different host arteries and also to assess the anastomotic stresses in order to minimise the risk of graft failure or injury in the host arteries, see Figure 5-10. One may notice the comparably higher stresses within the intimal layer of the host coronary artery due to the layer specificity of the model and the higher load bearing capacity of the intima in the aged human coronary arteries, see Figure 5-10.

The inflation and compliance test data shown exhibit considerable variation in the data, consistent with the variations observed in the tensile test data, and these variations demonstrate that the fabrication parameters for the BC need to be more precisely controlled.

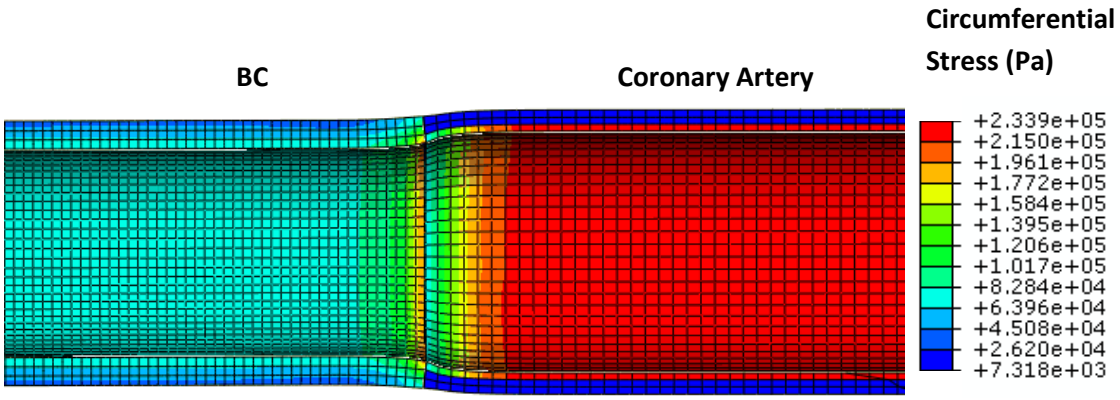

Figure 5-10: Circumferential stresses in a BC-Coronary artery anastomosis model under a luminal pressure of 120 mmHg, the unloaded diameter and thickness of the BC tube and the coronary artery were matched. (Layer specific properties were used for the coronary artery using the constitutive model outlined in Chapter 3 and 4)

Chapter 6

A multi-scale mechanobiological modelling framework using agent based models and finite element analysis; Application to vascular tissue engineering

Computational models of mechanobiological systems have been widely used to provide insight into these systems and also to predict their behaviour. In this context vascular tissue engineering benefits from further attention given the challenges involved in developing functional low calibre vascular grafts with long term patency. In this study a novel multi-scale mechanobiological modelling framework is presented which takes advantage of lattice free agent based models coupled with the FEM to investigate the dynamics of VSMC growth in vascular tissue engineering scaffolds. The results illustrate the ability of the mechanobiological modelling approach to capture complex multi-scale mechanobiological phenomena. Specifically, the framework enabled the study of the influence of scaffold compliance and loading regime in regulating the growth of VSMCs in vascular scaffolds and their role in development of intimal hyperplasia (IH). The mechanobiological framework presented provides a robust platform for testing hypotheses in vascular tissue engineering and lends itself to use as an optimisation design tool.

5.4 Mechanobiological Model

5.4.1 Mechanobiological model overview

A mechanobiological modelling framework was developed which comprised of two main coupled modules, (i) a module based on the FEM that quantifies cyclic strain (ε_{cyc}) and pore fluid velocity (V_{fluid}) as the main regulators of VSMC growth in TEBVs and (ii) a biological modelling module based on an agent based model which simulates the key responses of VSMCs growth, i.e. migration, proliferation, apoptosis and ECM synthesis in the vascular scaffold under the influence of the mechanical stimuli quantified in the FE module, see Figure

6-1. In the FE module the value of cyclic strain (ε_{cyc}) is calculated as the amplitude of the maximum principal strain at each element's centroid and the pore fluid velocity (V_{fluid}) was also calculated at each element's centroid as the mean fluid velocity throughout the loading cycle**.** The simulation starts in the FE module and the quantified values of the mechanical stimuli, i.e. (ε_{cyc}) and (V_{fluid}), are transferred to the agent based model where the growth of VSMCs is simulated under the influence of the mechanical stimuli. Following the agent based simulation of cell growth and ECM synthesis, the geometry, boundary conditions and mechanical properties of the tissue engineered construct are updated and the updated model is submitted to the FE module in order to take the influence of remodelling of mechanical properties due to cell growth into account. This iterative approach is repeated until the simulation reaches the desired simulation end time, see Figure 6-2. Given that the two modules are loosely coupled, it is essential to ensure that each iteration's time period is small enough to ensure that changes of mechanical properties are insignificant during each iteration's time period. Therefore, in this study each iteration's time period was set to two days which was chosen based on a sensitivity analysis, (see Appendix A-A.3).

A custom written routine was developed using python programming language to enable communication between the FE software Abaqus (Simulia, Providence, RI, USA) and the agent based modelling framework BREVE (www.Spiderland.org). The same routine also handled the tasks necessary for updating the input files of the FE analysis and data mining and processing. The agent based model was programmed using the STEVE language specific to the BREVE agent based modelling framework.

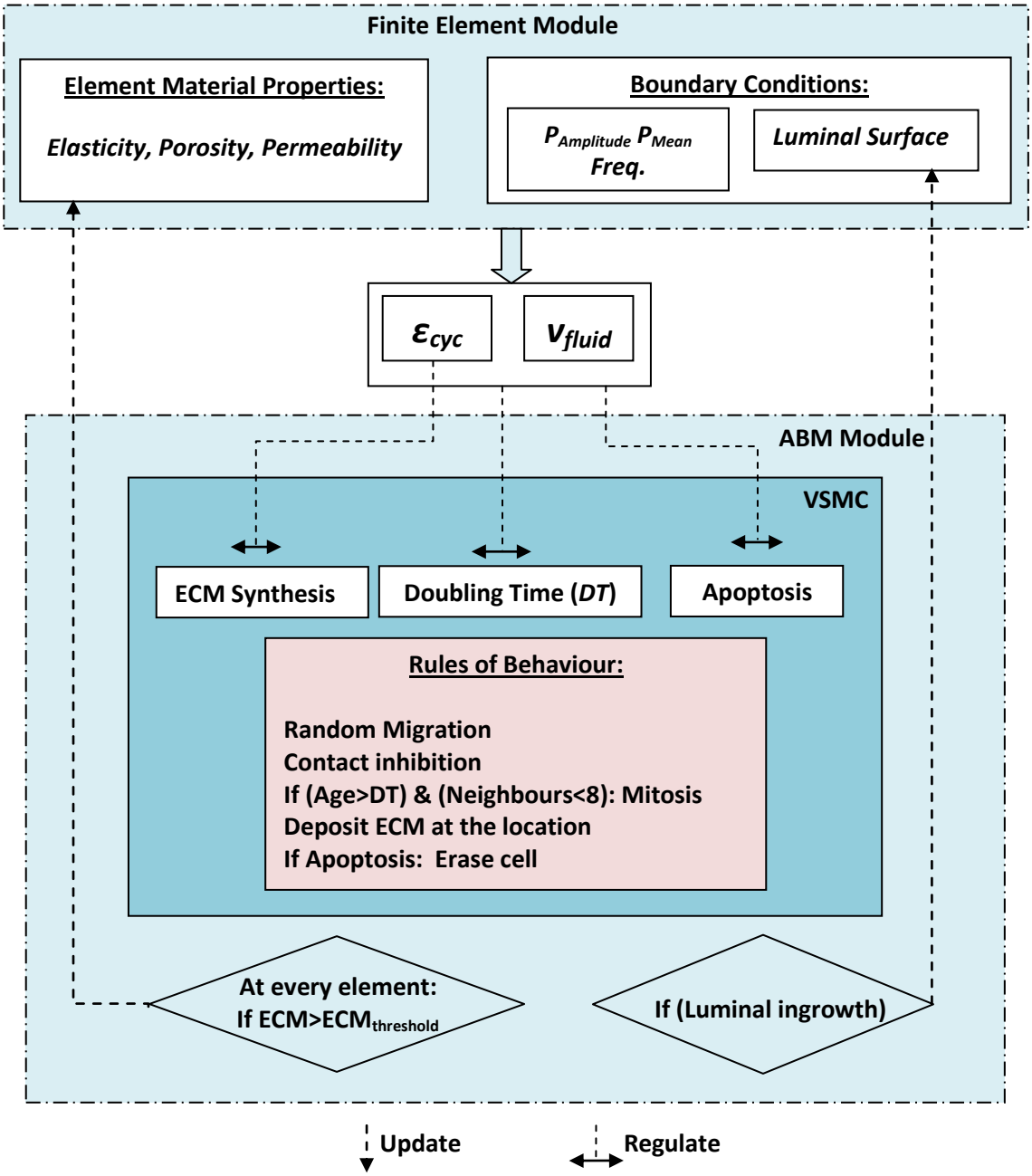

Figure 0-1: Detailed system diagram of the components and processes involved in the mechanobiological model. Mechanical stimuli quantified in the FE module regulate the doubling time, apoptosis rate and ECM synthesis of VSMCs in the ABM model. The mechanical properties of each finite element and also the new luminal surface are then updated based on the value of ECM synthesised in each element.

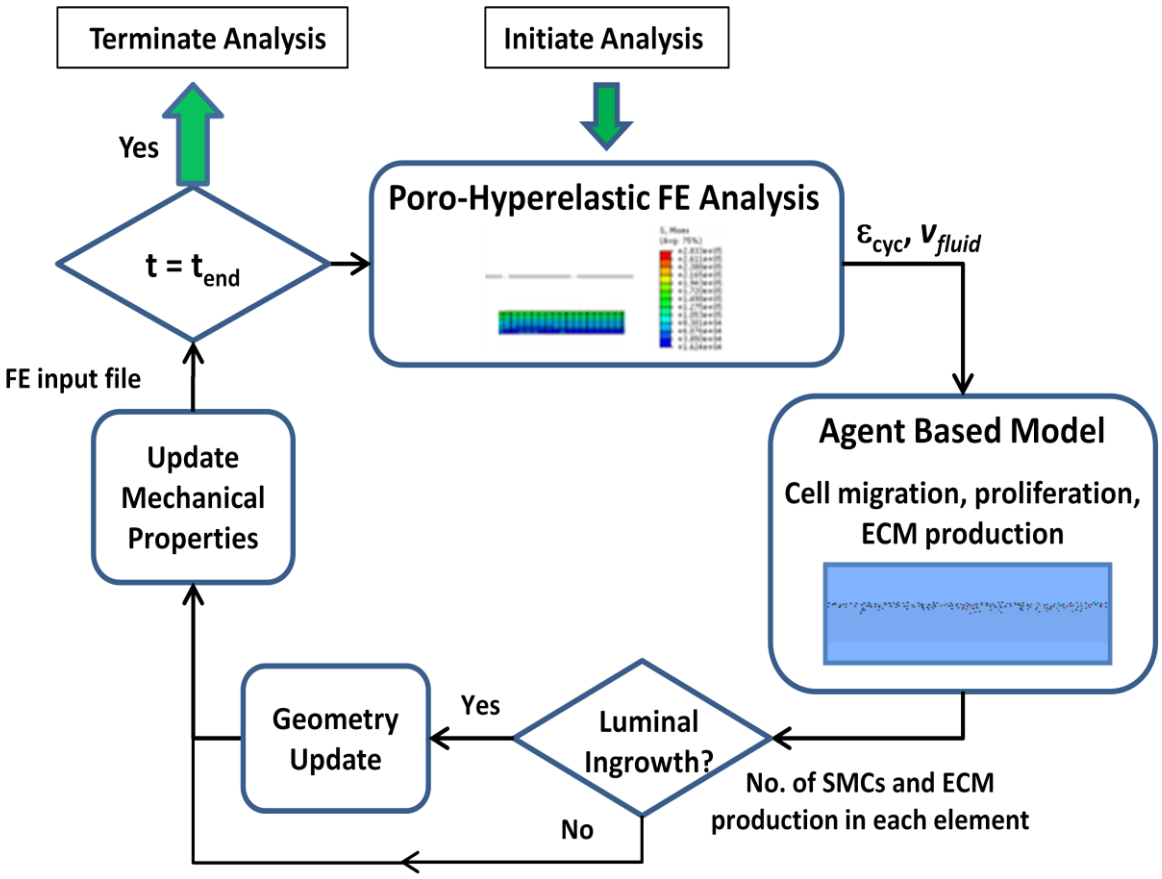

Figure 0-2: Overall schematic of the mechanobiological modelling framework, the simulation starts with a FE analysis where mechanical stimuli are quantified and then the ABM determines the VSMC growth under the influence of the mechanical stimuli. Following the ABM, the FE model is updated and the iterative approach continues until the simulation end time is achieved.

5.4.2 Finite element module

An axisymmetric poro-hyperelastic FE model of a tubular scaffold was used to quantify the cyclic strain (ε_{cyc}) and the pore fluid flow velocity (V_{fluid}) in the tissue engineered construct. Pressure and pore pressure boundary conditions were applied to the luminal surface of the tissue engineered construct depending on the lumen pressure while the two ends were longitudinally tethered and the pressure and pore pressure boundary conditions were set to zero (relative to the ambient pressure) at the abluminal surface. The model is composed of (11780) equilateral rectangular axisymmetric elements (Abaqus type CAX4RPH), 8740 of which are inactivated luminal elements that are added to the mesh connectivity upon VSMC proliferation into the luminal elements and synthesis of ECM. The python code could

automatically detect the new luminal surface and apply the pressure and pore pressure boundary condition to the new surface following each iteration. The tube was 8 mm long with a thickness of 0.673 mm and a luminal diameter of 4.18 mm, which was chosen based on dimensions of bacterial cellulose tubes used in Chapter 5 and published in Zahedmanesh *et al.,* (2011a) which have shown good potential for vascular tissue engineering. The model was discretised by 190 elements longitudinally and 62 elements radially. This mesh density was chosen based on mesh sensitivity studies (see Appendix A-A.3).

Poro-hyperelastic models couple the behaviour of the solid phase and the fluid phase of the material both of which are considered as incompressible. The approach employed in (Feenstra *et al.,* 2009 and Ayyalasomayajula *et al.,* 2010) was adopted which is based on an effective stress concept where an additive decomposition of the stress caused by external loading, $\bar{\sigma}$, into an effective stress on the matrix of the tissue, σ, and an isotropic pore pressure, P, is used as follows:

$$\bar{\sigma} = \sigma + P\mathrm{I} \qquad \textbf{Equation 0-1}$$

The pore pressure drives the pore fluid velocity field under the assumption of Darcy's flow (Darcy 1856) as:

$$V = \varphi V_{fluid} = -\mathrm{K}\nabla p \qquad \textbf{Equation 0-2}$$

where V is referred to as the effective fluid velocity, φ is the porosity of the material, V_{fluid} is the pore fluid velocity, K is the permeability of the material and p is the pore pressure (Feenstra *et al.*, 2009), see Table 6-1.

Table 0-1: Porosity and permeability values used in the simulations. Scaffold porosity and permeability for the remodelled scaffold were adapted from data in Koshiba *et al.,* (2007) and Feenstra *et al.,* (2009) respectively. The bare scaffold data is based on experiments on bacterial cellulose arterial scaffolds.

*(In Abaqus the permeability values should be input with dimensions (L/T) (Abaqus analysis user's manual v6.8), i.e. $\mathrm{k(m/s)} = \rho.\mathrm{g.K(m^4/N.s)}$, where ρ is the density of the wetting liquid, $1.05 \times 10^3\ \mathrm{kg/m^3}$, and g is the magnitude of the gravitational acceleration, $9.8\ \mathrm{m/s^2}$. Hence for the bare scaffold, $\mathrm{k} = 2.9 \times 10^{-9}\mathrm{(m/s)}$ and for the remodelled scaffold, $\mathrm{k} = 5.9 \times 10^{-12}\mathrm{(m/s)}$).

Scaffold	Initial Porosity of the Scaffold, φ_0	*Permeability of the Scaffold, K $(m^4/N.s)$
Bare scaffold	0.86	2.8e-13
Remodelled Scaffold	0.5	5.7e-16

The porosity in turn is a function of the determinant of the deformation tensor, J, and the initial (unloaded) porosity of the material, φ_0, as follows:

$$\varphi = 1 - J^{-1}(1 - \varphi_0) \qquad \textbf{Equation 0-3}$$

In order to calculate the effective stress, the following Ogden hyperelastic equation was used to model the stress-strain response of the scaffolds and IH tissue (Ogden 1972) considering them to be incompressible.

$$\overline{W} = \sum_{\mathrm{i}=1}^{3} \frac{2\mu_\mathrm{i}}{{\alpha_\mathrm{i}}^2}(\bar{\lambda}_1^{\alpha_i} + \bar{\lambda}_2^{\alpha_i} + \bar{\lambda}_3^{\alpha_i} - 3) \qquad \textbf{Equation 0-4}$$

Where, $\overline{W}$ denote the isochoric strain energy density, $\bar{\lambda}_\mathrm{i}$ denotes the deviatoric principal stretches and μ_i and α_i are the hyperelastic constants, see Table 6-2.

Table 0-2: Coefficients of the Ogden hyperelastic constitutive models (Zahedmanesh and lally 2009; Zahedmanesh *et al.,* 2011a)

Hyperelastic constants	Low compliance Scaffold	Arterial compliant scaffold
μ_1 (Pa)	-40,841,700.4	-1,231,144.96
μ_2 (Pa)	25,961,863.1	785,118.59
μ_3 (Pa)	14,911,467.2	453,616.46
α_1	6.860,889,05	16.59
α_2	8.517,152,27	16.65
α_3	3.735,167,42	16.50

Two types of scaffold were defined: a low compliance scaffold and a scaffold with a compliance similar to that of arteries (arterial compliant scaffold). The stress-strain response of a bacterial cellulose scaffold was chosen for the low compliance scaffold (Zahedmanesh *et al.,* 2011a) and the stress-strain response of human coronary medial layer was opted for the compliant scaffold (Zahedmanesh *et al.,* 2009). Where luminal ingrowth occurred, the mechanical properties of human coronary media were assigned to the luminal elements given that it is mainly composed of VSMCs, see Figure 6-3 and Table 6-2.

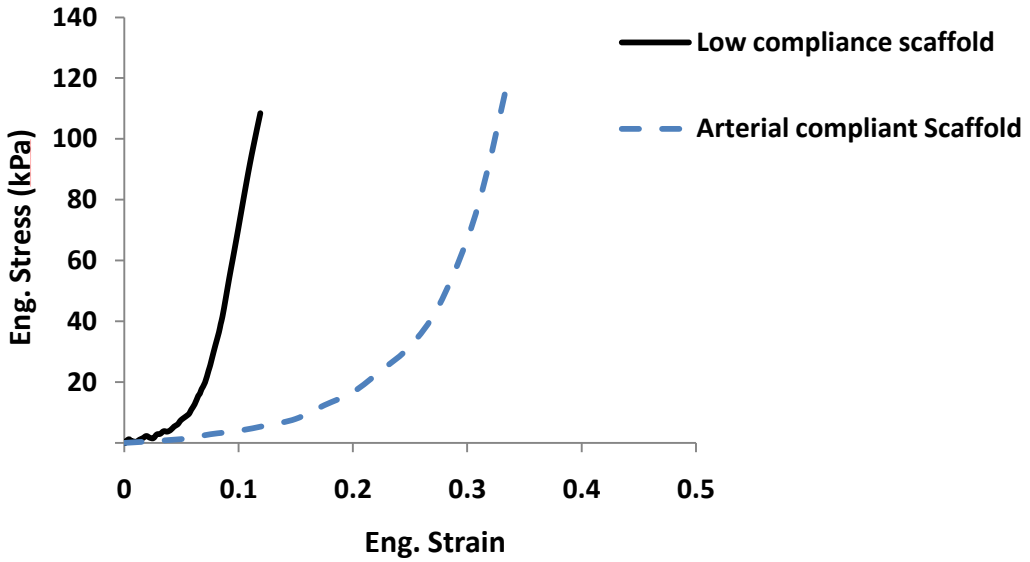

Figure 0-3: Stress-strain response of the low compliance scaffold (Zahedmanesh *et al.,* 2011a), arterial compliant scaffolds adapted from (Holzapfel *et al.*, 2005)

Once cells populate a scaffold they should ideally change its mechanical properties, such as compliance and permeability, to that of the native artery. Several scaffolds have shown this response such as in the study by Greisler *et al.,* (2004) where cell growth was found to increase the compliance of woven polyglactin 910 grafts implanted into rabbits and the study by Song *et al.,* (2010) which showed a lowering of initial stiffness of the Poly(Trimethylene Carbonate) scaffolds following VSMC culture. In addition, in the work by Roy *et al.,* (2005) decellularisation of porcine carotid arteries significantly reduced arterial compliance. Therefore remodelling of the mechanical properties of the scaffolds was represented by altering the initial mechanical properties of the scaffold i.e. stress-strain response, permeability and porosity to that of

arterial tissue (i.e. human coronary media given that media is mainly populated by VSMCs) in elements where the ECM content reached a threshold value of $ECM_{Threshold}$. In addition, the luminal elements were also activated when their ECM content reached $ECM_{Threshold}$. This element activation only concerned the FE model and for the agent based model all grid elements were available from the beginning. The collagen content in a native artery is approximately 3.1×10^{-4} μg/cell (Hahn *et al.,* 2007). Based on the dimensions of each finite element used in this study and dimensions of each VSMC, a maximum of two VSMCs can reside in each element. Hence a value of 6.2×10^{-4} μg/element is the arterial collagen content for each element in this study.

The remodelling threshold value $ECM_{Threshold}$, was chosen as 3.1×10^{-4} μg/Element which represents half the arterial collagen content per element given that once the ECM content in the construct is higher than this value its mechanical properties are more similar to arteries than the original scaffold.

5.4.3 Agent based module

An agent based model of VSMCs seeded confluently on the luminal and abluminal surfaces of a vascular scaffold was constructed by assigning one row of cells (250 cells distributed homogeneously) to the luminal and abluminal surfaces respectively. Following the FE analysis the values of the mechanical stimuli at each element of the FE model are exported to the ABM module. In the agent based model, for each mechanical quantity i.e. ε_{cyc} and V_{fluid}, a matrix $A_{i,j}$ is defined where i=the number of FE elements in the longitudinal direction and j=the number of FE elements in the radial direction. Each component of the matrix takes the value quantified at the centroid of the corresponding FE element. Hence at each point in the ABM domain, the value of the corresponding mechanical stimuli can be queried by referring to the related matrix component based on the coordinates of the point. This way the FE mesh domain could be easily super imposed on the ABM domain. The time step for the ABM simulations was set to 1 hour given that the experimental data used on cell processes such as cell migration and proliferation were obtained on a per hour basis.

5.4.3.1 Cell Migration

The agent based model was a lattice-free model and VSMCs were modelled as spheres with a radius equivalent to the average equivalent radius of VSMCs consistent with the approach taken in (Caiazzo *et al.,* 2009) in which VSMCs were modelled as spheres in a lattice free agent based model of coronary restenosis. VSMCs could migrate in a random walk fashion over the ABM domain, see Table 6-3. The same method used for super imposing the values of mechanical stimuli on the ABM domain was used to define the values of ECM synthesised by VSMCs throughout the ABM domain.

Table 0-3: Parameter values used for migration speed, dimension and ECM synthesis of VSMCs

Parameter	value	unit	Description and reference
VSMC migration speed	0.001	mm/hr	DiMilla *et al.,* (1993)
VSMC radius	12.96	μm	Adapted from Peirce *et al.,* (2004) ($6\times88\mu m^2$)
$ECM_{Threshold}$	0.00031	μg/element	ECM threshold for remodelling into arterial tissue. Adapted from Hahn *et al.,* (2007)
$ECM_{dep\text{-}baseline}$	1.12e-7	μg/cell.hr	Baseline ECM synthesis per hour. Adapted from Hahn *et al.,* (2007)

5.4.3.2 Cell Proliferation

Proliferation was modelled by defining *doubling time* for each individual cell consistent with the approach taken in the ABM model presented in (Peirce *et al.,* 2004). Each created cell records its age and once the age of the cell equals its doubling time the cell undergoes mitosis if there is a vacancy surrounding the cell. The age of the created daughter cells is then initiated at 0. Doubling time of VSMCs was defined in hours as a function of cyclic strain ε_{cyc} and pore fluid velocity V_{fluid} as follows:

$$Doubling\ Time\ (\varepsilon_{cyc}, V_{fluid}) = f(\varepsilon_{cyc}) + g(V_{fluid}) \qquad \textbf{Equation 0-5}$$

Where $f(\varepsilon_{cyc})$ determined the effect of cyclic strain on the doubling time of VSMCs and was derived from the experimental work by Colombo (2009) as defined by the following equation, see also Figure 6-4.

$$f(\varepsilon_{cyc}) = 13871.25\varepsilon_{\mathrm{cyc}}^2 - 48.225\varepsilon_{\mathrm{cyc}} + 43.257 \qquad \textbf{Equation 0-6}$$

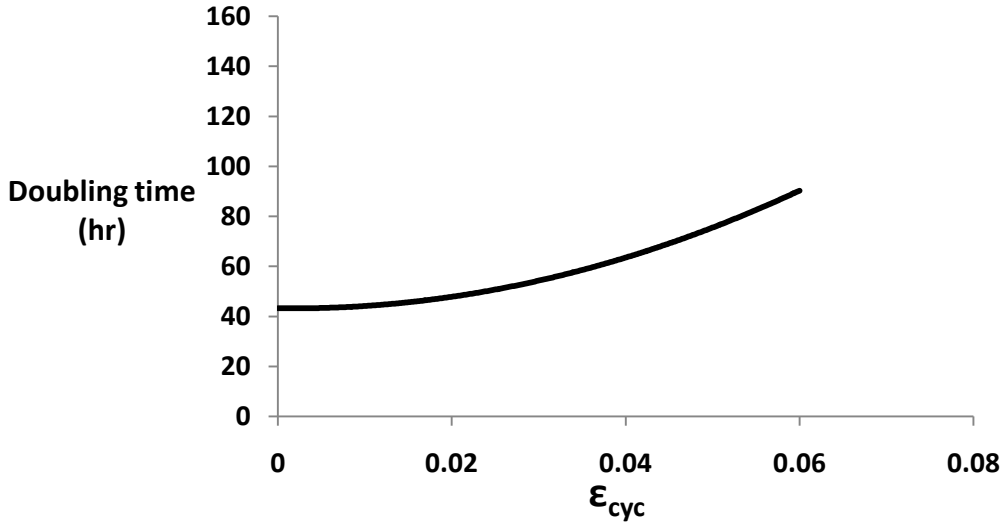

Figure 0-4: The influence of cyclic strain on the overall doubling time of VSMCs with maximal nutrient availability and waste removal.

Cartmell *et al.,*, (2003) studied the influence of pore fluid velocity on cell proliferation using a perfusion bioreactor for scaffold inlet flow rates of 0.01, 0.1, 0.2 and 1 ml/min (Cartmell *et al.,* 2003). The inlet flow rates were converted to pore fluid velocity using an analytical method where the mean pore pressure velocity within the scaffold was calculated using the following equation consistent with the approach taken in (Stops *et al.,* 2010; Jungreuthmayer *et al.,* 2009):

$$V_{fluid} = \frac{Q}{\pi \varphi r^2} \qquad \textbf{Equation 0-7}$$

Where V_{fluid} is the pore fluid velocity, Q is the external inlet flow rate, φ is the scaffold porosity and r in the chamber radius (Cartmell *et al.,* 2003).

The contribution of pore fluid velocity to the overall doubling time of VSMCs was then described using the data obtained from (Cartmell *et al.,* 2003) which presents the fold change in DNA content using the aforementioned flow rates and the static doubling time of VSMCs based on Jeong *et al.,* (2005) by the following phenomenological equation, see also Figure 6-5:

$$g(V_{fluid}) = 3.594 + 165.4 \times e^{-1075000 \times V_{fluid}} \qquad \textbf{Equation 0-8}$$

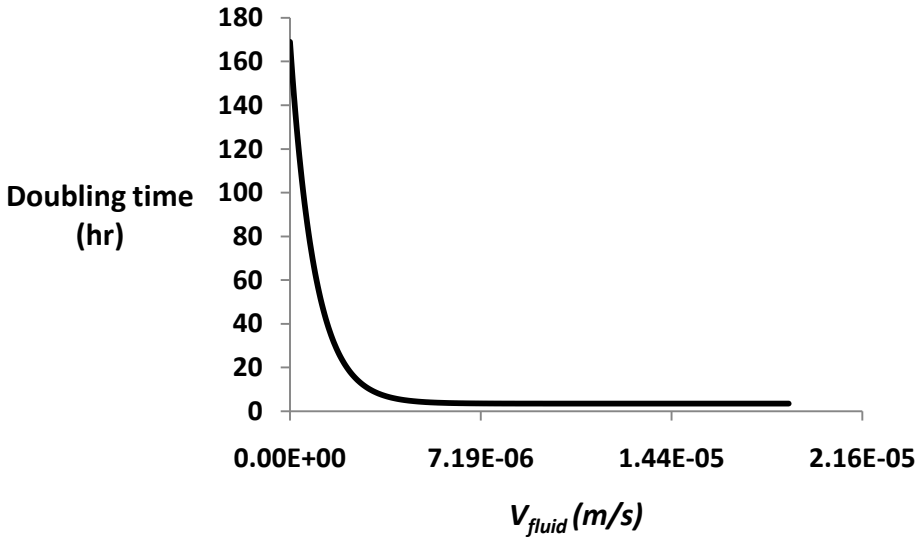

Figure 0-5: The influence of pore fluid velocity on the overall doubling time of VSMCs.

5.4.3.3 Cell death

Similar to the proliferation rate, apoptosis rate of VSMCs is dictated by the value of cyclic strain that the cells are exposed to (Colombo 2009) and the availability of nutrients and waste removal. Therefore the probability of apoptosis for each VSMC was defined as a function of the value of the cyclic strain and pore fluid velocity and the apoptotic cells were removed from the simulation following every iteration. The apoptosis rate reported in experimental studies determines the probability of apoptosis for each cell. A logical statement using a random number generator was defined within each cell which had a probability equivalent to the apoptosis probability of each cell. Where the statement was true the cell was removed. The following function was used to describe the probability of apoptosis for each VSMC:

$$Apoptosis(\%) = k(\varepsilon_{cyc}) + l(V_{fluid}) \qquad \textbf{Equation 0-9}$$

where $k(\varepsilon_{cyc})$ described the influence of cyclic strain on the apoptosis of VSMCs based on the data obtained from the experimental study by Colombo (2009) where the influence of cyclic strain on VSMC apoptosis was studied in an environment with maximal availability of nutrients and waste removal, see also Figure 6-6:

$$k(\varepsilon_{cyc}) = 80.35 \times \varepsilon_{cyc} + 0.357 \qquad \textbf{Equation 0-10}$$

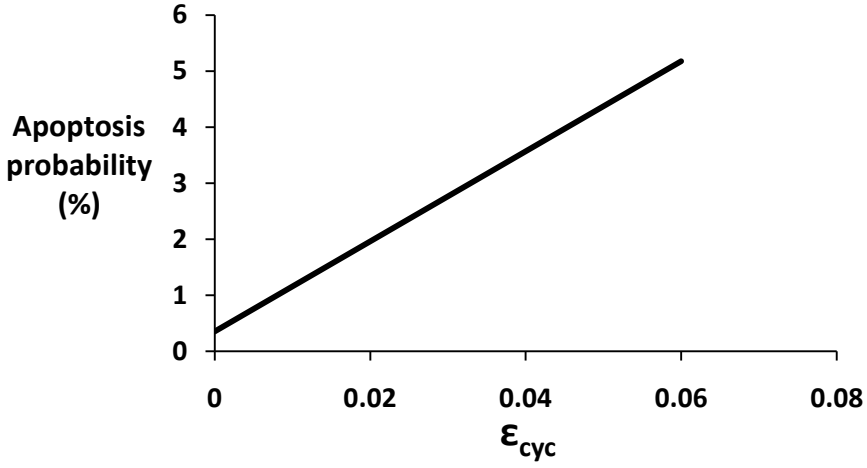

Figure 0-6: The influence of cyclic strain on the overall apoptosis of SMCs with ample availability of nutrients.

and $l(V_{fluid})$ described the influence of pore fluid velocity on Apoptosis of VSMCs based on the experimental data on VSMC number in static culture in a fibre matrix (Stankus *et al.,* 2006) and assuming an optimal pore fluid velocity above which cell death due to nutrient shortage and waste accumulation would not occur (Cartmell *et al.,* 2003) as follows, see also Figure 6-7:

$$l(V_{fluid}) = \begin{cases} -1808066.759 \times V_{fluid} + 13 & V_{fluid} < 7.19\text{E-}06\ (\mathrm{m/s}) \\ 0 & V_{fluid} > 7.19\text{E-}06\ (\mathrm{m/s}) \end{cases}$$

Equation 0-11

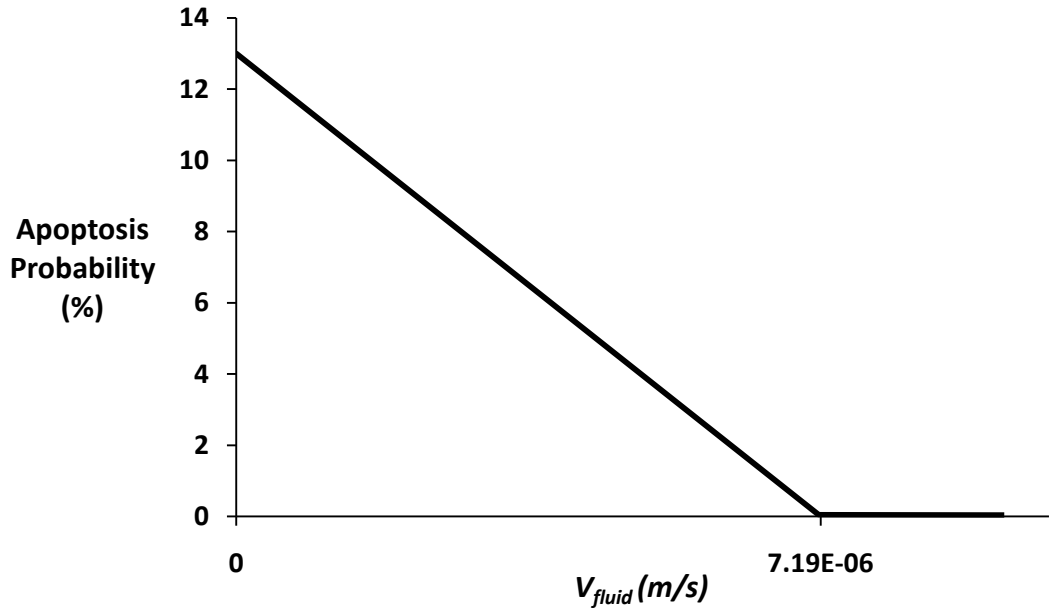

Figure 0-7: The influence of pore fluid velocity on the overall apoptosis of VSMCs.

5.4.3.4 Protein synthesis

At each time step of the simulation each cell deposited ECM with an amount of ($ECM_{deposition}$) representing the amount of collagen synthesis by VSMCs per hour at the corresponding FE element. It has been shown that cyclic strain upregulates synthesis of ECM by VSMCs. In the study by Kona *et al.,* (2009) collagen production in VSMCs was found to increase two-fold when the cells were exposed to 10% cyclic strain. Therefore a linear relation was assumed between the ECM synthesis and the value of the cyclic strain as follows in Equation 6-12:

$$ECM_{deposition}(\varepsilon_{cyc}) = ECM_{dep-baseline} + 10 \times (ECM_{dep-baseline} \times \varepsilon_{cyc}) \qquad \textbf{Equation 0-12}$$

Where, $ECM_{dep-baseline}$ is the baseline collagen synthesis per hour by VSMCs in static condition and ε_{cyc} is the value of the cyclic strain, see Table 6-3.

5.5 Application of the mechanobiological model

The following three main scenarios were simulated using the developed mechanobiological modelling framework in order to shed light on the influence of loading regime, remodelling of mechanical properties and the scaffold compliance on VSMC growth dynamics, scaffold remodelling and development of IH in TEBVs, see Figure 6-8.

(i) VSMCs were seeded on an arterial compliant scaffold and cultured under hypotensive (50-80 mmHg), normotensive (80-120 mmHg) and hypertensive (140-200 mmHg) luminal pressure and luminal pore pressure to investigate the role of loading regime for both *in-vivo* and *in-vitro* applications.

(ii) VSMCs were seeded on an arterial compliant scaffold and cultured under a pulsatile luminal pressure and pore pressure of 80-120 mmHg with a frequency of 1Hz vs. a non-pulsatile pressure of 100 mmHg to study the influence of pulsatile flow in *in-vitro* applications.

(iii) VSMCs were seeded on low compliance vs. arterial compliant scaffold and cultured under a pulsatile luminal pressure and luminal pore pressure of 80-120 mmHg with a frequency of 1Hz to study the influence of scaffold compliance for *in-vivo* and *in-vitro* applications.

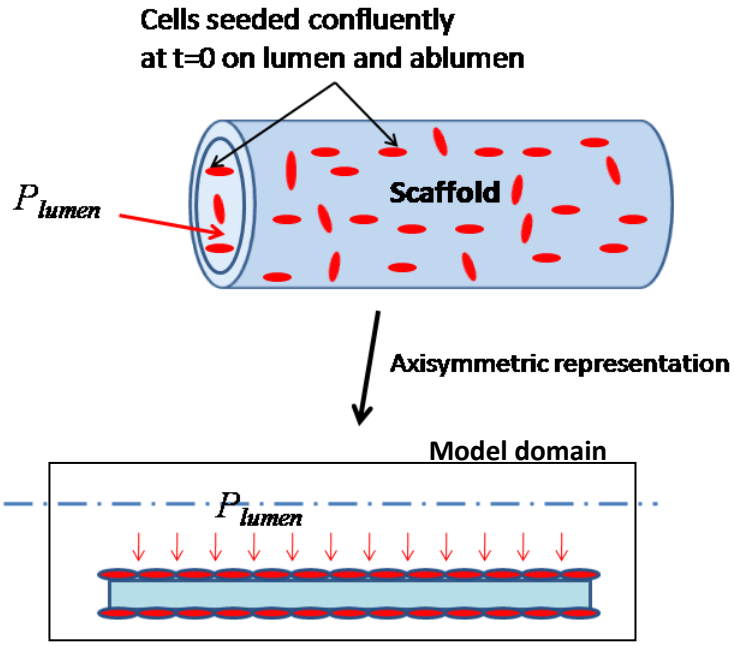

Figure 0-8: Schematic of the modelled tubular scaffold.

5.6 Results

The mechanobiological model enabled the influence of compliance and also the loading regime on growth dynamics of VSMCs in vascular scaffolds to be studied. The wall clock time for each simulation could reach up to 20 hours depending on the boundary conditions using a 2GHz processor and single core processing. The results clearly show that mechanical factors i.e. loading regime and scaffold compliance play a key role in regulating the growth of VSMCs.

Comparison of the influence of the three loading regimes of hypotensive, normotensive and hypertensive in scenario (i) in all three cases revealed a response composed of a toe and hill region where the number of cells increased to a peak value of 12 fold where the curve subsequently reached a plateau. At this stage the scaffold was fully packed with cells in all three cases, see Figure 6-9. Following 100 days, however, the cell number started to increase in all three cases. This increase in the cell number coincided with activation of luminal elements given that the amount of extracellular matrix produced in these elements exceeded the element activation ECM threshold.

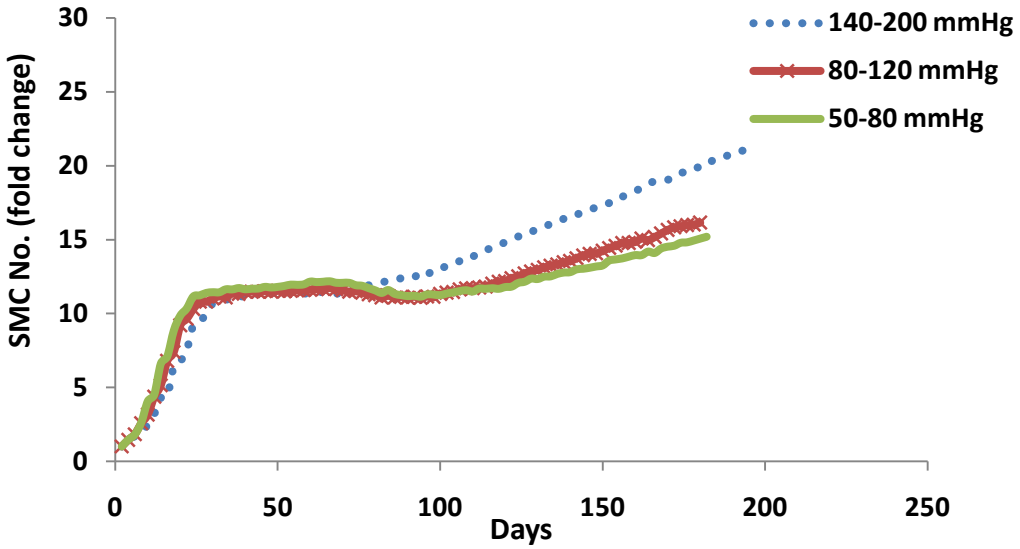

Figure 0-9: The results of scenario (i). Influence of pulsatile pressure on the number of viable cells over time in the arterial compliant scaffold, three loading regimes of hypotensive (50-80 mmHg), normotensive (80-120 mmHg) and hypertensive (140-200 mmHg) were compared.

The main difference in cell number among the three cases, however, started to emerge following this point where the cell number was highest in the hypertensive case and lowest in the hypotensive regime with values of 20 fold and 15 fold at day 180 respectively.

Figure 6-10 shows the alterations of pore fluid flow velocity and cyclic strain where the arterial compliant scaffold was subject to normotensive pulsatile pressure. It can be seen that pore fluid flow velocity, an indicator of nutrient transfer and waste removal, was reduced as the cells grew and populated the scaffold. One can notice concentrated zones of high pore fluid velocity at day 66 in elements which have a lower ECM content due to the randomness in the ABM. Given that the permeability of these elements was higher than the remodelled elements, fluid flow founds its way through these elements and hence zones of high fluid velocity were temporarily created at these elements. However, these elements were soon remodelled leading to a more homogeneous pore fluid velocity field. With the initiation of luminal ingrowth, the pore fluid velocity in the scaffold reduced even further given that the activated luminal elements further hindered fluid flow through the scaffold. At day 180 the pore fluid flow velocity in the core of the scaffold reduced to 0.3 μm/sec which is more than 99% reduction compared to day 0.

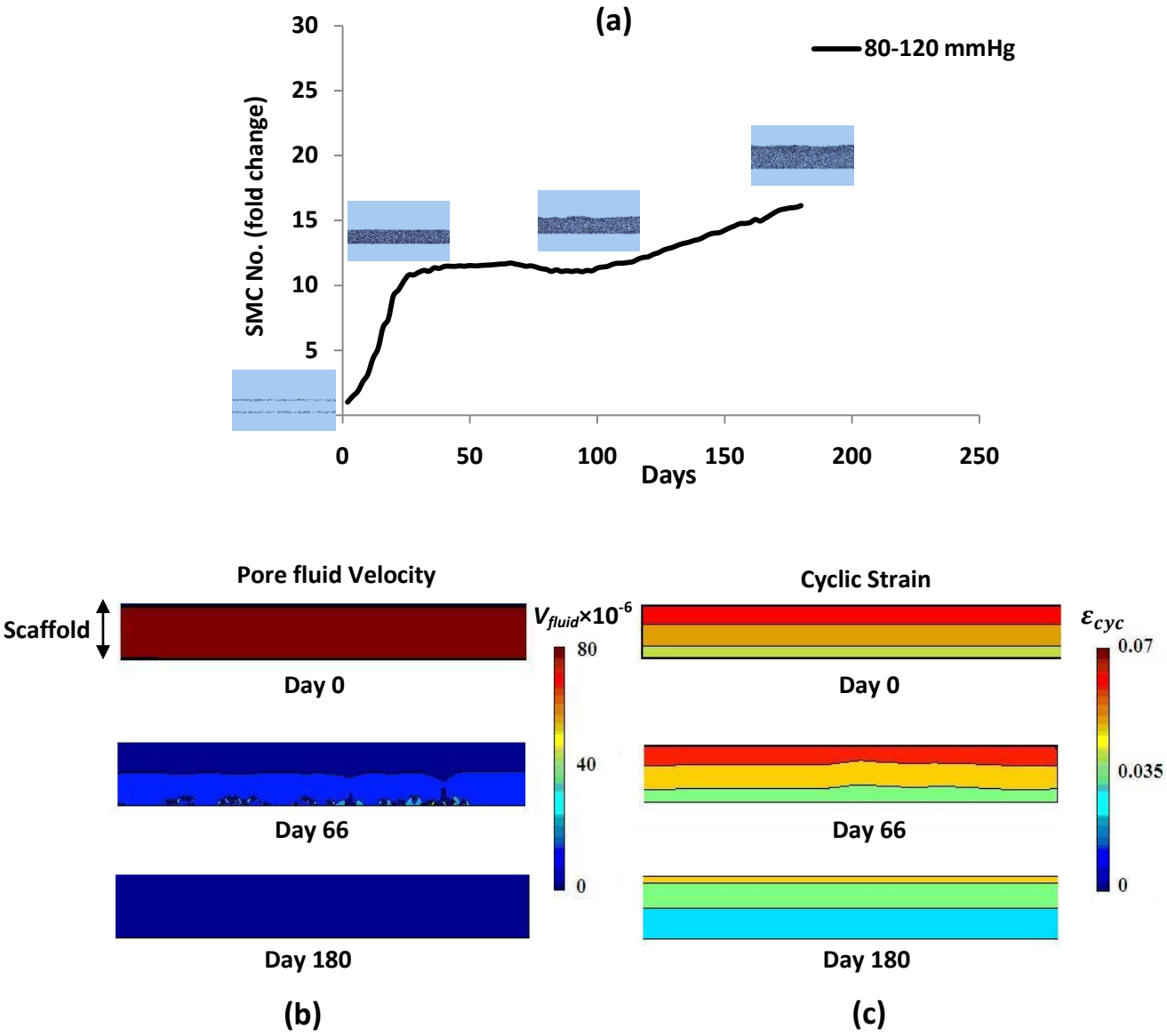

Figure 0-10: Influence of pore fluid velocity and cyclic strain on the cell number where the arterial compliant scaffold was subject to normotensive pulsatile pressure. (a) cell number evolution for 180 days. (b) mean medium flow velocity alterations throughout the 180 days.

Interestingly, the value of cyclic strain reduced 42% from a maximum initial value of 0.07 at day 0 to a value of 0.04 at day 180 which was due to the thickening of the TEBV wall following luminal ingrowth. Scenario (ii) on the other hand elucidates the role of pulsatile flow on VSMC growth dynamics. In this scenario the loading regime was changed from a pulsatile pressure of 80-120 mmHg to a constant non-pulsatile pressure of 100 mmHg. In the absence of cyclic strain the number of cells increased 31 fold in a period of 160 days with a positive slope showing that under this condition cells will continue to proliferate towards the lumen until the

vessel is fully occluded, see Figure 6-11. In stark contrast is the case with pulsatile luminal pressure where the number of cells was considerably lower and increased to a maximum of 14.8 fold in the same period. Figure 6-11 depicts the ABM domain showing the viable cells and also the amount of collagen synthesised by VSMCs in the scaffold and in the lumen. One can notice that the thickness of the TEBV is doubled where it was cultured under the static luminal pressure of 100mmHg compared to the pulsatile luminal pressure of 80-120mmHg. Interestingly, the amount of collagen synthesised within the scaffold was higher where the TEBV was subject to pulsatile luminal pressure compared to the static case with maximum values of 8×10^{-4} µg/element and 5×10^{-4} µg/element respectively. This is consistent with the findings of most *in-vitro* studies such as Hahn *et al.,* (2007) and Jeong *et al.,* (2005) which show enhanced collagen synthesis in pulsatile flow culture. The values of the collagen content are also consistent with the collagen content in arteries as discussed in the previous section.

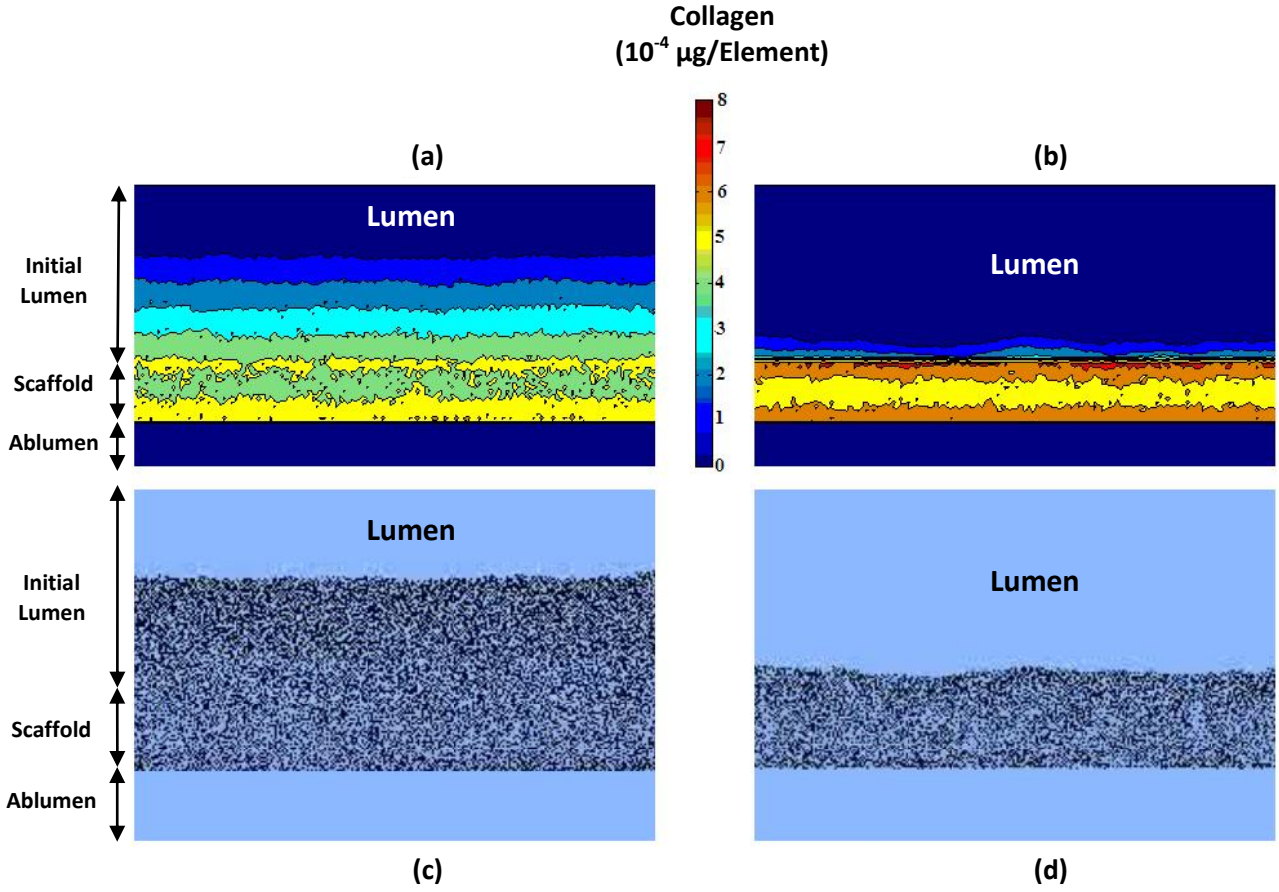

Figure 0-11: Results of scenario (ii). ECM synthesis and viable VSMCs at day 160 (a,c) the TEBV was cultured under static pressure of 100 mmHg (b,d) the TEBV was cultured under pulsatile pressure of 80-120mmHg.

In scenario (iii) the role of scaffold compliance was studied where a low compliance scaffold and the arterial compliant scaffold were compared. Consistent with the outcome of clinical studies which suggest low compliance of vascular grafts contributes to IH (Salacinski *et al.,* 2001), our results showed a significantly higher number of cells and luminal ingrowth using the low compliance scaffold. In the arterial compliant scaffold a plateau region in the cell number curve was achieved for a 75 day interval between the scaffold being fully populated with cells and the start of luminal ingrowth, following which the cell number started to increase slightly. In stark contrast, in the low compliance scaffold the cell number constantly increased and reached a value of 26 fold following 180 days of culture, see Figure 6-12.

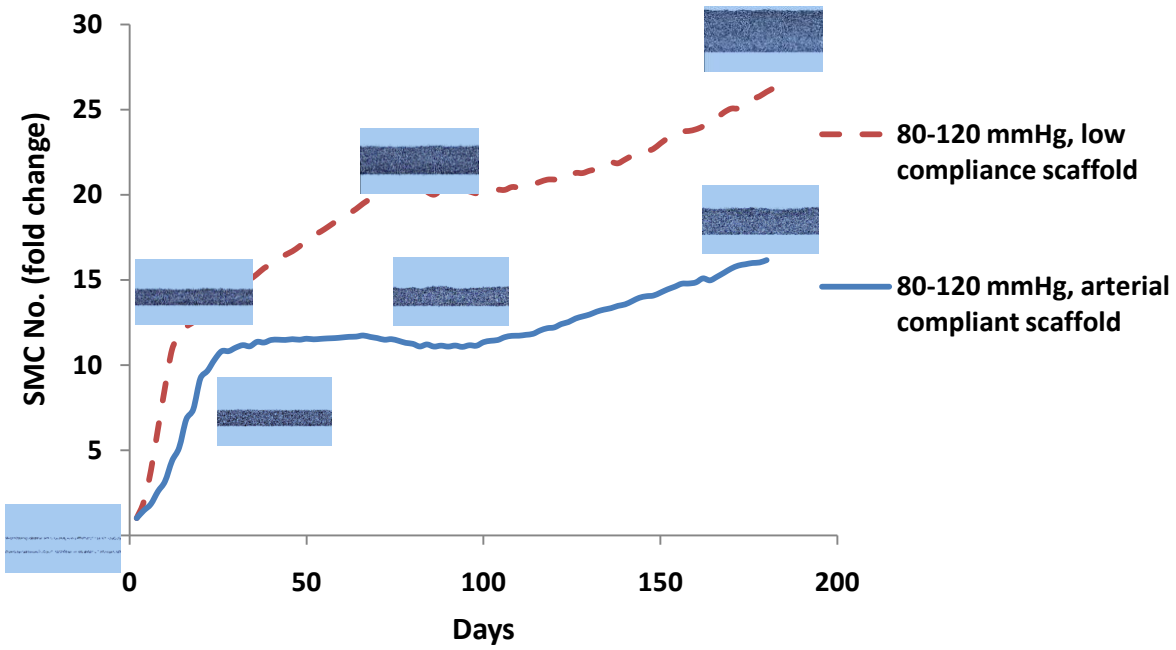

Figure 0-12: Results of scenario (iii) where the influence of scaffold compliance was studied.

5.7 Discussion

We have developed a mechanobiological modelling framework by coupling a lattice free agent based model with a FE model that can simulate growth of VSMCs in a TEBV and tissue remodelling. The framework allows the role of mechanical factors such as scaffold compliance and the loading regime on VSMCs growth to be explored. It also elucidates the significant regulatory role that mechanical factors play in vascular tissue engineering which can determine the fate of a TEBV and also highlights their role in development of IH.

One important advantage of the *in-silico* mechanobiological models is their capability to identify the role of each individual parameter involved in the complex multi-scale mechanobiological problems such as vascular tissue engineering. Given the numerous parameters involved in such systems and their intertwined role, it is often difficult to isolate the dominant cause and determine the contribution of each parameter to a specific behaviour using *in-vivo* or even *in-vitro* experiments. *In-silico* mechanobiological models enable the contribution of each of the involved parameters to the tissue level behaviour to be quantified in isolation. The current study illustrates a very good example in this context. The predicted nonlinear cell growth response, which is characterised by an increase in cell number to a peak value and a subsequent reduction in VSMC growth, is also observed in *in-vitro* cell culture studies on VSMC culture in compliant vascular scaffolds (Jeong *et al.,* 2005), however, the timescale of such experimental studies is limited to a few months at best and therefore they do not provide much data on luminal ingrowth and IH. It is known that the reduction in the permeability of the scaffold, the value of cyclic strain and also cell-cell contact, all play significant roles in VSMC growth dynamics, however, when they are all involved in the system, the contribution of each factor may not be easily quantified without a computational model. Even the influence of cyclic strain cannot be easily determined since although cyclic strain has an anti-proliferative and pro-apoptotic effect on VSMCs (Colombo 2009), it can also enhance the medium flow in a scaffold and hence improve the proliferation rate. The value of cyclic strain can alter along with cell growth due to the remodelling of mechanical properties of the

TEBV and also thickening of the TEBV wall. Therefore, determining the role of cyclic strain on a TEBV is a challenging task, yet the presented mechanobiological model provides considerable insights in this respect.

Several studies have highlighted the role of compliance on the development of IH and long term patency of vascular grafts (Salacinski *et al.,* 2001). Graft compliance can influence development of IH in two distinct ways, (i) perturbations of blood flow and shear stress and formation of recirculation and flow separation zones which can increase the particle residence time and hence increase the luminal concentration of mitogenic factors such as PDGF that stimulate luminal ingrowth of VSMCs (Lemson *et al.,* 2000; Salacinski *et al.,* 2001), and (ii) the low value of cyclic strain exerted on VSMCs in a graft increases their proliferation rate which leads to IH. It's a very challenging task to determine the contribution of each of these two different factors in the development of IH using *in-vivo* experiments. *In-vitro* experiments can also be challenging in this respect since IH is a long term process and *in-vitro* experiments can be very time consuming, laborious, expensive and prone to the risk of contamination when conducted over long timescales. However, the present mechanobiological model enables the influence of cyclic strain on IH to be studied in isolation over a long time scale which is one of its important advantages.

In this context, the results of scenario (i) clearly show that any subtle decrease of cyclic strain can initiate a maladaptive path towards occlusion of the TEBV due to IH. Indeed cyclic strain played a synergic role given that low cyclic strain contributed to more luminal ingrowth which in turn reduced the cyclic strain further and thereby expedited patency loss. Although using an arterial compliant scaffold with a normotensive pulsatile luminal pressure leads to a steady state cell number for up to 100 days, without an endothelium, VSMCs will still eventually grow into the lumen. Therefore, even though the results elucidate the determining role of biomechanics in vascular tissue engineering, they also highlight the significance of the endothelium and the need for vascular scaffolds with high endothelialisation rates. Such

insightful trends would be difficult to ascertain, even qualitatively, using *in-vitro* experiments, while the presented model enables quantitative evaluation of the influence of each parameter. Interestingly, the results of scenario (i) show that under a hypertensive luminal pressure the VSMC luminal ingrowth is higher compared to normotensive and hypotensive loading regimes. Given that the difference in cell number among the three cases emerged following 84 days by which the scaffold was fully populated by cells, this observation corroborates clinical studies which suggest that hypertension causes thickening and stiffening of arteries (London *et al.,* 2004). This was mainly due to the stress-stiffening response of the scaffold and IH tissue which stiffen at higher pressures and therefore undergo 22% lower cyclic strain in the hypertensive pressure compared to the normotenstive pressure.

The results of scenario (ii) and (iii) both signify the role of cyclic strain in regulating the remodelling of tissue engineered blood vessels and development of IH. In scenario (ii) the absence of cyclic strain due to bioreactor flow type (i.e. pulsatile vs. non-pulsatile flow) is studied while in scenario (iii) low cyclic strain due to mechanical properties of the scaffold is studied which can be deciphering both for *in-vivo* and in-*vitro* applications. As shown in Figure 6-11, the amount of extracellular matrix produced in the vascular scaffold is higher where a pulsatile flow culture was used. This is very interesting given that the cell number and luminal ingrowth were maintained considerably lower when pulsatile flow culture was used and one might presume that due to the higher cell proliferation in the non-pulsatile culture, ECM synthesis and therefore remodelling should be enhanced, whilst counter-intuitively the pulsatile flow enabled to maintain the cell number and IH at a considerably lower level and in the mean while enhance ECM synthesis and remodelling of the scaffold. Obviously this is due to the fact that cyclic strain increases ECM synthesis by each VSMC and also the fact that IH tissue which is lower in the pulsatile flow culture functions as a barrier to nutrient flow through the vessel which reduces cell growth in the scaffold while luminal cells receive ample nutrients to continue their ingrowth and increase IH level. In scenario (iii), the IH level is higher in the low compliance scaffold as expected intuitively, however one can notice that in the

lower compliance scaffold IH continues to increase even after cells populated and remodelled the scaffold. This is due to the fact that in the low compliance scaffold a higher level of luminal ingrowth occurred from the onset of growth which accounted for IH formation and therefore an increase in the thickness of the vessel, see Figure 6-12. Hence, in spite of the fact that the mechanical properties were remodelled to the more compliant arterial properties after being populated by cells, in the low compliance scaffold the added thickness due to IH reduced the cyclic strain value in comparison to the compliant scaffold where cell ingrowth was minimal from the onset of growth.

In order to highlight the influence of pore fluid velocity on VSMC growth, the arterial compliant scaffold was cultured under normotensive pulsatile pressure while pore fluid velocity was set to zero in Equations 6-8 in an artificial case to isolate the influence of pore fluid velocity in cell proliferation. The results showed a considerably lower VSMCs growth rate in the initial phase of the curve which prolonged the period of time required to fully populate the scaffold by cells. This reduced cell growth rate was maintained throughout the culture period as a lag in growth signifying the influence of pore fluid velocity on growth of VSMCs by enhancing nutrient transfer and waste removal, see Figure 6-13.

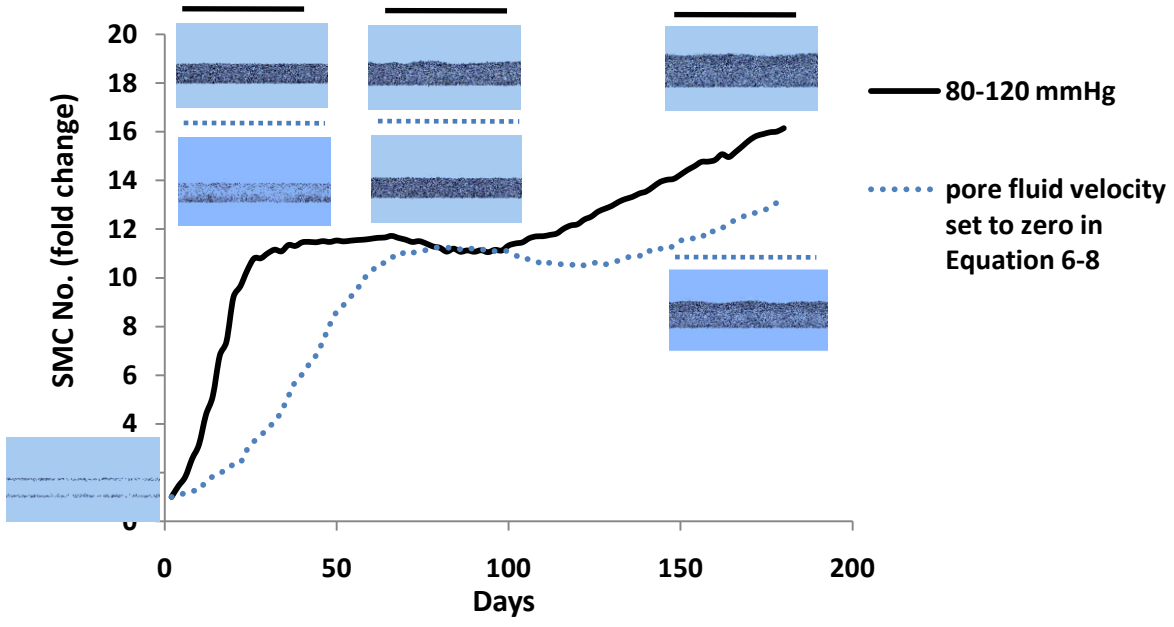

Figure 0-13: The influence of pore fluid velocity on VSMC growth dynamics. Pore fluid velocity was set to zero in Equation 6-8 to reveal the influence of pore fluid velocity.

The results also demonstrate the capability of the presented mechanobiological model to pinpoint an optimal tissue engineering approach that would yield the best results following implantation of a scaffold or in the *in-vitro* cell culture experiments. The simulations show that the optimal scaffold for vascular tissue engineering should have a compliance similar to arteries to minimise IH and enhance ECM synthesis and remodelling. In addition the results show that production of ECM at levels consistent with arterial tissue can take up to 6 month under optimal biomechanical conditions. Therefore one can conclude that in the context of scaffold design, the degradation of a vascular scaffold in the first 6 month period should be minimised to reduce the risk of failure. On the other hand in the context of *in-vitro* cell culture experiments the results imply that in order to enhance cell growth and reduce culture time an initial non-pulsatile luminal pressure can be used until cells fully populate the scaffold, following which a pulsatile luminal pressure can enhance ECM synthesis and scaffold remodelling.

The results clarify an important potential application of the model which is to serve as a platform to test existing hypotheses and also generate new hypotheses in vascular tissue engineering. The outcome of the simulations can then help to design new *in-vitro* experiments, reduce the experimentation costs, and come up with new tissue engineering strategies through identification of the most significant parameters involved which are informed by the *in-silico* model.

Also from a methodological standpoint, this study presents a novel, yet simple approach to achieve more realistic mechanobiological simulations utilizing agent based models by means of a straight forward method to couple the available ABM frameworks with FE packages. The usefulness of ABMs to investigate higher level patterns originating from local cell-environment interactions makes them ideal for tissue engineering applications. ABMs can provide insight into mechanisms which drive complex observed phenomena that are not easy to test in the laboratory and combining them with FEM can significantly increase their applicability and problem solving potential in mechanobiology.

In spite of the robustness and novelty of the developed mechanobiological modelling framework, the simulations presented in this study have their own limitations. No experimental data was used to directly validate the results of this study; however, every parameter employed was calibrated with published experiments. Pore fluid flow velocity is taken as the indicator of nutrient transport in the TEBV. Although this is a plausible approach as discussed earlier in the introduction and is adopted by other studies such as in Stops *et al.,* (2010), this study could benefit further from a more sophisticated model of nutrient transport and waste removal by solving advection-diffusion equations for the most important biochemicals i.e. glucose, oxygen and lactate. However, this would add tremendous complexity to the current model and was deemed beyond the scope of this study. While the influence of pore fluid flow on VSMCs is interpreted in the context of its effect on nutrient transport and waste removal, it can also influence cell behaviour through wall shear stress. Wall shear stress due to the luminal flow of medium or due to blood flow may also have an influence on the luminal VSMCs behaviour. However, the experiments in our lab show that the influence of shear stress on proliferation of VSMCs is trivial in comparison to the effect of cyclic strain. Nevertheless, excessively high values of pore fluid velocity and wall shear stress may have an adverse effect on VSMCs growth. In addition, given Cartmell *et al.,* (2003) used osteoblast-like cells in their experiments which formed the basis of the equations used in this study on the influence of pore fluid flow velocity on cell behaviour, Equations 6-8 and 6-11 need to be ascertained using experimental data dedicated specifically to VSMCs. After all, they serve to illustrate how the model can be applied provided such experimental data on VSMCs were available. Development of IH depends on several factors such as endothelialisation of the scaffold and the immune system activation, however, endothelialisation has been shown to be very poor on most available synthetic grafts (Zilla *et al.,* 2007) and was therefore excluded in this study. Nevertheless, this study aimed at elucidating the contribution of mechanical factors to remodelling and development of IH rather than prediction of the IH level. Another limitation of this study which benefits from further investigation is that the scaffold is assumed to be a

homogeneous medium, however most scaffolds have a heterogeneous microstructure which can have an important influence on the value of mechanical stimuli at the cell level and also on cell dynamics such as migration rate. The mechanical properties of the construct were updated depending on the value of ECM using a threshold based function. Although this is a simplification, a more realistic model requires experimental data on the evolution of mechanical properties i.e. permeability, porosity, and stress-strain relationship which was not available. Finally, Equation 6-6 concerning the role of cyclic strain on proliferation of VSMCs may not be applied to pathological levels of cyclic strain (>15%) given the different mechanisms of mechanotransduction at excessively high levels of cyclic strain.

Nevertheless, In spite of these simplifications, the model presented in this study is the first of its kind dedicated to the study of the mechanobiological environment of VSMCs in vascular tissue engineering and it clearly captures the key characteristics of VSMC growth in TEBVs comprising of nonlinear growth of TEBVs with time, ECM synthesis, remodelling and IH development.

Chapter 7

Final Discussion

Several mechanical factors are involved in the design of stents and vascular grafts which have a determining influence on their implantation outcome. Vascular injury caused by the stent due to high stresses in the vessel wall is identified as the main cause of in-stent restenosis (Schwartz *et al.,* 1992; Kornowski *et al.,* 1998; Mitra *et al.,* 2006). On the other hand mechanical compliance mismatch between vascular grafts and host arteries, usually due to the low compliance of vascular grafts, has been found to significantly contribute to intimal hyperplasia (Salacinski *et al.,* 2001). Furthermore, the important role of mechanoregulation in vascular tissue engineering has been shown by many studies (Seliktar *et al.,* 2003; Jeong *et al.,* 2005; Hahn *et al.,* 2007; Xu *et al.,* 2008). In these studies *In-vitro* mechanical stimulation of tissue engineered blood vessels has been shown to significantly enhance extracellular matrix synthesis and thereby improve the mechanical properties of vascular scaffolds, the majority of which suffer from low compliance and low burst pressure.

Computational technology enables us to simulate and quantify the complex *in-vivo* biomechanical environment in arteries and their interaction with implanted vascular devices. In many occasions computational modelling offers the only solution to the biomechanical challenges involved in vascular device technology. Such techniques, in conjunction with appropriately designed experiments, are helping us better understand the links between biomechanics and arterial pathologies.

One important advantage of computational models over experimental models is that computational models enable each individual biomechanical factor involved in the design of vascular devices to be studied in isolation. It is often extremely difficult to study the causative role of one single parameter using *in-vivo* and even *in-vitro* experiments. For instance, in this study, the influence of stent strut thickness on the level of arterial injury was studied from an arterial biomechanics viewpoint where the stresses induced in the arterial wall were the

matter of concern. The presented computational model complements the clinical studies such as ISAR-STEREO, which merely state a perceived causative link between stent-strut thickness and in-stent restenosis (Kastrati *et al.,* 2001) by elucidating the mechanisms by which strut thickness contributes to the level of in-stent restenosis. Hence, novel design solutions can be developed in light of the identified causative mechanisms. The computational model combined with the *in-vivo* studies such as ISAR-STERO then corroborates the general hypothesis that vascular injury is the main cause of in-stent restenosis.

A fundamental question which needs to be answered before developing computational models is to rationalise the extent to which the system of interest should be simplified. Indeed, modelling is nothing but simplification of complex phenomena to a level that we can deal with their complexity and still reasonably capture the key characteristic behaviours of the system. Obviously excessive simplification of a system will lead to a model that totally fails to capture the key responses of interest. On the other hand, including too many details will lead to a model which is as complex as the system itself, if not more complex. Therefore the key question that needs to be answered in order to develop a good model of a complex system such as the biomechanical systems is "How much simplification is plausible?". The modeller should come up with a rationale by which the key factors which contribute to the behaviours of interest can be determined. This constitutes the first and most critical step towards development of a deductive biomechanical model and is indeed an important distinctive feature of different models developed to study the same phenomena.

This study addresses some of the most complex challenges involved in the biomechanical modelling of vascular implants namely stents, vascular grafts and tissue engineered blood vessels. Hence the critical choice of the level of simplification was a main focus throughout all computational models presented in this study. Chapter 3 is specifically dedicated to address this crucial choice in modelling stent deployment procedures. Stent deployment procedures constitute a difficult problem from a biomechanical modelling perspective given the strong nonlinearity arising from the stress-strain response of arteries, the elasto-plastic response of

stents, the complex balloon geometry and its nonlinear unfolding response and last but not least, the contact problem between balloon-stent and stent-artery pairs. In spite of all the aforementioned challenges, the benefits that computational models bring have urged engineers to use computational models as an important part of the stent design cycle. Nonetheless, the majority of studies have resorted to a high level of simplification without providing a strong rationale for their choice of simplification. Considering the significant value of FEM as a formidable preclinical testing tool which can shorten the design cycle time for vascular stents and lower experimentation costs, it was necessary to thoroughly investigate the different levels of simplification used in stent deployment modelling and provide a basis for this critical choice as far as accuracy and efficiency of models are concerned. For this purpose a model with the minimum possible simplification was first developed and then stent deployment was modelled using the most widely used simplified models in order to determine the sensitivity of the models to the varying levels of simplification. Namely, the balloon deployment procedure was modelled including a realistic model of a three-fold balloon and later the same simulations were performed using the more simplified methods such as direct application of homogeneous pressure to inner stent surface with and without constraining elements. The results clearly showcased how critical the choice of simplification level is in a model. The study showed that the majority of the simplified methods fail to capture many key characteristics of stent expansion i.e. expansion diameter, dogboning and foreshortening, specifically in the transient phase. Furthermore, the study proposed a straight forward method to develop an exhaustive model of stent deployment procedures whereby all necessary details of stent response, its interaction with the vessel wall and the vessel stresses could be captured with high accuracy. An alternative and more efficient method was also proposed and its limitations were clearly discussed which can be used in certain circumstances, specifically when the transient phase of stent deployment is not the main interest of the modeller. The methods presented in Chapter 3 can be utilised in the stent design cycle to reduce the arterial

wall stresses and hence arterial injury in order to address the issue of in-stent restenosis as showcased in Chapter 4.

In the case of vascular grafts, however, the main biomechanical challenge is the issue of compliance mismatch and this study presented a method to ensure compliance matching with different host arteries using computational modelling. In chapter 5, a basis for modelling the *in-situ* mechanical response of vascular grafts is provided using custom-tailored experiments in conjunction with FE modelling. Arteries within the body have significantly different mechanical and geometrical properties depending on their type and function. Therefore in order to ensure compliance matching, grafts needs to be designed specifically for each different host artery. The presented method in chapter 5, whereby a constitutive model is presented for bacterial cellulose vascular grafts, enables the optimum graft material and geometrical design parameters to be determined in order to ensure compliance matching. Compliance matching not only reduces the level of intimal hyperplasia but also reduces the anastomotic stresses and thereby lowers the risk of graft rupture and injury to the host arteries. In addition, constitutive models for vascular grafts are necessary to study hemodynamics related factors which have also been postulated to contribute to development of intimal hyperplasia (Salacinski *et al.,* 2001). Hemodynamic related factors such as wall shear stress depend on the elastic properties of arteries which necessitates coupled field fluid-solid interaction models that require accurate constitutive models for wall mechanics. Even though, currently mechanical constitutive models are mainly developed based on experiments conducted on cadaveric tissues and the results are generalised, with recent developments in non-invasive methods such as intravascular ultrasound elastography (de Korte *et al.,* 2002), it would be possible to develop patient specific constitutive models for different arteries which would enable even better compliance matching of vascular grafts with host arteries using the FEM.

One important aspect of constitutive model development for mechanical response of materials is the appropriate choice of mechanical characterisation tests. Soft tissues are usually characterised using tensile tests. Several types of tensile tests may be conducted based

on the number of axes that extensions are applied to the material, including uniaxial, biaxial and multiaxial extension tests. Theoretically speaking, In order to fully characterise the three dimensional mechanical response of an incompressible isotropic material it is necessary to conduct biaxial experiments (Holzapfel *et al.,* 2009). However, uniaxial extension tests are very popular and many studies use them to develop constitutive models which are also used to model the response of vascular conduits under multi-axial loading conditions. This is mainly due to the fact that preparation of intact patches for biaxial tests is difficult to achieve and often not feasible at all. In addition, equi-biaxial experiments are often conducted rather than general biaxial tests given that availability of devices that allow independent control of extensions and stress in more than one direction is limited. Furthermore uniaxial extension tests allow for a higher level of extension compared to biaxial tests and therefore can better capture the nonlinear stress stiffening response of soft tissue. Nevertheless, it is necessary to verify that the constitutive models developed based on uniaxial extension tests can also accurately capture the response of material under more general loading cases such as inflation (Holzapfel *et al.,* 2009). In chapter 5, an approach was illustrated whereby a model of bacterial cellulose tubes under inflation was developed using a constitutive model based on uniaxial extension tests. The model results were then compared to actual inflation tests to verify the accuracy of the constitutive model in capturing the response of bacterial cellulose tubes under luminal pressures similar to those that the tubes undergo *in-vivo*. In this specific case where bacterial cellulose was under investigation, the constitutive model developed based on uniaxial tests was capable of accurately capturing the response of the bacterial cellulose tubes under inflation. There are also many studies which exemplify feasibility of using uniaxial tests to develop constitutive models for arteries such as the studies by Holzapfel *et al.,* (2000a, 2005a), however, this should not be over-generalised given that there are also materials such as human annulus fibrosus where uniaxial tests have been shown to be insufficient to characterise their *in-vivo* response (Bass *et al.,* 2004).

Complex biomechanics of the arteries and vascular devices only constitutes the first challenge in arterial biomechanics. The main complexity however, arises from the ability of arterial systems to remodel in response to the alterations in their mechanical environment by adapting their structure and morphology. Cells are central to this adaptation and therefore mechanobiological models are needed to determine how cells respond to the biomechanical signals received from their environment. The fact that mechanical loads are applied at tissue level and adaptation stems from cell level behaviours necessitate a multi-scale modelling approach whereby the mechanical signals that cells receive from their environment (cell level loads) are quantified based on the tissue level mechanical loads such as the pulsatile blood pressure in arteries. Then the quantified signals can be used to determine cellular behaviours. In addition to how cells respond to an altered mechanical environment, the most intriguing and yet complicated problem is that tissue level responses such as intimal hyperplasia in vascular grafts and tissue engineered blood vessel emerge not only from the behaviour of individual cells, but also from the intracellular interaction within cell societies. Hence, novel methods in computational biology such as agent based modelling have been developed which enable the response of multi-cellular biological systems or cell societies to be modelled based on interactions amongst cells. Agent based modelling is a robust and versatile platform whereby the collective response of cell societies can be modelled through defining simple rules of behaviour for each cell type and allowing the cells to interact based on the rules of behaviour, thereby the complex emergent collective behaviours of cell societies can be modelled. The rules of behaviour are defined at the cell level and include the important cell functions such as migration, mitosis, differentiation, protein synthesis and also how each individual cell responds to signals it receives from the neighbouring cells. Agent based modelling has been utilised in many studies which lend themselves to studying complex biological phenomena such as wound healing, tissue patterning, pathogensis of atherosclerosis, and tissue vascularisation (Walker *et al.,* 2004; Baily *et al.,* 2007; Pappalardo *et al.,* 2009). The novel idea which formed the basis of Chapter 6, was to combine agent based

modelling with the FEM to develop a robust mechanobiological modelling framework which allows some of the most important challenges in vascular tissue engineering to be addressed, namely mechanoregulation of remodelling and development of intimal hyperplasia.

Tissue engineering seems to be a promising approach in the treatment of vascular disease, however there are still several challenges that need to be addressed before it can be widely practiced clinically. An important challenge for tissue engineers is how mechanical factors can influence the remodelling of vascular scaffolds. However, in spite of the fact that computational models can provide significant insights in this context, a relatively small number of computational studies have focussed on vascular tissue engineering. A tremendous volume of data has been generated by *in-vitro* experiments in this field pertaining to the discovery of various chemo-mechano-biological pathways, however, they have not shed light on how these numerous factors and pathways combine to contribute to certain key characteristics of interest such as scaffold remodelling. This leads to the issue discussed earlier in this chapter regarding the rationale for simplification of complex systems in order to come up with models that can reasonably capture the key responses of interest in vascular tissue engineering. In addition to highly concentrated *in-vitro* and *in-vivo* studies focused on discovering new pathways, it is necessary to develop a platform that allows all the different pathways that are hypothesised to be involved in a complex matter such as remodelling, to be studied in a systematic and collective manner in order to come up with rationale which determine the key causative factors and mechanisms. Such a platform will then help to corroborate or rule out our hypotheses about the role of mechanical factors in remodelling and ultimately lend itself to developing novel methods in vascular tissue engineering informed by mechanics related cues.

The need for such a platform in vascular tissue engineering motivated the development of a robust and novel mechanobiological modelling framework by coupling agent based models with FE analysis as discussed in Chapter 6. The framework was used to study the influence of mechanical loading regime for *in-vivo* conditioning of vascular scaffolds to enhance their

remodelling. In addition the role of scaffold compliance on growth dynamics of vascular smooth muscle cells and development of intimal hyperplasia was investigated. In light of these findings, it may be concluded that it is possible to regulate the key characteristic behaviours of smooth muscle cell in tissue engineered blood vessels utilising a combination of strategies based on mechanical factors, i.e. scaffold compliance and external loads.

Interestingly, the mechanobiological modelling framework highlighted the significant role of cyclic strain in regulating the growth of VSMCs and development of IH which showed that VSMCs within TEBVs should undergo a physiological level of cyclic strain to minimise IH. In addition to the fact that this finding of the mechanobiological model is consistent with the clinical findings which suggest a direct relationship between the compliance of vascular grafts and their long term patency rates, it also relates to the findings of the clinical studies on stents such as ISAR-STEREO trial which show that the restenosis rate is lower when thin strut stents which are more compliant are used. Clearly therefore, the developed mechanobiological modelling framework could be employed to study restenosis following stent implantation.

Chapter 8

Conclusions & Future work

7.1 Conclusions

The overall aim of this study was to develop computational models which can help improve the performance of vascular stents and vascular grafts as the key vascular implants used in surgical treatment of vascular disease.

With regard to the stents the specific aim was to develop FE models that can accurately predict the mechanical behaviour of stents during stent deployment procedures and following stent placement which enable optimisation of stent design parameters in order to reduce arterial wall stresses and hence arterial injury which is the main cause of in stent restenosis. The findings of this study can be summarised as follows:

- The transient response of balloon expandable stents can only be captured using a balloon model and the simplified models where a uniform pressure is applied to the inner stent surface are incapable of capturing the transient response.
- Application of direct pressure to the inner stent surface was found to be incapable of accurately predicting the stress-strain field and the deformed configuration of the stent both in the transient phase and also following stent expansion and recoil. The use of restraining elements, however, which prevent expansion of the stent beyond the desired diameter combined with the application of a uniform pressure to the inner stent surface, with a magnitude high enough to achieve the desired expansion diameter, may be used as a computationally efficient method to predict the stress-strain field in the vessel wall following full stent expansion and recoil.
- Studying the influence of stent strut thickness on the arterial wall stresses revealed that thinner strut stents induce lower chronic stresses in the vessel wall which could

explain the lower restenosis rates using thin strut stents in comparison to thicker strut stents as reported by clinical trials such as ISAR-STEREO.

- This study supports the hypothesis that arteries develop restenosis in response to injury, where high vessel stresses are a good measure of that injury. The study points to a critical stress level in arteries, above which an aggressive healing response leads to in-stent restenosis in stented vessels. Stents can be designed to reduce stresses in this range in arteries using preclinical tools such as numerical modelling.

Vascular grafts were categorised into (i) synthetic vascular grafts and (ii) tissue engineered blood vessels and treated separately in this study.

The specific aim of this study with respect to synthetic vascular grafts was to use FE modelling to ensure compliance matching between vascular grafts and host arteries in order to minimise intimal hyperplasia. The findings of this study are as follows:

- Bacterial cellulose was identified as a suitable vascular scaffold based on compliance tests and preliminary cell seeding experiments.
- A preclinical test method has been developed which successfully provides a means to optimise graft material and scaffold or graft geometrical design parameters to ensure compliance matching and to prevent graft failure and injury in the host arteries.

With respect to tissue engineered blood vessels the specific aim was to develop a computational mechanobiological model to simulate mechanoregulation of remodelling in vascular tissue engineered scaffolds in order to develop novel strategies in vascular tissue engineering informed by biomechanics related cues. The main findings of this study in this context are as follows:

- Agent based models coupled with FE analysis can be used as a robust mechanobiological modelling framework for multi-scale mechanobiological modelling in vascular tissue engineering. By comparison to published *in-vitro* and *in-vivo* studies,

the mechanobiological modelling framework was found to capture the key characteristics of VSMC growth in TEBVs.

- The model generated valuable insights into the mechanobiological processes which drive the remodelling process and regulate VSMC growth dynamics in tissue engineered blood vessels and elucidated the role of mechanical factors such as scaffold compliance and loading regime.

7.2 Future work

Following on from the significant insights gained from the models presented in this thesis, the computational tools developed could be further improved and applied as follows:

- The influence of anisotropic arterial mechanical properties on the arterial wall stresses following stent deployment could be assessed.
- The influence of stent induced damage to the arterial wall on arterial wall stresses and stent recoil could be investigated by using an appropriate damage model for the arterial constitutive model
- The influence of inhomogeneous mechanical properties of atherosclerotic plaques could be studied using imaging modalities such as MRI and intra vascular ultrasound and also ultrasound elastography to better evaluate the stresses in the atherosclerotic arteries and also the risk of plaque rupture.
- *In-vitro* and *In-vivo* studies could be run to corroborate the mechanobiological modelling framework developed.
- By incorporating advection-diffusion equations in the mechanobiological modelling framework the transport of oxygen, glucose and lactate in tissue engineered constructs could be better modelled.
- The mechanobiological modelling framework could be applied to other areas such as skeletal tissue engineering and fracture healing.

- The mechanobiological modelling framework can be employed to study in-stent restenosis.

Bibliography

Abaqus analysis user's manual (v6.8), section 21.7.2, Permeability.

American Heart Association (2010a) Heart Disease and Stroke Statistics 2009 Updated, American Heart Association, Dallas, Tx.

American Heart Association (2010b) International Cardiovascular Disease Statistics 2009 Updated, American Heart Association, Dallas, Tx.

Andreykiv A., van Keulen F., Prendergast P.J. (2008) Simulation of fracture healing incorporating mechanoregulation of tissue differentiation and dispersal/proliferation of cells, *Biomechanics and Modeling in Mechanobiology*, Vol.7, pp443–461.

Auricchio F., Di Loreto M., Sacco E. (2001) Finite-element analysis of a stenotic revascularization through a stent insertion, *Computer Methods in Biomechanics and Biomedical Engineering,* Vol.4, pp249–264.

Ausk B.J., Gross T.S., Srinivasan S. (2006) An agent based model for real-time signaling induced in osteocytic networks by mechanical stimuli, *Journal of Bimechanics,* Vol.39, pp2638–2646.

Ayyalasomayajula A., Vande Geest J.P., Simon B.R. (2010) Porohyperelastic finite element modeling of abdominal aortic aneurysms, *Journal of Biomechanical Engineering*, Vol.132, pp104502–104510.

Bass E. C., Ashford F. A., Segal M. R., Lotz J. C. (2004) Biaxial Testing of Human Annulus Fibrosus and Its Implications for a Constitutive Formulation, *Annals of Biomedical Engineering*, Vol. 32, pp1231–1242.

Bäckdahl H., Esguerra M., Delbro D., Risberg B., Gatenholm P. (2008) Engineering microporosity in bacterial cellulose scaffolds, *Journal of Tissue Engineering and Regenerative Medicine*, Vol.2 , pp320–330.

Bäckdahl H., Helenius G., Bodin A., Nannmark U., Johansson B.R., Risberg B., Gatenholm P. (2006) Mechanical properties of bacterial cellulose and interactions with smooth muscle cells, *Biomaterials*, Vol.27, pp2141–2149.

Baily A.M., Thorne B.C., Peirce S.M. (2007) Multi-cell Agent based simulation of the microvasculature to study the dynamics of circulating inflammatory cell trafficking, *Annals of biomedical engineering*, Vol.35(6), pp916–936.

Bavry A.A., Kumbhani D.J., Helton T.J., Borek P.P., Mood G.R., Bhatt D.L. (2006) Late Thrombosis of Drug-Eluting Stents: A Meta-Analysis of Randomized Clinical Trials, *The American Journal of Medicine,* Vol.119, pp1056-1061.

Bedoya J., Meyer C.A., Timmins L.H., Moreno M.R., Moore Jr. J.E. (2006) Effects of Stent Design Parameters on Normal Artery Wall Mechanics, *Journal of Biomechanical Engineering–Transactions of ASME*, Vol.128, pp757–765.

Berglund J.D., Mohseni M.M., Nerem R.M., Sambanis A. (2003) A biological hybrid model for collagen-based tissue engineered vascular constructs, *Biomaterials*, Vol.24, pp1241–1254.

Berglund J.D., Nerem R.M., Sambanis A. (2004) Incorporation of intact elastin scaffolds in tissue-engineered collagen-based vascular grafts, *Tissue Engineering,* Vol.10, pp1526–35.

Bodin A., Ahrenstedt L., Fink H., Brumer H., Risberg B., Gatenholm P. (2007) Modification of nanocellulose with a xyloglucan–RGD conjugate enhances adhesion and proliferation of endothelial cells: Implications for Tissue Engineering, *Biomacromolecules,* Vol.8, pp3697–3704.

Bodin A., Backdahl H., Fink H., Gustafsson L., Risberg B., Gatenholm P. (2007) Influence of cultivation conditions on mechanical and morphological properties of bacterial cellulose tubes, *Biotechnology and Bioengineering*, Vol.97, pp425–434**.**

Boyle C.J., Lennon A.B., Early M., Kelly D.J., Lally C., Prendergast P.J. (2010) Computational simulation methodologies for mechanobiological modelling: a cell-centered approach to neointima development in stents, *Philosophical Transactions of the Royal Society A*, Vol.368, pp2919–2935.

Briguori C., Sarais C., Pagnotta P. (2002) In-stent restenosis in small coronary arteries: impact of strut thickness*, Journal of American College of Cardiology,* Vol.40, pp403– 409.

Byrne D.P., Lacroix D., Planell J.A., Kelly D.J., Prendergast P.J. (2007) Simulation of tissue differentiation in a scaffold as a function of porosity, Young's modulus and dissolution rate: Application of mechanobiological models in tissue engineering, *Biomaterials*, Vol.28 pp.5544–5554.

Byrne H., Drasdo D. (2009) Individual-based and continuum models of growing cell populations: a comparison, *Journal of Mathematical Biology*, Vol.58, pp.657–687.

Caiazzo A., Evans D., Falcone J.L., Hegewald J., Lorenz E., Stahl B., Wang D., Bernsdorf J., Chopard B., Gunn J., Hose R., Krafczyk M., Lawford P., Smallwood R., Walker D., Hoekstra A.G. (2009) Towards a complex automata multiscale model of in-stent restenosis, *Computational Science – ICCS*, Vol.5544, pp.705–714.

Canham P.B., Finlay H.M., Dixon J.G., Boughner D.R., Chen A. (1989) Measurements from light and polarised light microscopy of human coronary arteries fixed at distending pressure, *Cardiovascular Research*, Vol.23, pp973–982.

Cartmell S.H., porter B.D., Garcia A.J., Guldburg R.E. (2003) effects of medium perfusion rate on cell seeded three dimensional bone constructs in vitro, *Tissue engineering*, Vol.9(6), pp.1197–1203.

Catanese J., Cooke D., Maas C., Pruitt L. (1999) Mechanical properties of medical grade expanded polytetrafluoroethylene: the effects of internodal distance, density, and displacement rate, *Journal of Biomedical Material Research-B,* Vol.48, pp187–192.

Chapman G.B., Durante W., Hellums J.D., Schafer A.I. (2000) Physiological cyclic stretch causes cell cycle arrest in cultured vascular smooth muscle cells, *American Journal of Physiology-Heart and Circulation Physioliology,* Vol.278, pp H748–H754.

Clark M., Glagov S., (1979) Structural integration of the arterial wall. I. Relationships and attachments of medial smooth muscle cells in normally distended and hyperdistended aortas, *Labratory investigation*, Vol.40, pp587–602.

Coletti F., Macchietto S., Elvassore N. (2006) Mathematical modeling of three-dimensional cell cultures in perfusion bioreactors, *Industrial and Engineering Chemistry Research*, Vol.45(24), pp8158–8169.

Colombo A. (2009) The role of altered cyclic strain patterns on proliferation and apoptosis of vascular smooth muscle cells - implications for in-stent restenosis, *PhD thesis, Dublin City University (http://doras.dcu.ie/14917/)*.

Colombo A., Zahedmanesh H., Toner D., Cahill P., Lally C. (2010) A method to develop mock arteries suitable for cell seeding and in-vitro cell culture experiments, *Journal of the Mechanical Behavior of Biomedical Materials*, Vol.3, pp470-477.

Darcy H. (1856) Les Fontaines Publiques de la Ville de Dijon, Dalmont, Paris.

Daemen J., Wenaweser P., Tsuchida K., Abrecht L., Vaina S., Morger C., Kukreja N., Jüni P., Sianos G., Hellige G., van Domburg R.T., Hess O.M., Boersma E., Meier B., Windecker S., Serruys P.W. (2007) Early and late coronary stent thrombosis of sirolimuseluting and paclitaxel-eluting stents in routine clinical practice: data from a large two-institutional cohort study, *Lancet,* Vol.369, pp 667–678.

De Beule M., Mortier P., Carlier S.G., Verhegghe B., Van Impe R., Verdonck P. (2008) Realistic finite element-based stent design: the impact of balloon folding, *Journal of Biomechanics,* Vol.41, pp383–389.

De Beule M., Van Impe R., Verhegghe B., Segers P., Verdonck P., (2006) Finite element analysis and stent design: reduction of dogboning, *Technology and Health Care*, Vol.14, pp233–241.

de Quadros A.S., Sarmento-Leite R., Gottschall C.A., Silva G.V., Perin E.C. (2006) Hyperexpansion of coronary stents and clinical outcomes, *Texas Heart Institute Journal,* Vol.33, pp437–44.

De Korte C.L., Carlier S.G., Mastik F., Doyley M.M., van der Steen A.F. W., Serruys P.W., Bom N. (2002) Morphological and mechanical information of coronary arteries obtained with intravascular elastography, Feasibility study in vivo, *European Heart Journal*, Vol.23, pp405–413.

Den Buijs J.O., Lu L., Jorgensen S.M., Dragomir-Daescu D., Yaszemski M.J., Ritman E.L. (2009) Solute Transport in Cyclically Deformed Porous Tissue Scaffolds with Controlled Pore Cross-Sectional Geometries, *Tissue Engineering: part A*, Vol.15(8), pp1989–1999.

DiMilla P.A., Stone J.A., Quinn J.A., Albelda S.M., Lauffenburger D.A. (1993) Maximal migration of human smooth muscle cells on fibronectin and type IV collagen occurs at an intermediate attachment strength, *Journal of Cellular Biology,* Vol.122, pp729–737.

Dumoulin C., Cochelin B. (2000) Mechanical behaviour modelling of balloon-expandable stents, *Journal of Biomechanics*, Vol.33, pp1461–1470.

Duraiswamy N., Schoephoerster R.T., Moreno M.R., Moore Jr. J.E. (2007) Stented artery flow patterns and their effects on the artery wall, *Annual Review of Fluid Mechanics*, Vol.39, pp357–382.

Durante W., Liao L., Reyna S.V., Peyton K.J., Schafer A.L. (2000) Physiological cyclic stretch directs L-arginine transport and metabolism to collagen synthesis in vascular smooth muscle, *FASEB Journal,* Vol. 14(12), pp1775–1783.

Early M., Lally C., Prendergast P.J., Kelly D.J. (2008) Stresses in peripheral arteries following stent placement: a finite element analysis, *Computer Methods in Biomechanics and Biomedical Engineering*, Vol.12, pp25–33.

European Heart Network (2010) European Cardiovascular Disease Statistics 2008 Updated, Brussels, Belgium.(http://www.ehnheart.org/).

Feenstra P.H., Taylor C.A. (2009) Drug transport in artery walls: A sequential porohyperelastic-transport approach, *Computer Methods in Biomechanics and Biomedical Engineering*, Vol.12, pp263–276.

Fink H., Faxälv L., Monlár G.F., Drotz K., Risberg B., Lindahl T.L., Sellborn A. (2010) Real-time measurements of coagulation on bacterial cellulose and conventional vascular graft materials, *Acta Biomaterialia,* Vol.6, pp1125–1130.

Fischman D.L., Leon M.B., Baim D.S. (1994) A randomized comparison of coronary-stent implantation with balloon angioplasty in patients with coronary artery disease, *New England Journal of Medicine*, Vol.331, pp496–501.

Fung Y. (1990) Biomechanics: motion, flow, stress, and growth. Springer-Verlag, New York.

Fung Y. (1993) Mechanical Properties of living tissues. Second Edition. Springe-Verlag. New York.

Geris L., Liedekerke P.V., Smeets B., Tijskens E., Ramon H. (2010c) A cell based modelling framework for skeletal tissue engineering applications*, Journal of Biomechanics*, Vol.43, pp887–892.

Geris L., Schugart R., Van Oosterwyck H. (2010a) *In silico* design of treatment strategies in wound healing and bone fracture healing, *Philosophical Transactions of the Royal Society A*, Vol.368(1920), pp2683–2706.

Geris L., Vander Sloten J., Van Oosterwyck H. (2010b) Connecting biology and mechanics in fracture healing: an integrated mathematical modeling framework for the study of nonunions, *Biomechanics and Modelling in Mechanobiology*, In press. doi: 10.1007/s10237-010-0208-8

Gerlee P., Andersona A.R.A. (2008) hybrid cellular automaton model of clonal evolution in cancer: the emergence of the glycolitic phenotype, *Journal of theoretical Biology*, Vol.250, pp705–722. doi:10.1016/j.jtbi.2007.10.038

Gervaso F., Capelli C., Petrini L., Lattanzio S., Virgilio L.D., Migliavacca F., (2008) On the effects of different strategies in modelling balloon-expandable stenting by means of finite element method, *Journal of Biomechanics*, Vol.41, pp1206–1212.

Gijsen F.J.H., Migliavacca F., Schievano S., Socci L., Petrini L., Thury A., Wentzel J.J., van der Steen A.F.W., Serruys P.W.S., Dubini G., (2008) Simulation of stent deployment in a realistic human coronary artery, *BioMedical Engineering OnLine*, Vol. 6, pp7–23.

Greisler H.P., Joyce K.A., Kim D.U., Pham S.M., Berceli S.A., Borovetz H.S. (2004) Spatial and temporal changes in compliance following implantation of bioresorbable vascular grafts, *Journal Biomedical Material Research*, Vol.26, pp1449–1461. doi: 10.1002/jbm.820261105

Greisler H.P., Joyce K.A., Kim D.U., Pham S.M., Berceli S.A., Borovetz H.S. (2004) Spatial and temporal changes in compliance following implantation of bioresorbable vascular grafts. *Journal of Biomedical Material Research*, Vol.26, pp1449–1461.

Grewe P.H., Deneke T., Machraoui A., Barmeyer J., Muller K.M. (2000) Acute and chronic tissue response to coronary stent implantation: pathologic findings in human specimens*, Journal of American College of Cardiology*, Vol.35, pp157–163.

Guo Z., Sloot P. M.A., Tay J.C. (2008) a hybrid agent based approach for modeling microbiological systems, *Journal of Theoretical Biology*, Vol.255, pp163–175. doi:10.1016/j.jtbi.2008.08.008

Hahn M.S., Mchale M.K., Wang E., Schmedlen R.H., West J.I. (2007) Physiologic pulsatile flow bioreactor conditioning of poly(ethyleneglycol)-based tissue engineered vascular grafts, *Annals of Biomedical Engineering,* Vol.35(2), pp190–200. doi: 10.1007/s10439-006-9099-3

Hall G.J., Kasper E.P., (2006) Comparison of element technologies for modelling stent expansion, *Journal of Biomechanical Engineering*, Vol.128, pp751–756.

Halka A.T., Turner N.J., Carter A., Ghosh J., Murphy M.O., Kirton J.P., Kielty C.M., Walker M.G. (2008) The effects of stretch on vascular smooth muscle cell phenotype in vitro, *Cardiovascular Pathology,* Vol.17, pp98–102.

Hara H., Nakamura M., Palmaz J.C., Schwartz R.S. (2006) Role of Stent Design and Coatings on Restenosis and Thrombosis, *Advanced Drug Delivery Reviews*, Vol.58, pp377–386.

Hara H., Nakamura M., Palmaz J.C., Schwartz R.S., (2006) Role of stent design and coatings on restenosis and thrombosis, *Advanced Drug Delivery Reviews*, Vol. 58, pp377–386.

Helenius G., Backdahl H., Bodin A., Nannmark U., Gatenholm P., Risberg B. (2006) In vivo biocompatibility of bacterial cellulose, *J Biomed Mater Res-A*, Vol.76(2), pp 431–438.

Health-EU, The public Health Portal of the European Union (2010) Cardiovascular Diseases, Brussels, Belgium. (http://ec.europa.eu/health-eu).

Heyligers J.M., Arts C.H., Verhagen H.J., de Groot P.G., Moll F.L.(2005) Improving small-diameter vascular grafts: from the application of an endothelial cell lining to the construction of a tissue-engineered blood vessel, *Annals of Vascular Surgery*, Vol.19, pp448–456.

Hibbett, Karlsson and *Sorenson* Inc., 1998 ABAQUS Version 5.8 User's Manual.

Hinds M.T., Rowe R.C., Ren Z., Teach J., Wu P.C., Kirkpatrick S.J., Breneman K.D., Gregory K.W., Courtman D.W. (2006) Development of a reinforced porcine elastin composite vascular scaffold*, Journal of Biomedical Material Research A,* Vol.77(3), pp458–469.

Hoffmann R., Mintz G.S. (2000) Coronary in-stent restenosis — predictors, treatment and Prevention*, European Heart Journal,* Vol.21, pp1739–1749. doi: 10.1053/euhj.2000.2153

Holzapfel G.A., Gasser T.C., Ogden R.W. (2000a) A new constitutive framework for arterial wall mechanics and a comparative study of material models, *Journal of Elasticity*, Vol.61, pp1–48.

Holzapfel G.A. (2000b) Nonlinear solid mechanics. A continuum approach for engineering. John Wiley & Sons, Chichester.

Holzapfel G.A., Sommer G., Gasser C.T., Regitnig P. (2005a) Determination of layer-specific mechanical properties of human coronary arteries with nonatherosclerotic intimal thickening and related constitutive modelling, *American Journal of Physiology—Heart and Circulatory Physiology*, Vol.289, pp2048–2058. doi:10.1152/ajpheart.00934.2004

Holzapfel G.A., Stadler M., Gasser T.C. (2005b) Changes in the mechanical environment of stenotic arteries during interaction with Stents: computational assessment of parametric stent designs, *Journal of Biomechanical Engineering -T ASME*, Vol.127, pp166–180.

Holzapfel G.A., Ogden R.W. (2009) On planar biaxial tests for anisotropic nonlinearly elastic solids. A continuum mechanical framework, *Mathematics and Mechanics of Solids*, Vol.14, pp474–489.

Humphrey J.D., Delange S.L. (2004) An introduction to biomechanics, solids and fluids, analysis and design, Springer.

Hwang C.W., Wu D., Edelman E.R. (2001) Physiological transport forces govern drug distribution for stent-based delivery, Circulation, Vol.104, pp600–605.

Hwang M, Garbey M, Berceli SA, Tran-Son-Tay R (2009) Rule based simulation of multi-cellular biological systems-a review of modelling techniques. *Cellular and molecular bioengineering* Vol.2(3), pp285–294. doi: 10.1007/s12195-009-0078-2

Iakovou I., Schmidt T., Bonizzoni E., Ge L., Sangiorgi G.M., Stankovic G., Airoldi F., Chieffo A., Montorfano M., Carlino M., Michev I., Corvaja N., Briguori C., Gerckens U., Grube E., Colombo A. (2005) Incidence, predictors, and outcome of thrombosis after successful implantation of drug-eluting stents, *JAMA,* Vol.293(17), pp2126–2130. doi: 10.1001/jama.293.17.2126

Isenberg B.C., Williams C., Tranquillo R.T. (2006) Endothelialization and flow conditioning of fibrinbased media-equivalents, *Annals of Biomedical Engineering*, Vol.34, pp971–985.

Issaksson H., van Donkelaar C.C., Huiskes R., Ito K. (2008) A mechano-regulatory bone-healing model incorporating cell-phenotype specific activity, *Journal of Theoretical Biology,* Vol.252(2), pp230–246. doi:10.1016/j.jtbi.2008.01.030

Jeong S.I., Kwon J.H., Lim J.I., Cho S.W., Jung Y.M., Sung W.J., Kim S.H., Kim Y.H., Lee Y.M., Kim B.S., Choi C.Y., Kim S.J. (2005) Mechano-active tissue engineering of vascular smooth muscle using pulsatile perfusion bioreactors and elastic PLCL scaffolds*, Biomaterials*, Vol.26, pp1405–1411. doi:10.1016/j.biomaterials.2004.04.036

Ju F., Xia Z., Sasaki K., (2008) On the finite element modelling of balloon-expandable stents, *Journal of the Mechanical Behavior of Biomedical Materials*, Vol.1, pp86–95.

Jungreuthmayer C., Donahue S.W., Jaasma M.J., Al-Munajjed A.A., Zanghellini J., Kelly D.J., O'Brien F.J. (2009) A comparative study of shear stresses in collagen-glycosaminoglycan and calcium phosphate scaffolds in bone tissue-engineering bioreactors, *Tissue Engineering Part A*, Vol.15(5), pp1141–1149. doi:10.1089/ten.tea.2008.0204

Kastrati A., Mehilli J., Dirschinger J. *et al*. (2001) Intracoronary stenting and angiographic results: strut thickness effect on restenosis outcome (ISAR-STEREO) trial, *Circulation,* Vol.103, pp2816– 2821.

Kim J., Kang Y.H., Choi H.H., Hwang S.M., Kang B.S. (2002) Comparison of implicit and explicit finite-element methods for the hydroforming process of an automobile lower arm, *International Journal of Advanced Manufacturing Technology*, Vol.20, pp407–413.

Kiousis D.E., Wulff A.R., Holzapfel G.A. (2009) Experimental studies and numerical analysis of the inflation and interaction of vascular balloon catheter-stent systems, *Annals of Biomedical Engineering*, Vol.37, pp315–330.

Kleemann R., Zadelaar S., Kooistra T. (2008) Cytokines and atherosclerosis: a comprehensive review of studies in mice, *Cardiovascular Research*, Vol.79, pp360–376. doi:10.1093/cvr/cvn120

Kona S., Chellamuthu P., Xu H., Hills S.R., Nguyen K.T. (2009) Effects of cyclic strain and growth factors on vascular smooth muscle cell responses, *The open biomedical engineering journal*, Vol.3, pp28–38. doi: 10.2174/1874120700903010028

Kornowski R., Hong M.K., Tio F.O., Bramwell O., Wu H., Leon M.B. (1998) In-stent restenosis: contributions of inflammatory responses and arterial injury to neointimal hyperplasia, *Journal of the American College of Cardiology*, Vol.31, pp224–230.

Koshiba N., Ando J., Chen X., Hisada T. (2007) Multiphysics simulation of blood flow and LDL transport in a porohyperelastic arterial wall model, *Journal of Biomechanical Engineering*, Vol.129(3), pp374–385.

Kozai T., Eto M., Yang Z., Shimokawa H., Lüscher T.F. (2005) Statins prevent pulsatile stretch-induced proliferation of human saphenous vein smooth muscle cells via inhibition of Rho/Rho-kinase pathway, *Cardiovascular Research*, Vol.68, pp475–482.

Lally C., Dolan F., Prendergast P.J. (2005) Cardiovascular Stent Design and Vessel Stresses: A Finite Element Analysis*, Journal of Biomechanics*, Vol.38, pp1574–1581.

Lee R.T., Loree H.M., Cheng G.C., Lieberman E.H., Jaramillo N., Schoen F.J., (1993) Computational structural analysis based on intravascular ultrasound imaging before in vitro angioplasty: prediction of plaque fracture locations. *Journal of the American College of Cardiology*, Vol.21, pp777–782.

Lemson M.S., Tordoir J.H., Daemen M.J., Kistslaar P.J. (2000) Intimal hyperplasia in vascular grafts, *European Journal of Endovascular Surgery*, Vol.19, pp336–350.

Li N.Y.K., Verdolini K., Clermont G., Mi Q., Rubinstein E.N., Hebda P.A., Vodovotz Y. (2008) A patient–specific in silico model of inflammation and healing tested in acute vocal fold injury, *PLoS ONE,* Vol.3(7), e2789. doi: 10.1371/journal.pone.0002789

Liang D.K., Yang D.Z., Qi M., Wang W.Q. (2005) Finite Element Analysis of the Implantation of a Balloon-Expandable Stent in a Stenosed Artery, *International Journal of Cardiology*, Vol.104, pp314–318.

Liu B, Qu M.J., Qin K.R., Li H., Li Z.K., Shen B.R., Jiang Z.L. (2008) Role of Cyclic Strain Frequency in Regulating the Alignment of Vascular Smooth Muscle Cells In Vitro, *Biophysics Journal*, Vol. 94(4), pp1497–1507.

London G.M., Marchais S.J., Guerin A.P., Pannier B. (2004) Arterial stiffness: pathophysiology and clinical impact, *Clinical Experimental Hypertension*, Vol.26, pp689–699.

Long J.L., Tranquillo R.T. (2003) Elastic fiber production in cardiovascular tissue-equivalents, *Matrix Biology*, Vol.22, pp339–350.

Loree H.M., Grodzinsky A.J., Park S.Y., Gibson L.J., Lee R.T. (1994) Static circumferential tangential modulus of human atherosclerotic tissue, *Journal of Biomechanics*, Vol.27, pp195–204.

McClean R., Eigler N.L. (2002) Stent Design: Implications for Restenosis, *Reviews in Cardiovascular Medicine*, Vol.3, S16–S22.

McFadden E.P., Stabile E., Regar E., Cheneau E., Ong A.T.L., Kinnaird T., Suddath W.O., Weissman N.J., Torguson R., Kent K.M., Pichard A.D., Satler L.F., Waksman R., Serruys P.W. (2004) Late thrombosis in drug-eluting coronary stents after discontinuation of antiplatelet therapy, *Lancet*, Vol.364: pp1519–21.

Merks R.M.H., Perryn E.D., Shirinfard A., Glazier J. (2008) Contact-inhibited chemotaxis in De Novo and Sprouting blood vessel growth, *PLoS Computational Biology*, Vol.4(9), e1000163. doi: 10.1371/journal.pcbi.1000163

Messenger J.C., Chen S.Y., Carroll J.D., Burchenal J.E., Kioussopoulos K., Groves B.M., (2001) 3D coronary reconstruction from routine single-plane coronary angiograms: clinical validation and quantitative analysis of the right coronary artery in 100 patients, *International Journal of Cardiac Imaging*, Vol.16, pp413–427.

Michaels A.D., Chatterjee K. (2002) Angioplasty Versus Bypass Surgery for Coronary Artery Disease, *Circulation,* Vol.106, e187.

Migliavacca F., Gervaso F., Prosi M., Zunino P., Minisini S., Formaggia L., Dubini G. (2007) Expansion and drug elution model of a coronary stent*, Computer Methods in Biomechanics and Biomedical Engineering*, Vol.10, pp63–73.

Migliavacca F., Petrini L., Colombo M., Auricchio F., Pietrabissa R. (2002) Mechanical behavior of coronary stents investigated through the finite element method, *Journal of Biomechanics*, Vol.35, pp803–811.

Migliavacca, F., Petrini, L., Montanari, V., Quagliana, I., Auricchio, F., Dubini, G., 2005. A predictive study of the mechanical behaviour of coronary stents by computer modelling, *Medical Engineering and Physics,* Vol.27, pp13–18.

Mitchell RN. (2009) Graft Vascular Disease: Immune Response Meets the Vessel wall, *Annual Review of Pathology: Mechanisms of Disease,* Vol.4, pp19–47.

Mitra A.K., Agrawal D.K. (2006) In stent restenosis: bane of the stent era, *Journal of Clinical Pathology*, Vol.59, pp232–239.

Mooney D.J., Mazzoni C.L., Breuer C., McNamara K., Hern D., Vacanti J.P., Langer R. (1996) Stabilized polyglycolic acid fibre-based tubes for tissue engineering*, Biomaterials*, Vol.17, pp115–124.

Mooney M. (1940) A theory of large elastic deformation, *Journal of applied physics*, Vol.11, pp582–592.

Morice J.C., Serruys P.W., Sousa J.E., *et al.,* (2002) A randomized comparison of a sirolimus eluting stent with a standard stent for coronary revascularization, *New England Journal of Medicine*, Vol.346, pp1773–1780.

Morrow D., Sweeney C., Birney Y.A., Cummins P.M., Walls D., Redmond E.M., Cahill P.A. (2005) Cyclic strain inhibits notch receptor signaling in vascular smooth muscle cells in vitro, *Circulation Research*, Vol. 96, pp567–575.

Morrow D., Sweeney C., Birney Y.A., *et al*. (2005) Cyclic Strain Inhibits Notch Receptor Signaling in Vascular Smooth Muscle Cells In Vitro, *Circulation Research*, Vol.96, pp567–75.

Morton A.C., Crossman D., Gunn J. (2004) The influence of Physical Stent Parameters Upon Restenosis, *Pathological Biology*, Vol.52, pp196–205.

Murphy B.P., Savage P., McHugh P.E., Quinn D.F. (2003) The stress-strain behaviour of coronary stent struts is size dependent, *Annals of Biomedical Engineering*, Vol.31, pp686–691.

National Heart Long and Blood Institute (2010) Diseases and conditions index, Heart and Vascular Diseases, Coronary Angioplasty, National Heart Long and Blood Institute, National Institute of Health, U.S Department of Health & Human Services, (Accessed online, December, 2010, http://www.nhlbi.nih.gov/health/dci/Diseases/Angioplasty/Angioplasty_howdone.html).

Nerem R.M., Seliktar D. (2001) Vascular tissue engineering, *Annual Reviews of Biomedical Engineering*, Vol.3, pp225–243.

Nigg B.M., Herzog W. (2001) Biomechanics of the Musculo-skeletal System, 3rd Edition, Wiley.

Niklason L.E., Gao J., Abbott W.M., Hirschi K.K., Houser S., Marini R., Langer R. (1999) Functional arteries grown in vitro, *Science*, Vol.284, pp489–93.

Nikolovski J., Kim B.S., Mooney D.S. (2003) Cyclic strain inhibits switching of smooth muscle cells to an osteoblast-like phenotype, *The FASEB Journal*, Vol.17, pp455–457.

Numaguchi K., Eguchi S., Yamakawa T., Motley E.D., Inagami T. (1999) Mechanotransduction of rat aortic vascular smooth muscle cells requires RhoA and intact actin filaments, *Circulation Research,* Vol.85, pp5–11.

Ogden R.W. (1972) Large deformation isotropic elasticity: on the correlation of theory and experiment for incompressible rubberlike solids, *Proceedings of the Royal Society of London A- Mathematical and Physical Sciences*, Vol.326, pp565–584. doi: 10.1098/rspa.1972.0026

Ogden R.W., Saccomandi G., Sgura I., (2004) Fitting hyperelastic models to experimental data, Computational Mechanics, 34(6), pp484–502.

Ogdens R.W. (1984) Nonlinear elastic deformations, John Wiley and Sons, New York.

Opitz F., Schenke-Layland K., Cohnert T.U., Starcher B., Halbhuber K.J., Martin D.P., Stock U.A. (2004) Tissue engineering of aortic tissue: dire consequence of suboptimal elastic fiber synthesis in vivo, *Cardiovascular Research*, Vol.63, pp719–730.

Pache J., Kastrati A., Mehilli J. *et al*., (2003) Intracoronary Stenting and Angiographic Results: Strut Thickness Effect on Restenosis Outcome (ISAR-STEREO-2), Trial. *Journal of the American College of Cardiology*, Vol.41, pp1283–1288.

Pankajakshan D., Agrawal D.K. (2010) Scaffolds in tissue engineering of blood vessels, *Canadian Journal of Physiology Pharmacology*, Vol.88(9), pp855–873. doi:10.1139/Y10-073

Pappalardo F., Cincotti A., Motta A., Pennisi M. (2009) Agent based modelling of Atheresclerosis: A Concrete help in Personalized treatments, *Lecture Notes in Computer Science*, Vol.5755, pp386–396. doi: 10.1007/978-3-642-04020-7_41

Patel A., Fine B., Sandig M., Mequanint K. (2006) Elastin biosynthesis: The missing link in tissue-engineered blood vessels, *Cardiovascular Research*, Vol.71, pp40–49.

Pedrizzetti G., Perktold K. eds. (2003) CardioVascular Fluid Mechanics. Springer-Verlag Wien New York (ISBN 3-211-00538-2)

Peirce S.M., Van Gieson E.J., Skalak T. (2004) Multicellular simulation predicts microvascular patterning and in silico tissue assembly, *The FASEB journal*, doi:10.1096/fj.03-0933fje. doi: 10.1096/fj.03-0933fje

Pomposelli F.B. Jr., Arora S., Gibbons G.W., Frykberg R., Smakowski P., Campbell D.R., Freeman D.V., LoGerfo F.W. (1998) Lower extremity arterial reconstruction in the very elderly: Successful outcome preserves not only the limb but also residential status and ambulatory function*, Journal of Vascular Surgery*, Vol.28, pp215–225.

Prendergast P.J., Lally C., Daly S., Reid A.J., Lee T.C., Quinn D., Dolan F. (2003) Analysis of prolapse in cardiovascular stents: a constitutive equation for vascular tissue and finite-element modeling, *Journal of Biomechanical Engineering*, Vol.125, pp692–699.

Rhodin J.A.G. (1980) Architecture of vessel wall in Handbook of physiology, The Cardiovascular System*. Bethesda, MD: The Americal Physiological Society*, Sect. 2, Vol. 2, Chapt. 1, pp1–32.

Rivlin R.S. (1948a) Large elastic deformations of isotropic materials I, Fundamental concepts, *Philosophical Transations of the Royal Society of London A*, Vol.240, pp. 459–490.

Rivlin R.S. (1948b) Large elastic deformations of isotropic materials IV, Further developments of the general theory, *Philosophical Transactions of the Royal Society of London A*, Vol.241, pp. 379–397.

Roach M.R., Burton A.C. (1957) The reason for the shape of the distensibility curves of arteries, *Canadian Journal Biochemistry and Physiology*, Vol.35, pp181–190.

Rogers C., Tseng D.Y., Squire J.C., Edelman E.R., (1999) Balloon–artery interactions during stent placement: a finite element analysis approach to pressure, compliance, and stent design as contributors to vascular injury, *Circulation Research*, Vol.84, pp378–383.

Roy S., Silacci P., Stergiopulos N. (2005) Biomechanical proprieties of decellularized porcine common carotid arteries, *American Journal of Physiology- Heart and Circulation Physiology*, Vol.289, H1567–H1576. doi:10.1152/ajpheart.00564.2004

Salacinski H.J., Goldner S., Giudiceandrea A., Hamilton G., Seifalian A.M., Edwards A., Carson R.J. (2001) The mechanical behavior of vascular grafts: A review, *Journal of Biomaterial Applications*, Vol.15, pp241–278.

Sarkar S., Salacinski H.J., Hamilton G., Seifalian A.M. (2006) The mechanical properties of infrainguinal vascular bypass grafts: Their role in influencing patency, *European Journal of Vascular Endovascular Surgery*, Vol.31, pp627–636.

Sarkar S., Sales K.M., Hamilton G., Seifalian A.M. (2007a) Addressing thrombogenicity in vascular graft construction, *Journal of Biomedical Material Research-B*, Vol.82, pp100–108.

Sarkar S., Hamilton T.S.G., Seifalian A.M. (2007b) Achieving the ideal properties for vascular bypass grafts using a tissue engineered approach: a review, *Medical and Biological Engineering and Computing,* Vol.45, pp327–336.

Schepers A., de Vries M.R., Daha M., van Bockel J.H., Quax P.H.A. (2006) Blocking complement activation in general, and complement factor 5a in particular, inhibits intimal hyperplasia and accelerated atherosclerosis in murine vein grafts, *Vascular Pharmacology*, Vol.45, e1–e17.

Schwartz R.S., Huber K.C., Murphy J.G., Edwards W.D., Camrud A.R., Vlietstra R.E., Holmes D.R., (1992) Restenosis and the proportional neointimal response to coronary artery injury: results in a porcine model, *The American Journal of Cardiology*, Vol.19, pp267–274.

Seliktar D., Nerem R.M., Galis Z.S. (2003) Mechanical strain-stimulated remodeling of tissue-engineered blood vessel constructs, *Tissue Engineering*, Vol.9, pp657–666. doi:10.1089/107632703768247359

Serruys P.W., Kutryk M.J.B. (1998) Handbook of Coronary Stents, 2nd ed., Martin Dunitz Ltd., United Kingdom.

Serruys P.W., Kutryk M.J.B. (2000) Handbook of Coronary Stents, 3rd ed., Martin Dunitz Ltd., United Kingdom.

Serruys P.W., Kutryk M.J.B., Ong A.T.L. (2006) Coronary–artery stents—drug therapy, *New England Journal of Medicine*, Vol.354, pp483–495.

Shadwick R.E. (1999) Mechanical design in arteries, *The Journal of Experimental Biology*, Vol.202, pp3305–3313.

Shin'oka T., Imai Y., Ikada Y. (2001) Transplantation of a tissue-engineered pulmonary artery, *New England Journal of Medicine*, Vol.344, pp532–533.

Shin'oka T., Matsumura G., Hibino N., Naito Y., Watanabe M., Konuma T., Sakamoto T., Nagatsu M., Kurosawa H. (2005) Midterm clinical result of tissue-engineered vascular autografts seeded with autologous bone marrow cells, *Journal of Thoracic and Cardiovascular Surgery*, Vol.129, pp1330–1338.

Shum-Tim D., Stock U., Hrkach J., Shinoka T., Lien J., Moses M.A., Stamp A., Taylor G., Moran A.M., Landis W., Langer R., Vacanti J.P., Mayer J.E. Jr. (1999) Tissue engineering of autologous aorta using a new biodegradable polymer, *Annals of Thoracic Surgery*, Vol.68, pp2298–304.

Simoons M.L. (2003) Cardio-vascular disease in Europe: challenges for the medical profession, *European Heart Journal*, Vol.24, pp. 8–12.

Song Y., Wennink J.W.H., Kamphuis M.M.J., Sterk L.M.T., Vermes I., Poot A.A., Feijen J., Grijpma D.W. (2010) Dynamic Culturing of Smooth Muscle Cells in Tubular Poly(Trimethylene Carbonate) Scaffolds for Vascular Tissue Engineering. Tissue Eng Part A, In press. doi:10.1089/ten.tea.2009.0805

Sotoudeh M., Li Y., Yajima N., Chang C., Tsou T., Wang Y., Usami S., Ratcliffe A., Chien S., Shyy J.Y. J. (2002) Induction of apoptosis in vascular smooth muscle cells by mechanical stretch, *American Journal of Physiology-Heart and Circulation Physiology*, Vol.282, pp1709–1716.

Sousa J.E., Costa M.A., Abizaid A. *et al.*, (2005) Four-year angiographic and intravascular ultrasound follow-up of patients treated with sirolimus-eluting stents, *Circulation,* Vol.111, pp2326–2329.

Stankus J.J., Guan J., Fujimoto K., Wagner W.R. (2006) Microintegrating smooth muscle cells in a biodegradable elastomeric fibre matrix, *Biomaterials*, Vol.27(5), pp735–744. doi:10.1016/j.biomaterials.2005.06.020

Stary H.C., Chandler A.B., Dinsmore R.E., Fuster V., Glagov S., Insull W. Jr., Rosenfeld M.E., Schwartz C.J., Wagner W.D., Wissler R.W. (1995) A definition of advanced types of atherosclerotic lesions and a histological classification of atherosclerosis. A report from the Committee on Vascular Lesions of the Council on Arteriosclerosis, *Circulation*, Vol.92, pp1355–1374.

Stary H.C., Blankenhorn D.H., Chandler A.B., Glagov S., Insull W. Jr., Richardson M., Rosenfeld M. E., Schaffer S.A., Schwartz C.J., Wagner W.D., Wissler R.W. (1992) A definition of the intima of human arteries and of its atherosclerosis-prone regions. A report from the Committee on Vascular Lesions of the Council on Arteriosclerosis, *Circulation*, Vol.85, pp391–405.

Steinberg D., (2005) An interpretive history of the cholesterol controversy, part III: mechanistically defining the role of hyperlipidemia, *Journal of Lipid Research*, Vol.46, pp2037–2051.

Steinman D.A., Vorp D.A., Ethier C.R. (2003) Computational modeling of arterial biomechanics: Insights into pathogenesis and treatment of vascular disease, *Journal of Vascular Surgery*, Vol.37, pp1118–1128.

Stewart S.F., Lyman D.J. (1992) Effects of a vascular graft/natural artery compliance mismatch on pulsatile flow, *Journal of Biomechanics*, Vol.25, pp297–310.

Stewart S.F., Lyman D.J. (2004) Effects of an artery/vascular graft compliance mismatch on protein transport: a numerical study, *Annals of Biomedical Engineering*, Vol.32, pp991–1006.

Stoneman V.E.A., Bennett M.R. (2004) Role of apoptosis in atherosclerosis and its therapeutic implications, *Clinical Science*, Vol.107, pp343–354.

Stops A.J.F., erati K.B., Browne M., O'Brien F.J., McHugh P.E. (2010) A prediction of cell differentiation and proliefartion within a collagen-glycosaminoglycan scaffold subjected to mechanical strain and perfusive fluid flow, *Journal of Biomechanics*, Vol.43, pp618–626. doi:10.1016/j.jbiomech.2009.10.037

Subbaraj K., Ghista D.N., Viviani G.R. (1989) Presurgical finite element simulation of scoliosis correction, *Journal of Biomedical Engineering*, Vol.11(1), pp9–18. doi:10.1016/0141-5425(89)90159-3

Subbotin V.M. (2007) Analysis of arterial intimal hyperplasia: review and hypothesis, *Theoretical Biology and Medical Modeling*, Vol.31, pp4–41.

Tai N.R., Salacinski H.J., Edwards A., Hamilton G., Seifalian A.M. (2000) Compliance properties of conduits used in vascular reconstruction, *British Journal of Surgery*, Vol.87, pp1516–1524.

Takashima K., Kitou T., Mori K., Ikeuchi K. (2007) Simulation and experimental observation of contact conditions between stents and artery models, *Medical Engineering and Physics*, Vol.29, pp326–335.

Tarry C.W., Walsh D.B., Birkmeyer N.J. O., Fillinger M.F., Zwolak R.M., Cronenwett J.L. (1998) Fate of the contralateral leg after infrainguinal bypass, *Journal of Vascular Surgery*, Vol.27, pp1039–1048.

Teebken O.E., Bader A., Steinhoff G., Haverich A. (2000) Tissue engineering of vascular grafts: human cell seeding of decellularised porcine matrix, *European Journal of Vascular and Endovascular Surgery*, Vol.19, pp381–386.

Thorne B.C., Bailey A.M., Peirce S.M. (2007) Combining experiments with multi-cell agent based modeling to study biological tissue patterning, *Briefings in bioinformatics*, Vol.8(4), pp245–257. doi: 10.1093/bib/bbm024

Tickner E.G., Sacks A.H. (1967) A theory for the static elastic behavior of blood vessels, *Biorheology,* Vol.4, pp151–168.

Timmins L.H., Moreno M.R., Meyer C.A., Criscione J.C., Rachev A., Moore J.E. Jr. (2007) Stented artery biomechanics and device design optimization, *Medical and Biological Engineering and Computing*, Vol.45(5), pp505–513.

Toner D., Dolan F., Lally C. (2007) Validation of Numerical Models of Stent Expansion Using an In-Vitro Compliant Artery Model, *In Proceedings of Bioengineering in Ireland (13) and the 27th Meeting of the Northern Ireland Biomedical Engineering Society*, Enniskillen, N. Ireland, pp61.

Treloar L.R.G. (1944) Stress-strain dat for vulcanised rubber under various types of deformation, *Transactions of the Faraday Society*, Vol.40, 59-70.

Tseng D.Y., Edelman E.R. (1998) Effects of amide and amine plasma-treated ePTFE vascular grafts on endothelial cell lining in an artificial circulatory system, *Journal of Biomedical Material Research*, Vol.42(2), pp188–198.

van Andel C.J., Pistecky P.V., Borst C. (2003) Mechanical Properties of Porcine and Human Arteries: Implications for Coronary Anastomotic Connectors, *Annals of Thoracic Surgery*, Vol.76, pp58–65.

Vernhet H., Demaria R., Juan J.M., Oliva-Lauraire M.C., Senac J.P., Dauzat M. (2001) Changes in wall mechanics after endovascular stenting in the rabbit aorta: comparison of three stent designs*, American Journal of Roentgenology*, Vol.176, pp803–807.

Viceconti M. (2010) What is a model? A tentative taxonomy of biomedical models. *Proceedings of the European society of biomechanics*, Edinburgh, UK.

Volkmer E., Drosse I., Otto S., Stangelmayer A., Stengele M., Kallukalam B.C., Mutschler W., Schieker M. (2008) Hypoxia in static and dynamic 3D culture systems for tissue engineering of bone, *Tissue Engineering Part A*, Vol.14(8), pp1331–1340. doi:10.1089/ten.tea.2007.0231

Von der Mark K. (1981) Localization of collagen types in tissues, *International Reviews of Connective Tissue Research,* Vol.9, pp265–324.

Vukovic I., Arsenijevic N., Lackovic V., Todorovic V. (2006) The origin and differentiation potential of smooth muscle cells in coronary atherosclerosis, *Experimental and Clinical Cardiology*, Vol.11(2), pp123–128

Walker D.C., Hill G., Wood S.M., Smallwood R.H., Southgate J. (2004) Agent based compuatationl modelling of wounded epithelial cell monolayers, *IEEE Transactions on Nanobioscience*, Vol.3(3), pp153–163.

Wang J.H. C., Thampatty B.P. (2006) An introductory review of cell Mechanobiology, *Biomechanics and Modeling in Mechanobiology*, Vol.5, pp1–16. doi: 10.1007/s10237-005-0012-z

Wang W.Q., Liang D.K., Yang D.Z., Qi M., (2006) Analysis of the transient expansion behavior and design optimization of coronary stents by finite element method, *Journal of Biomechanics*, Vol.39, pp21–32.

Watton P.N., Selimovic A., Raberger N.B., Huang P., Holzapfel G.A., Ventikos Y. (2010) Modelling evolution and the evolving mechanical environment of saccular cerebral aneurysms, *Biomechanics and Modeling in Mechanobiology*, Vol.10, pp109-132. doi: 10.1007/s10237-010-0221-y

Weinberg C.B., Bell E. (1986) A blood vessel model constructed from collagen and cultured vascular cells*, Science*, Vol.231, pp397–400.

Welt F.G., Rogers C. (2002) Inflammation and restenosis in the stent era, Arteriosclerosis, *Thrombosis and Vascular Biology*, Vol.22(11), pp1769–1776.

Wieneke H., Haude M., Knocks M., Gutersohn A., von Birgelen C., Baumgart D. and Erbel R. (1999) Evaluation of Coronary Stents in the Animal Model: A Review, *Materialwissenschaft und Werkstofftechnik*, Vol.30, pp809–813.

Wu W., Wang W.Q., Yang D.Z., Qi M., (2007) Stent expansion in curved vessel and their interactions: a finite element analysis, *Journal of Biomechanics*, Vol.40, pp2580–2585.

Xu Z.C., Zhang W.J., Li H., Cui L., Cen L., Zhou G.D., Liu W., Cao Y. (2008) Engineering of an elastic large muscular vessel wall with pulsatile stimulation in bioreactor, *Biomaterials,* Vol.29, pp1464–1472. doi:10.1016/j.biomaterials.2007.11.037

Zhang W.J., Liu W., Cui L., Cao Y. (2007) Tissue engineering of blood vessel, *Journal of Cellular and Molecular Medicine*, Vol.11, pp945–957.

Zilla P., Bezuidenhout D., Human P. (2007) Prosthetic vascular grafts: Wrong models, wrong questions and no healing, *Biomaterials*, Vol.28, pp5009–5027.

Zahedmanesh H., Lally C. (2009) Determination of the influence of stent strut thickness using the finite element method: implications for vascular injury and in-stent restenosis, *Medical and Biological Engineering and Computing*, Vol. 47, pp385-393.

Zahedmanesh H., Kelly D., Lally C. (2010) Simulation of a balloon expandable stent in a realistic coronary artery; Determination of the optimum modelling strategy, *Journal of Biomechanics*, Vol.43, pp2126–2132.

Zahedmanesh H., Mackle J, Selborn A., Bodin A., Drotz C., Gatenholm P., Lally C. (2011a) Bacterial cellulose as a potential vascular graft: Mechanical characterisation and constitutive model development, *Journal of Biomedical Material Research-Part B*, Vol.97(1), pp105-13. doi: 10.1002/jbm.b.31791

Zahedmanesh H., Lally C. (2011b) A multiscale mechanobiological model using agent based models; Application to vascular tissue engineering, *Biomechanics and Modeling in Mechanobiology*, In press.

Appendix A

A.1: Mesh sensitivity for the simulations presented in Chapter 3

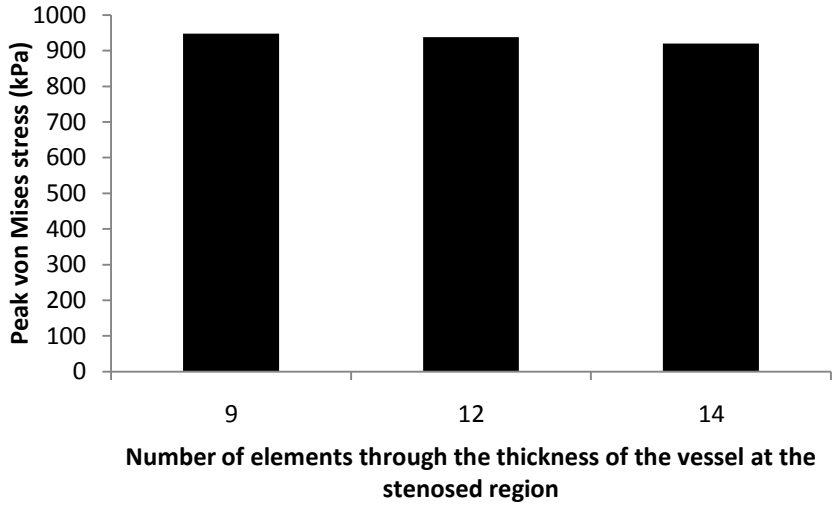

Figure A-9-1: Mesh sensitivity analysis for the stent deployment simulations using restraining elements.

A.2: Mesh sensitivity for the simulations presented in Chapter 5

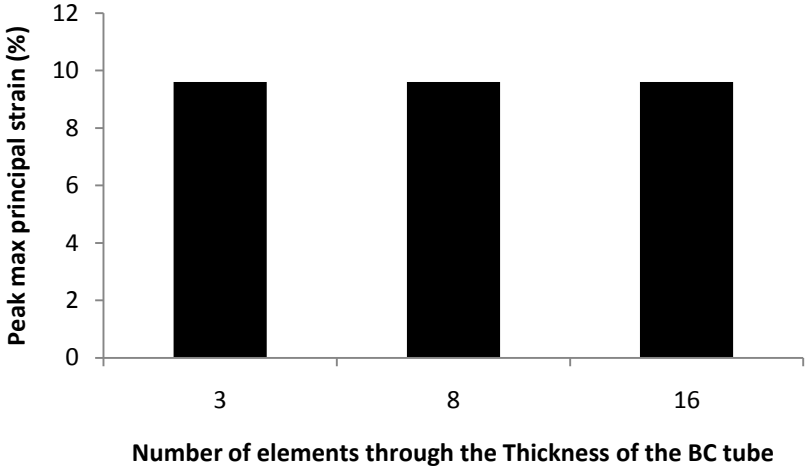

Figure A-9-2: Mesh sensitivity analysis for FE model of BC tubes inflation using the constitutive model developed for BC tubes, 3 elements through the thickness of the BC tubes proved adequate to model their inflation response.

A.3 Sensitivity analyses for simulations presented in Chapter 6

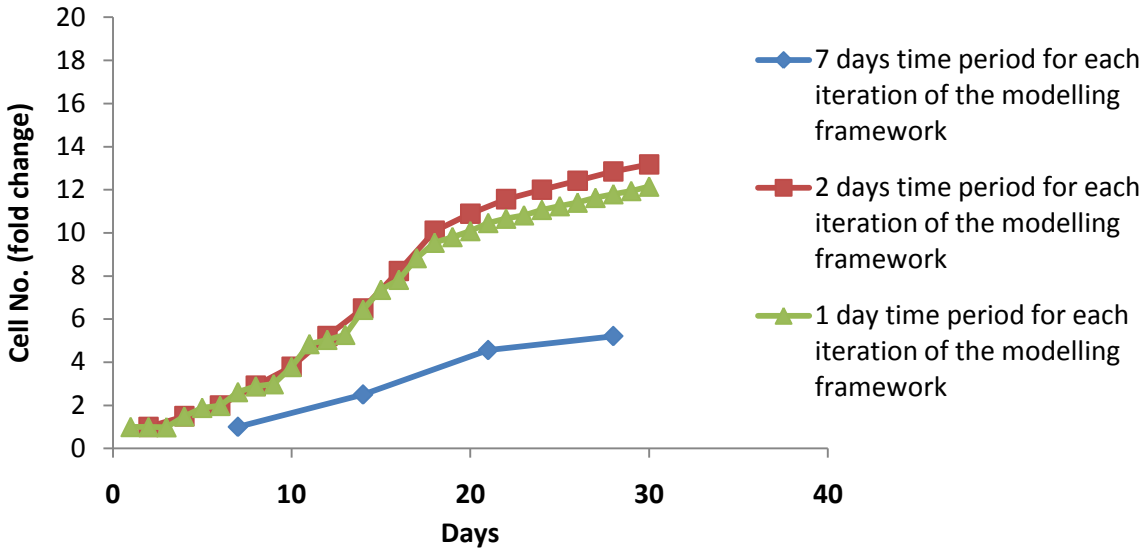

Figure A-9-3: The sensitivity of the simulation results to each iteration's time period. A test simulation was run using three different time periods of 7 days, 2 days and 1 day for each iteration's time period based on which a period of two days was chosen for the simulations.

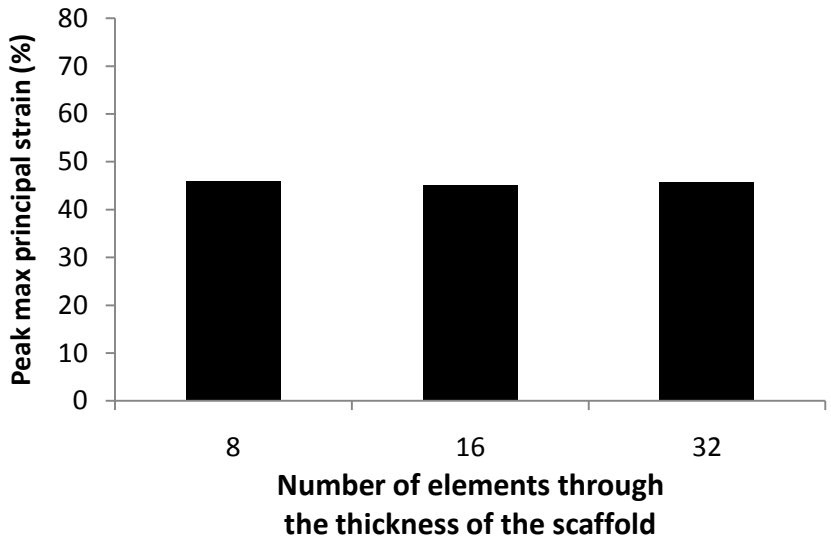

Figure A-9-4: Mesh convergence analysis where compliant scaffold was studied. 16 elements through the thickness of the scaffold proved sufficient.